Informing the practice of ground heat exchanger design through numerical simulations

by

Simon R. Haslam

A thesis
presented to the University of Waterloo
in fulfillment of the
thesis requirement for the degree of
Master of Applied Science
in
Civil Engineering

Waterloo, Ontario, Canada, 2013

© Simon R. Haslam 2013

I hereby declare that I am the sole author of this thesis. This is a true copy of the thesis, including any required final revisions, as accepted by my examiners.

I understand that my thesis may be made electronically available to the public.

Abstract

Closed-loop ground source heat pumps (GSHPs) are used to transfer thermal energy between the subsurface and conditioned spaces for heating and cooling applications. A basic GSHP is composed of a ground heat exchanger (GHX), which is a closed loop of pipe buried in the shallow subsurface circulating a heat exchange fluid, connected to a heat pump. These systems offer an energy efficient alternative to conventional heating and cooling systems; however, installation costs are higher due to the additional cost associated with the GHX. By further developing our understanding of how these ground loops interact with the subsurface, it may possible to design them more intelligently, efficiently, and economically.

To gain insight into the physical processes occurring between the GHX and the subsurface and to identify efficiencies and inefficiencies in GSHP design and operation, two main research goals were defined: comprehensive monitoring of a fully functioning GSHP and intensive simulation of these systems using computer models.

A 6-ton GSHP was installed at a residence in Elora, ON. An array of 64 temperature sensors was installed on and surrounding the GHX and power consumption and temperature sensors were installed on the system inside the residence. The data collected were used to help characterize and understand the function of the system, provide motivation for further investigations, and assess the impact of the time of use billing scheme on GSHP operation costs.

To simulate GSHPs, two computer models were utilized. A 3D finite element model was employed to analyse the effects of pipe configuration and pipe spacing on system performance. A unique, transient 1D finite difference heat conduction model was developed to simulate a single pipe in a U-tube shape with inter-pipe interactions and was benchmarked against a tested analytical solution. The model was used to compare quasi-steady state and transient simulation of GSHPs, identify system performance efficiencies through pump schedule optimization, and investigate the effect of pipe length on system performance. A comprehensive comparison of steady state and pulsed simulation concludes that it is possible to simulate transient operation using a steady state assumption for some cases. Optimal pipe configurations are identified for a range of soil thermal properties. Optimized pump schedules are identified and analysed for a specific heat pump and fluid circulation pump. Finally, the effect of pipe spacing and length on system performance is characterized. It was found that there are few design inefficiencies that could be easily addressed to improve general design practice.

Acknowledgements

A huge thank you goes to Prof. James R. Craig, my supervisor and endless source of knowledge at the University of Waterloo. Thank you for your constant help, motivation, and guidance. Your thorough edits and revisions helped to transform this document into what it is and your positive feedback helped to keep the project forever moving forward.

This project would not have been nearly as successful without the teamwork provided by Richard Simms, the other half of the 'Geoexchange Research Department' at the University of Waterloo. Richard was a constant source of brainstorming and insight in all areas of this project. Thanks for your hard work, patience, and understanding my lack of understanding when necessary.

The research presented herein was completed in partnership with NextEnergy Inc. based out of Elmira, ON. NextEnergy offered industry experience and some of the facilities needed to perform the work presented. The knowledge and funding that has been made available by NextEnergy assisted in all areas of this research.

David Brodrecht from NextEnergy Inc. provided significant insight into a variety of aspects of this project, including brainstorming, much needed mechanical descriptions and lessons, and guidance in helping to understand GHX design. Thanks David.

Peter and Jane Robertson, with the support of NextEnergy and Rapid Cooling, generously provided their fully function horizontal residential GSHP in Elora, ON, for analysis. Thank you to the Robertsons for your hospitality and cooperation throughout this research.

Thanks to Terry Ridgeway from the University of Waterloo for his technical assistance and guidance in preparation for the installation of the monitoring equipment at the Elora Field Site.

Sean McGregor from WILO Canada Inc. helped to assist with identification of fluid circulation pump specifications necessary for GSHP system performance investigations. Thank you Sean.

A big thank you goes to NextEnergy Inc., NSERC, OCE, the University of Waterloo, and Rapid Cooling for their financial support throughout this project.

Finally, thank you to Angela for her continued support, much needed revisions, constant motivation, and her ability to distract me just enough to keep me sane through this project.

Dedication

This thesis is dedicated to my parents, Pam and Steve. Thank you for the physical, emotional, and financial support throughout my life that has lead me to this point. No matter how much of this document you may understand, understand that it could not have happened if I wasn't the man you shaped me into.

Table of Contents

List of Tables

List of Figures

Nomenclature

α thermal diffusivity [m^2/s]

β_1 conductance term describing heat transfer between fluids in adjacent pipes [1/s]

β_2 conductance term describing the heat transfer between the fluid in the pipe and the soil at the intermediate radius [1/s]

β_3 conductance term describing the heat transfer between the fluid in the pipe and the soil at the intermediate radius [1/s]

β_4 conductance term describing the heat transfer between the soil at the intermediate radius and the far field [1/s]

ΔE_{fluid} change in energy in the fluid due to external sources [J]

ΔT prescribed change in temperature between the inlet and outlet temperatures [°C]

Δt time step [s]

$\Delta T_{fluid}^{source}$ change in temperature between the external source (fluid in adjacent pipe or surrounding soil) and the fluid in the pipe [°C]

Δx length of the control volume [m]

$\forall$ volume [m^3]

$\forall_s$ volume of soil between the outer pipe radius and the intermediate soil radius [m^3]

$\forall_\infty$ volume of the hollow cylinder of soil created between the intermediate soil radius and the radius of influence [m^3]

μ dynamic viscosity [Pa·s]

ν kinematic viscosity [m^2/s]

ρ density [kg/m^3]

ρ_s density of the soil [kg/m^3]

ρ_{fluid} fluid density [kg/m^3]

$\rho_{fluid}c_{p_{fluid}}$ volumetric heat capacity (VHC) of the fluid [$J/(m^3K$]

A cross sectional area perpendicular to heat flow [m^2]

a matrix coefficient [1/s]

A_p cross sectional area of the inner pipe perpendicular to flow [m^2]

A_s cross sectional area perpendicular to fluid flow of the soil to the intermediate radius with the area of the pipes removed [m^2]

A_∞ cross sectional area perpendicular to fluid flow of the annulus between the intermediate soil and the far field [m^2]

b matrix coefficient [1/s]

c matrix coefficient [1/s]

c_p specific heat capacity [J/(kgK)]

c_{p_s} specific heat capacity of the soil [J/(kgK)]

$c_{p_{fluid}}$ specific heat capacity of the fluid [J/(kgK)]

Cd heating correction factor

D dispersion coefficient [m^2/s]

d matrix coefficient [1/s]

D_H hydraulic length (pipe inner diameter) [m]

D_L longitudinal dispersion coefficient [m^2/s]

E thermal energy [J]

f friction factor of fluid flowing through a pipe [-]

i degree of freedom [-]

k thermal conductivity [J/(smK)]

k_{pipe} thermal conductivity of the pipe material [J/(smK)]

k_{soil} thermal conductivity of the soil between the pipes [J/(smK)]

L total pipe length [m]

N number of equations in each model segment: outgoing and incoming pipes and soil [-]

n node number [-]

Nu Nusselt number [-]

Nu_0^0 approximation of the asymptote of the Nusselt number as $Pr \to 0$ and $Re \to 0$ [-]

Nu_i approximation of the asymptote of the Nusselt number in transition to laminar flow

Nu_t approximation of the Nusselt number for turbulent flows [-]

Nu_{lc} approximation of the Nusselt number [-] at Re = 2100

Nu_{lc} approximation of the Nusselt number [-] at Re = 2100

Nu_{max} Nusselt number [-] for the maximum flow rate considered in the model

$Nu_{non-turbulent}$ Nusselt number [-] for a non-turbulent flow rate

P total power (or energy per unit time) extracted from the subsurface by one circuit of the loop [J/s]

Pr Prandtl number [-], which is equivalent to the ratio of kinematic viscosity to thermal diffusivity ($Pr = \nu/\alpha$)

Q volumetric flow rate of fluid through the heat pump [m^3/s]

q heat flow [J/s]

Q_{source} thermal energy conduction through the pipe wall [J/sm]

Q_{source}^{pipes} heat flux from the adjacent pipe per metre [J/sm]

Q^{soil}_{source} heat flux from the subsurface per metre [J/sm]

R effective thermal resistance [smK/J]

R^* absolute thermal resistance [sK/J]

r_1 radius of cylinder 1 [m]

r_2 radius of cylinder 2 [m]

r_i inner radius of the pipe [m]

r_o outer radius of the pipe [m]

R_p effective thermal resistance between the fluids in each of the pipes [smK/J]

R_s effective thermal resistance between the fluid in the pipe and the intermediate soil [smK/J]

r_s intermediate soil radius [m]

r_{1_o} outer radius of one pipe [m]

r_{2_o} outer radius of adjacent pipe [m]

R_∞ effective thermal resistance of the annulus of soil between the intermediate radius and the far field [smK/J]

r_∞ radius of influence [m]

R_{abs} absolute thermal resistance of the conducting material between the two parallel cylinders [sK/J]

R_{eff} effective thermal resistance across the pipe wall [smK/J]

R^{source}_{eff} effective thermal resistance between the external source (fluid in adjacent pipe or surrounding soil) and the fluid in the pipe [smK/J]

R_{eq} equivalent effective thermal resistance across the pipe wall modified for non-turbulent flow [smK/J]

R_{inter} effective thermal resistance between either of the pipes and the soil at an intermediate radius [smK/J]

R_{pipe} effective thermal resistance of the pipe wall [smK/J]

R_{soil}^{pipes} effective thermal resistance of the medium between the two pipes [smK/J]

Re Reynolds number [-]

$T'(x,t)$ fluid temperature in the adjacent pipe [°C]

$T(x,t)$ fluid temperature in the pipe of interest [°C]

T^n temperature during current time step [°C]

T^{n+1} temperature during next time step [°C]

t_R fluid residence time in the pipe [s]

$T_s(x,t)$ temperature of the soil at the intermediate soil radius as a function of distance along the pipe and time [°C]

T_∞ far field temperature at the radius of influence [°C]

T_{inner} temperature on the inside of the pipe wall [°C]

T_{in} fluid temperature at the pipe inlet [°C]

T_i temperature at node i [°C]

T_{outer} temperature on the outside of the pipe wall [°C]

T_{out} fluid temperature at the pipe outlet [°C]

T_{s_i} soil temperture at node i [°C]

v mean fluid flow velocity [m/s]

VHC volumetric heat capacity [J/(m^{3}K]

w half the distance between the pipe centres [m]

w_1 distance from y-axis to centre of cylinder 1 [m]

w_2 distance from y-axis to centre of cylinder 2 [m]

Chapter 1

Introduction

Ground source heat pumps (GSHPs) utilize stored energy in the subsurface to provide efficient heating and cooling for buildings. A basic GSHP will return between two and half to four units of energy per one unit consumed while in heating mode, and the equivalent of between ten and twenty units while in cooling mode (NRCan, 2009). A typical GSHP is a combination of a ground heat exchanger (GHX), which consists of a heat exchange fluid circulating through a closed pipe circuit buried in the shallow subsurface and a heat pump. Currently, GHXs are intentionally overdesigned to account for the uncertainty in our understanding of subsurface energy processes.

1.1 Motivation

GSHPs offer a renewable method for heating and cooling applications. Thermal energy, whose original source is predominantly solar energy, can either be extracted from the Earth, heating a building, or injected into it, cooling a building. These systems have the ability to provide efficient heating and cooling for a range of buildings in Ontario and when comparing efficiency in operation costs to that of heating and cooling systems utilizing conventional fuel sources, GSHPs offer the most economical option (Etcheverry et al., 2004). However, since conventional systems have significantly lower initial costs, the use of GSHPs is not as wide spread as it could be. The Oakridge National Laboratory (2008) states that the high capital cost of GSHPs is the number one barrier to adoption to consumers. This barrier is most significant for those properties where land area is limited, thus requiring that a more expensive vertical system be used rather than a horizontal system. Horizontal systems can be more economical but require larger land areas than the vertical equivalent. By reducing horizontal GHX size through better loop design procedures, horizontal GSHPs could become more logistically feasible for a larger range of properties, making them attainable for more building owners. Therefore, an investigation into methods through which the initial size and cost of GSHPs could be reduced would help to identify potential improvements in the application of these systems.

1.2 Problem Statement

While GSHPs are not an entirely new technology, they have been understudied in research circles (OSU, 1988). The main goal of this thesis was to investigate GHX design and system operation and performance through field measurements and numerical simulation to provide insight into their function and identify potential areas for improvement.

This goal was addressed by enhancing our understanding of the heat transfer mechanisms in the subsurface and the interactions between soils and horizontal GHXs. Improving our understanding in this area should lead to improved methods for GHX design, which would allow installers to safely design their systems more efficiently. Upgrading the efficiency of GHX design may lead to decreased installation costs by reducing land area and material requirements; therefore, increasing the feasibility of these systems for smaller residential lots.

Currently, horizontal GHXs require large areas of land to meet existing design guidelines. Typically, it is assumed that approximately 230 m^2 (2500 ft^2) of land area is needed per ton of heating (McQ, 2002), where 1 ton is equivalent to 3516 J/s (12000 BTU/h). This assumption, along with other empirically-based design calculations, have likely led to the improper design of many horizontal ground loop systems (Spitler and Cullin, 2008). While this amount of land area may be necessary for some installations, updated horizon-

tal loop design methods may be able to determine land required on a unit-specific basis. By identifying optimal ground loop configurations and developing novel design methods based on insights into the physics of heat transfer processes, it should be possible to design less conservatively and more intelligently. Ideally, such techniques will lead to reduced materials, costs, and land area requirements, allowing for installation of horizontal GHXs on smaller properties, increasing their utility.

1.3 Thesis Scope

The research presented helps to further the understanding of GSHP operation and the physical processes between the pipe and the subsurface with the purpose of improving GHX design techniques. This thesis provides a review of previous work, a summary of field measurements, a presentation of a developed numerical model, and analyses of measured and simulated data.

A field site in Elora, ON, consisting of a fully functioning horizontal GSHP, was thoroughly monitored throughout this research. The data collected was analysed and is presented in various forms, including total energy usage, operation costs, and temperature measurements.

A transient one dimensional (1D) finite difference heat conduction model of a U-tube

shaped GHX in a cylindrical soil domain was developed to provide a tool through which a range of test cases could be simulated and investigated. While a variety of informative numerical models exist in the literature, a specialized model was developed to analyse specific aspects of GHXs. For this research it was necessary for the model to adequately represent the physical system on small time scales to analyse heat transfer on time scales less than the pipe residence time. Also, the model was required to be fully transient, have the ability to directly define the heat transfer between adjacent, parallel pipes, and be computationally efficient for the time scales of interest (approximately the duration of a heating season in Ontario). The developed 1D finite difference model is presented herein, benchmarked against an existing analytical solution. It was used to analyse the effects of modelling a transient system using a quasi-steady state approximation, investigate the effect that pump scheduling has on overall GSHP performance using the coefficient of performance (COP) metric, and further understand heat transfer between adjacent parallel pipes in a GHX.

An investigation into the effects of horizontal GHX configuration on performance using model simulations is also presented. Simms (2013) developed a three dimensional (3D) model using the finite element method (FEM) to simulate the interactions between horizontal ground loops and the subsurface. The thermal energy flux within the system was assessed based on the temperature gradient between the inside of the pipe and the

surrounding soil. The model is capable of simulating a system with multiple pipes and multiple trenches in various orientations. The model output includes the fluid temperature within the ground loop and measures of system performance and efficiency over time. This model was used in this thesis to investigate the variations in performance between a range of different horizontal GHX configurations and the effects of pipe spacing on system efficiency. These investigations were conducted with the purpose of determining the optimum horizontal GHX configuration to maximize GSHP performance and efficiency over time. The conclusions made help to improve knowledge of specific details of GHX design. This model is discussed in detail in Chapter 2.

Chapter 2

Background

This chapter describes the basic design and operation of GSHPs. Several existing numerical models created to simulate the interaction between a GHX and the subsurface are presented to summarize the current state of the science. Basic GSHP design techniques are discussed and the Canadian standard design method is summarized.

2.1 Ground Source Heat Pumps

A closed-loop ground source heat pump (GSHP) is a combination of a ground heat exchanger (GHX) and a heat pump. These systems are utilized for the heating and cooling of conditioned spaces. A GHX consists of a heat exchange fluid circulating through a

closed pipe circuit buried in the shallow subsurface (typically <200 m). This pipe circuit is connected to a heat pump, whose function it is to transfer thermal energy between the circulating fluid and a conditioned space, typically inside a building. In heating mode, the heat pump extracts energy from the fluid and transfers it to the space and in cooling mode, the heat pump rejects energy from the building into the fluid, changing the temperature of the fluid as it flows across the heat pump. The GHX acts to moderate the temperature of the circulating fluid to that of the ground temperature, providing a thermal energy source or sink to the building depending on the operation mode of the heat pump.

A GHX can be of a variety of configurations. In typical GSHPs, the pipe is installed vertically in a borehole, or series of boreholes, between 20 and 200 m deep or horizontally in shallow trenches between the Earth's surface and a depth of 3 m (OSU, 1988). Figure 2.1 is a schematic representation of the two main types of GHX configurations.

Vertical GHXs are most commonly installed in a U-tube shape. This configuration involves two parallel pipes being installed in a single borehole, forming a U-bend connection at the bottom of the borehole. Vertical systems with two U-tubes installed in the same borehole are also common. Vertical borehole heat exchangers (BHEs) can exist as a single borehole or an array of boreholes connected near the ground surface. A variety of vertical GHX configurations are described by OSU (1988, 2009).

A range of horizontal GHX configurations are used in practice. Typical designs include

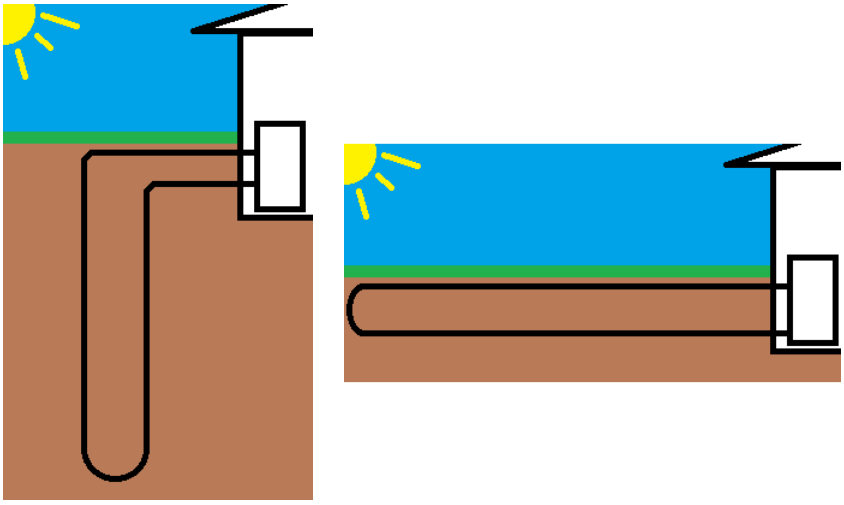

(a) (b)

Figure 2.1: Typical GSHP ground loop configurations: (a) vertical and (b) horizontal - not to scale

1 to 4 pipes buried in a single trench. These pipes can be buried within a single trench or in multiple trenches connected by a common manifold trench. A slinky-loop configuration is also common in horizontal GHX applications. This configuration involves a single coiled pipe spread along the bottom of the trench or multiple coiled pipes spread adjacently along a wider excavation. Some of the most widely used horizontal configurations are described and investigated in Section 5.4. A variety of standard horizontal GHX configurations are described in OSU (1988), OSU (2009), and IGSHPA (1994). Several horizontal GHX configurations are further discussed in Chapter 5 (Figure 5.13).

Horizontally bored configurations can also be used as GHXs; however, these systems are

less common. Horizontally bored systems are constructed similarly to vertical BHE systems with boreholes installed horizontally at shallower depths. Such systems are beneficial for installing the GHX beneath existing infrastructure or landscape while minimizing the disturbance at the Earth's surface.

2.1.1 Existing GHX Models

A variety of numerical models examining specific aspects of the heat transfer mechanisms between GHXs and the subsurface exist. However, the majority of these models focus on vertical systems, or borehole heat exchangers (BHEs), while only a few exist which describe horizontal systems and even fewer which directly describe the heat transfer between adjacent, parallel pipes. A number of previously proposed numerical, semi-numerical, and basic design models are described below.

One of the original models using the finite element method to simulate BHEs was developed by Muraya (1994). This model used an equivalent radius to simulate the two pipes in a BHE and an effectiveness parameter to account for heat transfer between the pipes.

Yavuzturk et al. (1999) presented a transient two dimensional (2D) finite volume model to simulate U-tube shaped BHEs. This model was based on a thermal conduction equation

in polar coordinates and utilized a fully implicit finite volume approach using radial coordinates to represent the U-tube shape of the pipe in a BHE. While this model does simulate both pipes in the U-tube system it does not directly simulate the thermal interactions between the pipes.

Al-Koury et al. (2005) developed a 3D steady state finite element model describing BHEs and their interactions with the subsurface. This model used finite elements to represent the U-tube shaped system. Each element was divided into two pipe segments and two borehole grout segments to represent the physical processes between: the up pipe and the borehole grout material, the down pipe and the borehole grout material, adjacent grout material, and the borehole grout material and the subsurface. This model uses the grout material to couple the heat transfer between pipes. Therefore, thermal energy transfer occurs between each pipe and the grout surrounding that pipe and between adjacent grout segments but the model does not consider direct interactions between pipes. Also, all components of the BHE are combined into single elements. This model was extended by Al-Koury and Bonnier (2006) to the transient system.

The model presented by Al-Koury and Bonnier (2006) was further improved upon by Diersch et al. (2011a). They developed a transient 3D model of single and multiple vertical U-tube BHEs by using the finite element method and implementing the numerical techniques described by Al-Koury et al. (2005) and analytical techniques described by Eskilson

and Claesson (1988) in the FEFLOW simulator. Again, the numerical model presented by Diersch et al. (2011a) uses a division of elements into segments of up pipe, down pipe, and two borehole grout material segments. The inclusion of additional segments in the grout helped to improve this model over that described by Al-Koury and Bonnier (2006). This change improved the accuracy of the model and allowed for the simulation of additional U-tube geometries in the BHE. The Diersch et al. (2011a) model has the ability to simulate a double U-tube system, in which case there is an element segment for each of the four pipes and the corresponding four borehole grout segments. This model is shown to produce results agreeable with analytical solutions for a variety of test cases as benchmarked by Diersch et al. (2011b). However, similar to Al-Koury et al. (2005), there is no direct heat transfer between the pipes in this model and the heat transfer is strictly between the pipes and their corresponding grout segments, adjacent grout segments, and the grout segments and the surrounding subsurface, and computational efficiency is dependent on the optimization of the mesh configuration.

The analytical method employed by Diersch et al. (2011b) was originally described by Eskilson and Claesson (1988), extended for additional BHE pipe geometries, and implemented in the FEFLOW simulator. This method was originally proposed as a method for the steady state simulation of an array of thermally interacting BHEs for only long term analyses. Diersch et al. (2011a) found the analytical method accurate, highly efficient, and

robust for long term analyses but not applicable for short term simulations.

Nabi and Al-Khoury (2012a) proposed a 3D finite volume model for BHEs. This model separates the soil domain and the BHE domain, solving each one as a heat source to the other. It is an extension of the work presented by Al-Koury et al. (2005) and Al-Koury and Bonnier (2006).

A variety of other finite element based numerical models describing vertical BHEs have previously been proposed analysing a range of specific processes. For example, Raymond et al. (2011), among others, used this numerical method to simulate BHEs with the purpose of understanding the heat transfer during thermal response tests for the quantification of thermal properties.

The finite element method has also been used to investigate ground water flow interactions with BHEs. Muraya (1994), Rees et al. (2004), and He et al. (2011) have proposed finite element models that include the effects of soil moisture and the presence of ground water on the heat transfer between the subsurface and certain types BHEs.

For horizontal ground heat exchangers much less modelling work has been done; however, some analyses have been completed using numerical modelling techniques. Stevens (2002) presented a numerical model to simulate the heat transfer between a single buried cylindrical pipe and the surrounding semi-infinite subsurface. This model, developed us-

ing the finite difference method, examined the heat transfer differences between the fluid and the subsurface for the steady pumping of a fluid through the pipe and the case of intermittent pumping of a fluid through the pipe.

An earlier model proposed by Mei and Emerson (1985) described the behaviour of a GHX as a single buried coil. This model included intermittent pumping and the freezing effects of moisture in the soil surrounding the buried pipe.

Philippe et al. (2011) proposed a semi-analytical model to simulate the axial fluid temperatures and pipe temperatures in a horizontal, serpentine ('S'-shaped) GHX. Several techniques are combined by Philippe et al. (2011) to simulate this system. The finite difference method is used to approximate the axial heat transfer between the fluid and the pipe. An analytical cylindrical heat source solution first proposed by Baudoin (1988) was employed to define a reference heat transfer problem that was used to describe the heat transfer between the pipe and the soil. Finally, for longer simulations, the heat transfer between adjacent pipes was described using spatial superposition of all the adjacent pipe segments. An empirical temperature penalty was assigned to the subsurface at the location of each pipe based on the effects of the other pipes in the system. These solution methods were coupled iteratively through time to describe the fluid and pipe temperatures. To include the ground surface boundary condition for longer simulations Philippe et al. (2011) utilized mirror image pipe sections above the ground surface.

Fontaine et al. (2011) describe a transient analytical model based on the finite line source that examines horizontally buried GHX pipes. The model was developed with the goal of assessing the ability of GHXs to keep the subsurface below a building's foundation frozen in regions of permafrost while providing the energy required to heat the building. However, the model does not directly describe the heat transfer between adjacent horizontal pipes. The analytical model presented by Fontaine et al. (2011) was verified using the 3D finite element simulation software COMSOL Multiphysics 3.5a (COM, 2008).

2.2 Current Design Techniques

In this section a brief introduction to a few of the available methods and software packages for GHX design is provided to summarize the current state of the science of GSHP simulation and design.

A common practice in GHX design is the use of correlations describing thermal resistances for transient conductive heat transfer between the buried pipe and the undisturbed subsurface at a distance (Philippe et al., 2011). These correlations describe heat transfer based on thermal conduction shape factors presented in ASHRAE (2009) for typical GHX geometries. The thermal resistance correlations were originally presented by Kavanaugh and Rafferty (1997) and are based on a modified version of an analytical solution describ-

ing thermal conduction shape factors for a line source in a conductive medium presented by Carslaw and Jaeger (1947). The solution treats the GHX as a solid cylinder of specific radius and depends on the duration of system operation and thermal diffusivity of the subsurface. It is used to approximate the thermal resistance between the pipe and the subsurface for a range of GHX geometries, soil characteristics, and pumping durations that are then used in ground loop design.

Philippe et al. (2011) presented a simple procedure to estimate BHE length using spreadsheet calculations. The procedure utilizes the cylindrical heat solution developed by Carslaw and Jaeger (1947) with temporal superposition proposed by Ingersoll and Plass (1948). While the spreadsheet offers a simple method for preliminary calculation of BHE lengths, more rigorous software exists for detailed designs.

One widely used design method for basic GSHP implementation was developed by OSU (1988) and OSU (2009). This method involves a well defined design procedure that utilizes various properties of the GHX configuration, pipe material and dimensions, and geographic location to estimate the required GHX length for a specified heat pump. The method considers the heat pump efficiency, pipe thermal resistance, estimated subsurface thermal resistance, basic local meteorological data, and basic details of the system load requirements. The method utilizes the thermal resistance correlations described above and provides an estimate of the required pipe length per unit of heating or cooling capacity

based on the defined inputs.

Two similar design techniques for smaller systems are implemented within the software packages *GeoDesigner®* developed by *ClimateMaster®* and *WaterFurnace® Energy Analysis (WFEA)* by *WaterFurnace®*. These software packages can be employed for the design of residential or light commercial GHX system design. Loop length estimates are calculated using an iterative process attempting to create a GHX with the necessary capacity as defined by user inputs. While extensive descriptions of the design processes are not available, the calculation procedures are based on an amalgamation of various meteorological, geological, and mechanical inputs and empirical coefficients based on GHX configuration and soil type (WaterFurnace, n.d.).

For more complex systems, more intensive design software packages are employed. One such package is *Ground Loop Design™* developed by *Gaia Geothermal* (2010). This software allows the user to estimate GHX design requirements for a variety of vertical and horizontal configurations. When considering a vertical BHE, the software utilizes one of two calculation methods. The first is fundamentally based on the cylindrical heat solution developed by Carslaw and Jaeger (1947), while the second method is based on the analytical solution for heat conduction in a homogeneous medium solution proposed by Eskilson (1987). The *Ground Loop Design™* utilizes the second method for constant heat extraction cases.

When considering horizontal GHXs, *Ground Loop Design*^{TM} is again fundamentally based on the cylindrical heat solution developed by Carslaw and Jaeger (1947). The software has the ability to estimate GHX design requirements when using slinky type horizontal configurations, using the approximation outlined by IGSHPA (1994).

2.3 GHX Design Guidelines and Standards

The design requirements for a GHX in a certain jurisdiction are dependent on the association responsible for the governance of GSHP design. The most widely accepted method is that described in the *ASHRAE Handbook* (ASHRAE, 2009) as mentioned above. These guidelines are typically referenced in standards pertaining to GSHP design.

In Canada, the standard design method is outlined in *CSA Standard C448: Design and Installation of Earth Energy Systems* (CSA, 2009). The design procedures for residential GHX applications outlined by CSA (2009), referred to as the Multiple Measure Method, are similar to other methods in the industry but applicable only for heating dominate GHX designs. A summary of these guidelines is provided in Appedix A.

2.4 3D Finite Element Model

The 3D finite element model developed by Simms (2013) was used extensively in this thesis because of its ability to simulate horizontal GHXs in a variety of configurations. This model was composed of a 3D soil continuum model, representing the subsurface, coupled to a 1D pipe model, representing the GHX. The continuum model characterizes a soil medium with heterogeneous, isotropic thermal conductivity. The governing equation for the continuum was defined by Simms (2013) as:

$$\rho c \frac{\partial T}{\partial t} = \vec{\nabla} \cdot (\boldsymbol{k} \cdot \vec{\nabla} T) + \vec{q} \tag{2.1}$$

where $\vec{q}$ is the volumetric heat flux from the GHX [J/(sm^3)]; $\boldsymbol{k}$ is the thermal conductivity tensor of the soil [J/(smK)]; ρc is the volumetric heat capacity of the soil [J/(m^{3}K)]; and ∇T is the temperature gradient [K/m] in the soil (Simms, 2013). A Dirichlet fixed temperature boundary condition was specified on the surface of the continuum domain, while Neumann zero flux boundary conditions were specified on all sides and the bottom of the continuum domain (Simms, 2013). The surface boundary condition was defined using the shallow surface temperature data collected from the Elora Field Site discussed in Chapter 3. Additional soil temperature data from the field site were used to define the initial conditions of the continuum model, which were defined as a temperature varying

with depth (Simms, 2013).

The 1D pipe model describes the in-pipe advection-dispersion in a GHX and defines the volumetric heat flux, $\vec{q}$ in Equation 2.1, to the continuum model. The governing equation for the pipe model was defined by Simms (2013) as:

$$\frac{\partial T_p}{\partial t} = -v\frac{\partial T_p}{\partial \overline{x}} + (D_L + \alpha_f)\frac{\partial^2 T_p}{\partial \overline{x}^2} - \frac{K_p}{\rho \cdot c_p \cdot L}(T_p - T) \tag{2.2}$$

where $T_p(\overline{x}, t)$ is the temperature of the fluid in the pipe [K]; $v(t)$ is the velocity of the fluid within the pipe [m/s]; D_L is the in-pipe longitudinal dispersivity caused by mechanical mixing [m^2/s]; α_f is the thermal diffusivity of the fluid [m^2/s]; ρ and c_p are the density [kg/m^3] and specific heat capacity [J/(kgK)] of the fluid, respectively; L is the effective thickness of the pipe wall [m]; K_p is a representative thermal conductivity of the pipe wall [J/(smK)]; and $T(\overline{x}, t)$ is the temperature [K] of the soil continuum immediately adjacent to the outside of the pipe wall at distance $\overline{x}$ down the pipe, determined using Equation 2.2 (Simms, 2013). The inlet boundary condition to the pipe model was defined as a temperature difference between the pipe inlet and outlet fluid temperatures, which acts as a forcing term. Along the length of the pipe, the difference in temperature between the soil and the fluid acts as a Dirichlet boundary condition for the pipe model. The initial fluid temperature in the pipe model was defined as the temperature of the soil immediately

surrounding the pipe, defined in the initial condition of the continuum model (Simms, 2013).

The coupling of the continuum and pipe models was iterative bidirectional. The soil temperatures were used to define the Dirichlet boundary condition along the length of the pipe, which allowed for the generation of a solution to fluid temperatures in the pipe model. Using this fluid temperature profile, the thermal energy flux between the fluid and the soil could be determined, defining the source term to the continuum model from the pipe. The solution to the soil continuum model was then determined, updating the temperatures of the soil continuum, ending a time step of the full model. This process was then repeated for the duration of the simulation (Simms, 2013).

Chapter 3

Elora Field Site

A fully functioning residential ground source heat pump was installed in Elora, Ontario in partnership with NextEnergy, Inc., Rapid Cooling, and the residents, the Robertsons. The site was fitted with a range of temperature and power consumption monitoring equipment to analyse the performance of the ground source heat pump (GSHP) and the temperature changes on the ground heat exchanger (GHX), or ground loop, and in the subsurface immediately surrounding the pipe.

The Robertsons agreed to the installation of the monitoring equipment and granted access to their home for the necessary interior work. No special instructions were given to the Robertsons and they used the system as it would typically be used for residential heating and cooling.

The temperature and power consumption data acquired from the Elora Field Site, while very much consistent with expectations, were analysed to gain insight into specific objectives for this research, including investigations into the performance effects of pump scheduling, GHX configurations, and pipe spacing.

3.1 Ground Loop Design

Figure 3.1 shows the GHX design of the Elora Test site. The drawing is an accurate representation of the as-built GHX based on measurements taken during installation.

The ground loop design represented in Figure 3.1 was designed by the *NextEnergy* dealer *Rapid Cooling*. It is a standard *NextEnergy* design procedure to use the *GeoDesigner®* software package to estimate required GHX length (Brodrecht, 2010). This package was used to simulate a design similar to that installed at the Robertson's home. The details of this design are shown in Appendix B. This design yielded a required trench length of 279 m (915 ft), which is similar to the approximately 260 m (850 ft) of loop trench installed at the Robertson's home. The presented design is meant only to provide insight into the design process.

Appendix B shows an operating cost and performance comparison of the GSHP to two conventional heating and cooling systems: an air-to-air heating and cooling system and

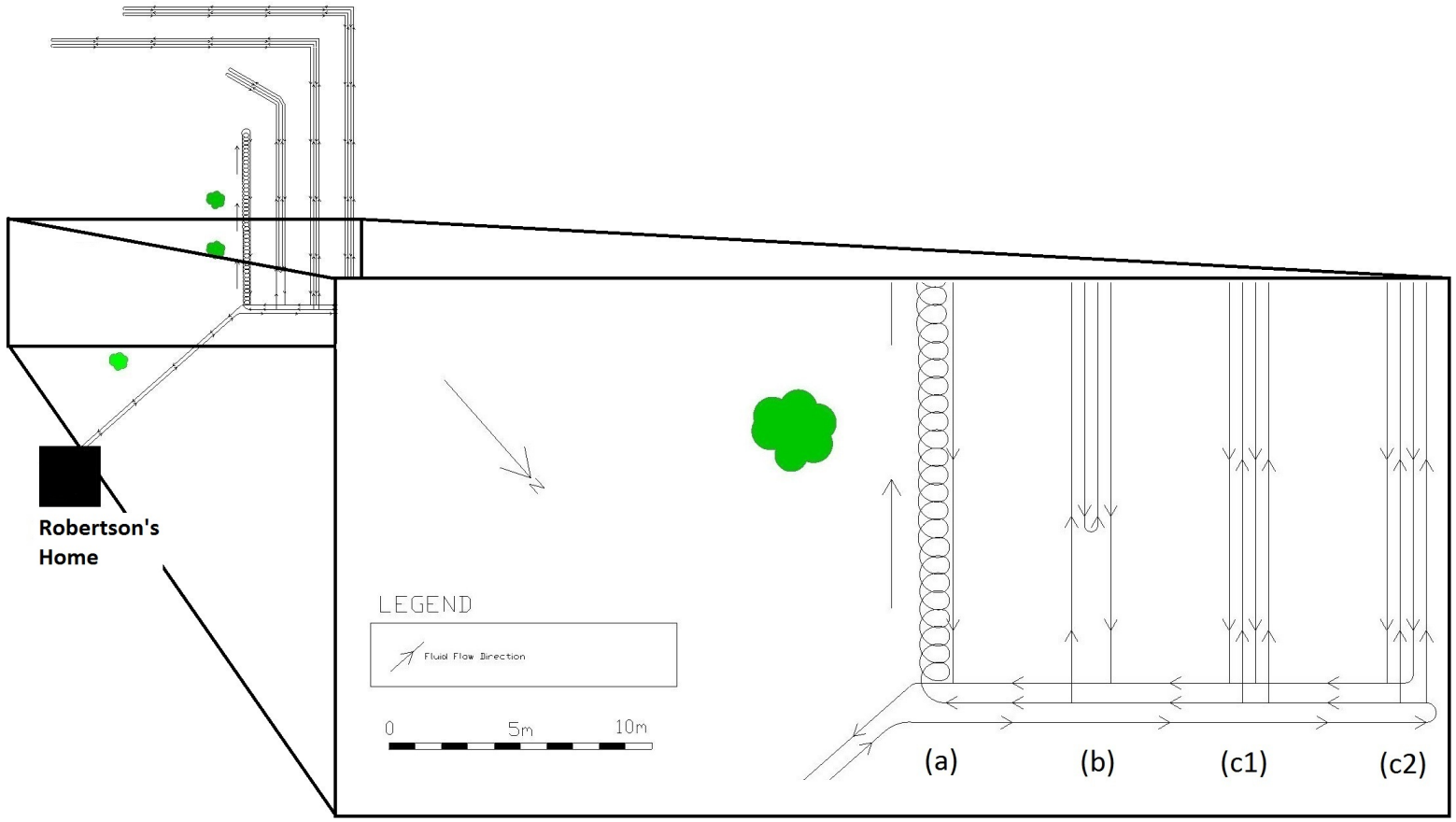

Figure 3.1: Approximate as-built representation of Elora Field Site ground loop design with: (a) slinky loop configuration, (b) rabbit loop configuration, and (c1) & (c2) "side-by-side" loop configurations

a mid-efficiency natural gas heating system with a standard air conditioning unit. This comparison concludes that the GSHP is the most economical of these 3 systems to operate on a annual basis.

The installed GHX utilized three different pipe configurations in four trenches. Figure 3.2 is a schematic representing how these three pipe configurations are positioned in a 1.5 m (5 foot) wide trench. Configuration (b) is referred to as the "rabbit" loop and consists of one pipe 183 m (600 feet) in length; (a) is a "slinky" loop and consists of one pipe 183 m in length; and configuration (c), referred to as a "side by side" loop, consists of two separate 183 m pipes. Two trenches with configuration (c) were installed at the Elora Test Site. The system was designed for each 183 m length of pipe to have a heating capacity of 1 ton, or 3516 J/s (12000 BTU/h). Therefore, configurations (a) and (b) each represent one ton of heating capacity, while each configuration (c) represent two tons of heating capacity, for a total of six tons of heating capacity.

The 4 loop trenches are connected by a perpendicular trench referred to as the manifold trench. This manifold trench is connected to the house by an approximately 35 m trench housing single supply and return pipes. This trench is referred to as the header trench.

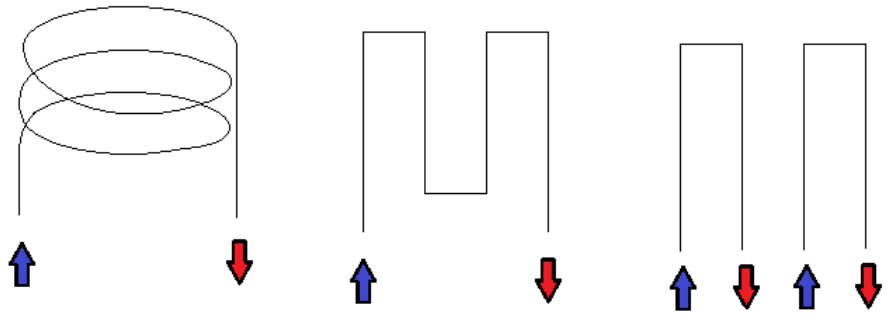

Figure 3.2: Pipe configurations installed at Elora Test Site: (a) slinky loop, (b) rabbit loop, and (c) side-by-side loops - not to scale

3.2 Ground Loop Monitoring

A total of 64 thermistors were calibrated and installed at the Elora Field Site to monitor temperature at various locations in the subsurface. The absolute values measured by the thermistors were of electrical conductivity of the surrounding medium. These absolute measurements were used to calculate the temperature at each sensor using the calculation method and thermistor calibration procedure summarized in Appendix C. Figure 3.3 shows the locations and depths of all thermistors along and surrounding the GHX and the locations of the data loggers. The figure shows two heavily instrumented cross sections. One cross section was installed with the purpose of monitoring the temperatures surrounding the header trench in close proximity to the house. The sensor locations of the header trench cross section are shown in Figure 3.4.

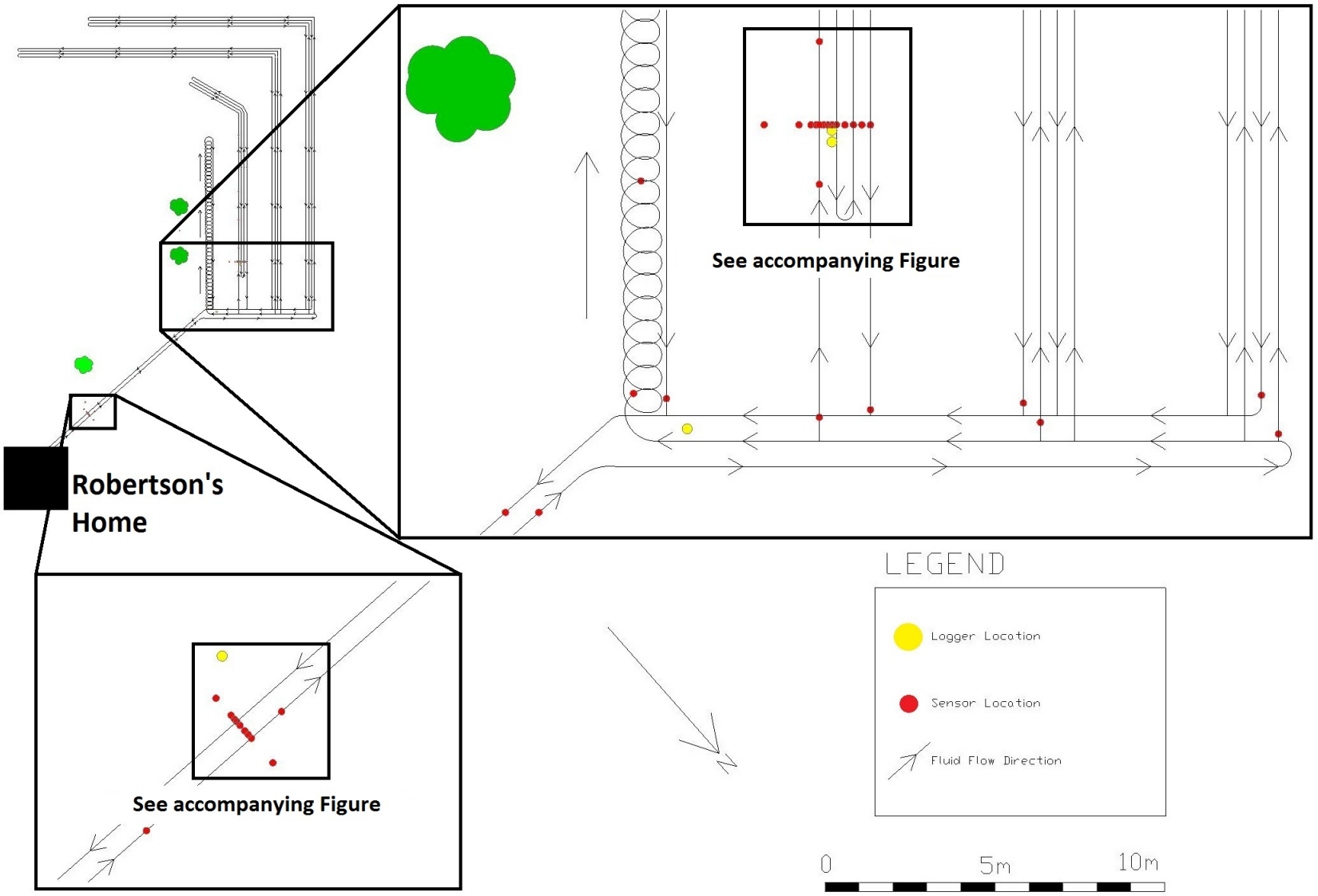

Figure 3.3: Approximate as-built representation of Elora Field Site ground loop design with sensor array showing heavily instrumented cross sections of header trench (Figure 3.4) and rabbit trench (Figure 3.7)

The header trench is where the temperature difference between two adjacent pipes is largest throughout the GHX due to the significant temperature change across the ground loop. The goal of this monitoring location was to analyse the effects of the proximity of the supply and return pipes in the header trench on GSHP performance. Temperature sensors were installed as shown in Figure 3.4 to monitor the subsurface temperature at locations on a horizontal line through the two pipes, perpendicular to fluid flow.

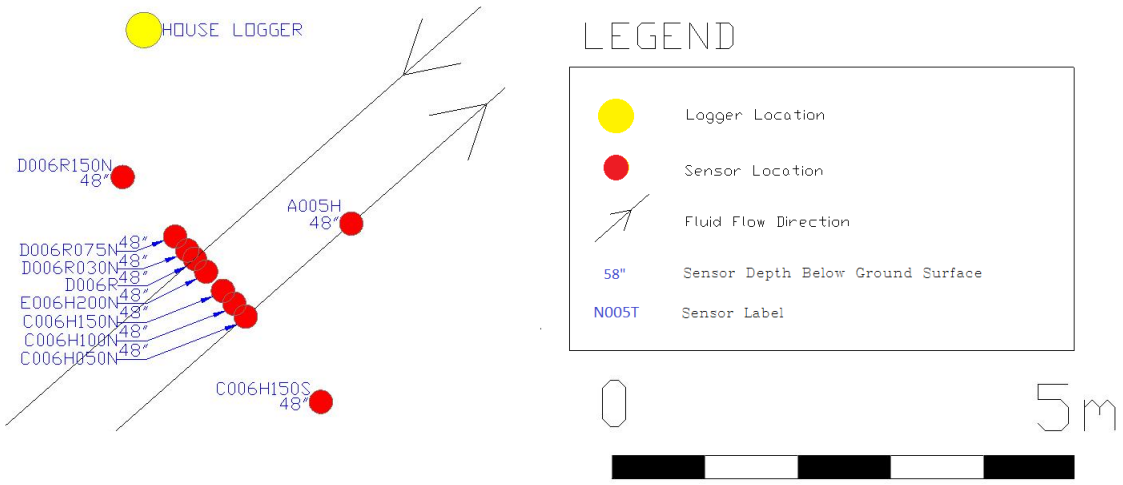

Figure 3.4: Sensor locations at header trench cross section

A photograph of the temperature sensors across the header trench taken during installation of the GHX and the monitoring equipment is displayed in Figure 3.5.

Figure 3.6 shows a snapshot temperature measurement profile generated from each of the thermistors across the header trench. This snapshot was taken on December 8, 2010

Figure 3.5: Photograph of sensor locations at header trench cross section during installation

while the GSHP was operating in heating mode. Figure 3.6 shows the cooler supply pipe on the left in dark blue and the warmer return pipe on the right in light blue. The figure shows how the GHX is extracting thermal energy from the surrounding subsurface, reducing the temperature in the soil around the pipes. It is shown that the temperature in the soil between the two pipes is significantly lower than that in the soil at a distance away from the pipes. Therefore, a reduction in efficiency is experienced at this location. However, the temperature between the pipes is still warmer than that of the return pipe, suggesting that direct energy transfer between the adjacent pipes is unlikely, only that energy transfer into the return pipe may be diminished due to the effects of the adjacent supply pipe. This idea is investigated in Chapter 5.4 to quantify the effects of header pipe spacing.

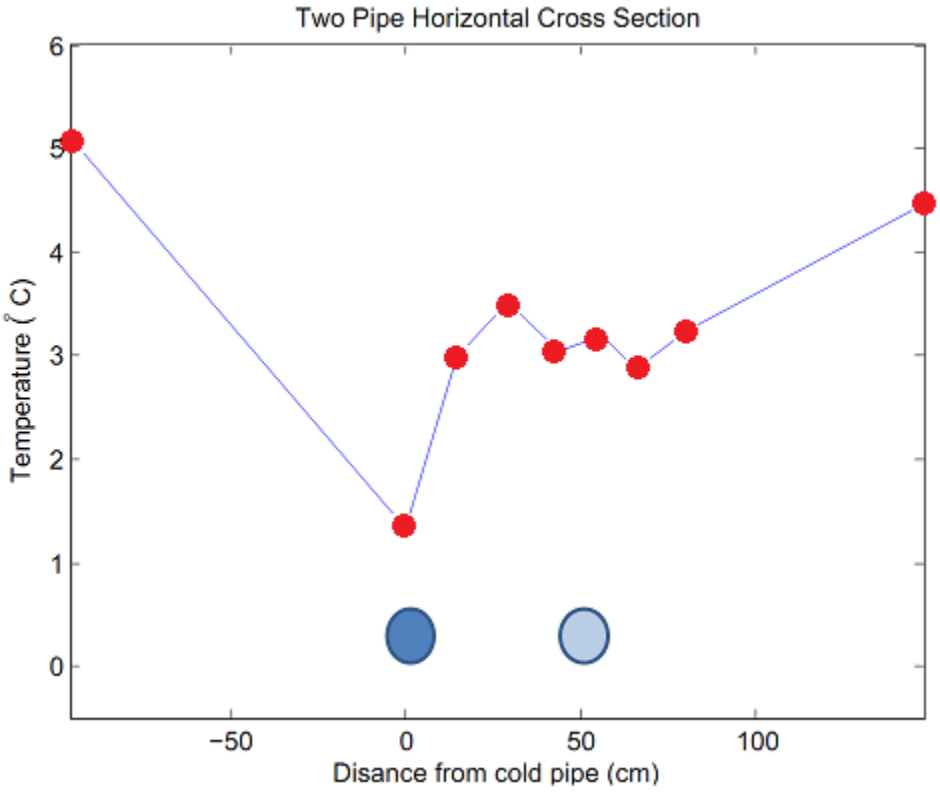

Figure 3.6: Snapshot of temperature across heat trench at Elora Test Site taken during GSHP heating mode on December 8, 2010. Red circles indicate sensor locations across the trench - all sensors located at a depth of 48 inches below ground surface.

The other heavily instrument cross section shown in Figure 3.3 is located across the rabbit loop trench approximately 9.5 m from the manifold. To analyse the temperature in the rabbit trench several groups of thermistors were installed in various orientations relative to the trench. Figure 3.7 shows the locations and depths of the temperature sensors along this cross section. A group of thermistors were installed across the trench with a sensor on

each pipe and several between the pipes and outside the trench. A line of 4 thermistors was installed along the trench on approximately 5 m intervals. Finally, 10 thermistors were installed in a vertical line passing through the supply pipe between 10 cm and 275 cm below ground surface.

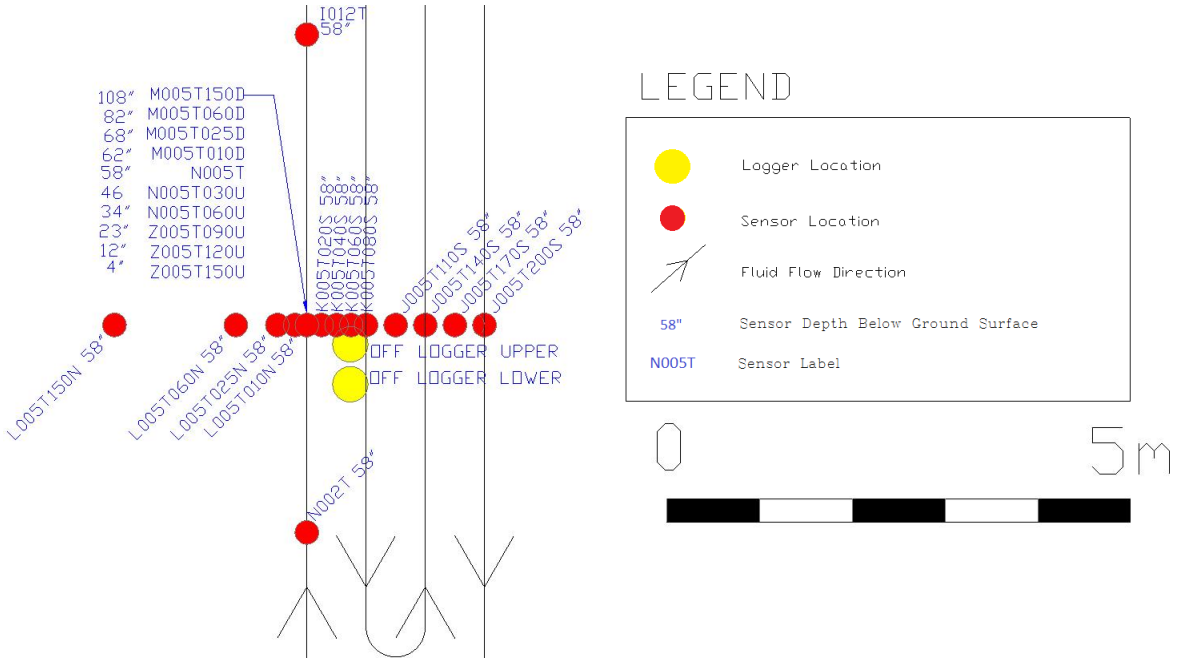

Figure 3.7: Sensor locations at rabbit trench cross section

Undisturbed soil temperature measurements were gathered at an off-loop monitoring location. This location, shown in Figure 3.8, was over 5 m away from the GHX and consisted of four thermistors at depths between 10 cm and 150 cm. This location was used to determine background soil temperatures throughout the monitoring period.

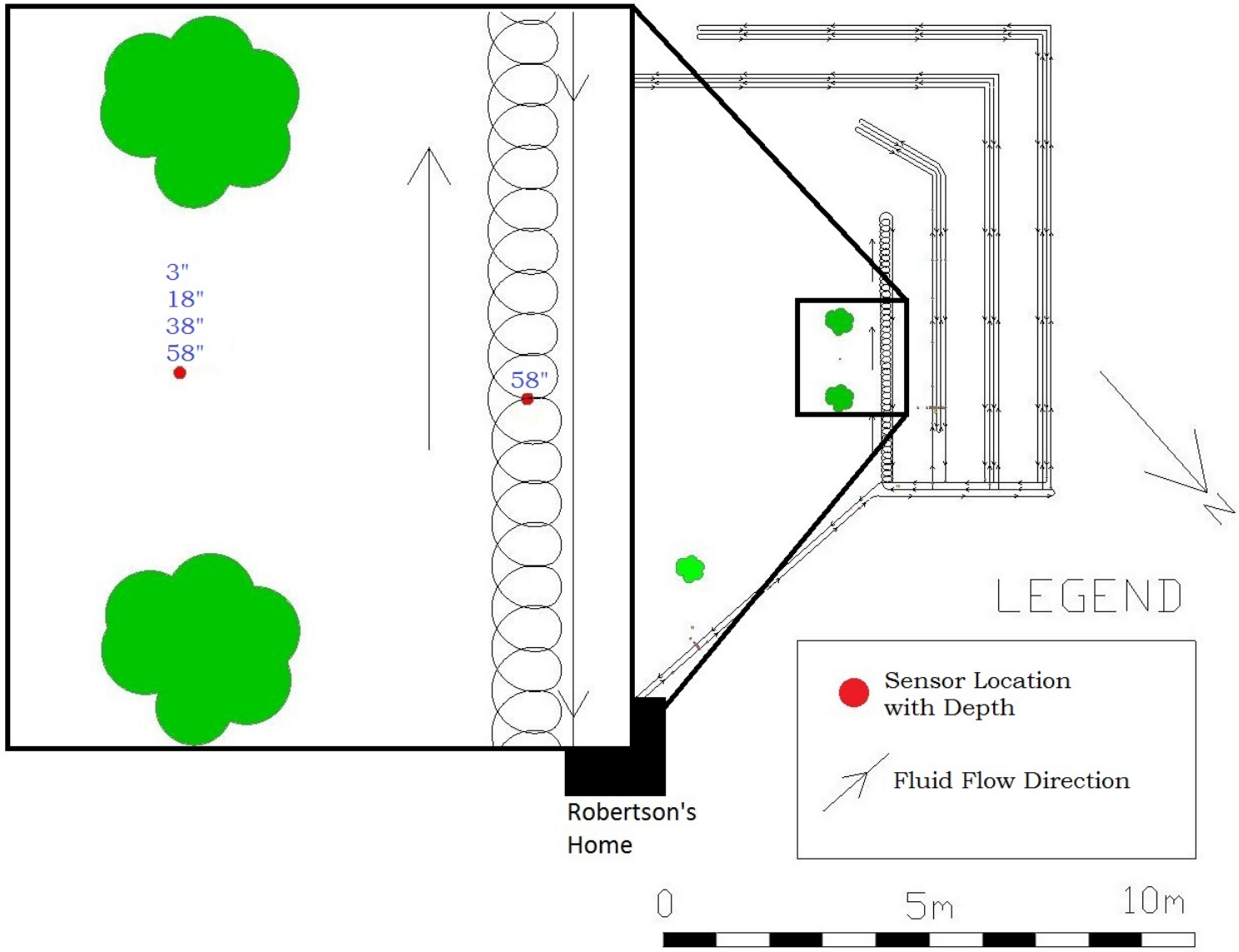

Figure 3.8: Sensor locations at the off-loop location

The installed thermistors were connected to four data loggers for data collection purposes. Measurements were gathered on 5 minute intervals between December 2010 and December 2012.

The data collected were used by Simms (2013) to determine various effective soil parameter values at the Elora Field Site, including equivalent homogeneous values for soil thermal conductivity, soil thermal diffusivity, soil volumetric heat capacity, and undisturbed soil temperature. Values determined by Simms (2013) are used herein where described.

3.3 Interior Monitoring

Typically, the efficiency of ground source heat pumps is defined using the energy efficiency ratio (EER) for cooling operation and the coefficient of performance (COP) for heating operation (OSU, 1988). The EER is a ratio of the total cooling capacity of the system to the power input during cooling operation (OSU, 1988). The COP is a ratio of the heating capacity of the system to the power input during heating operation (OSU, 1988). Therefore, to fully understand the efficiency of a GSHP it is necessary to monitor both energy consumption and generation, thus the Elora Field Site was fitted with a range of sensors on the heat pump system, or 'furnace', inside the house to quantify system performance. These sensors included those used to monitor the power consumption of

the various components of the furnace and those for measuring temperatures at various supply and return ports. To briefly summarize the power monitoring apparatus, four energy sensors were used to directly monitor the power consumed by the main components of the GSHP: the air circulation fan (blower), the fluid circulation pump, the heat pump compressor, and the auxiliary electric heating system. The power consumption data were used to analyse the operating costs of the GSHP at the Elora Filed Site.

3.3.1 GSHP Operation Costs

The power monitoring equipment at the Elora Field Site was continuously collecting data on the power consumption of the main components of the installed GSHP. Figure 3.9 depicts the total energy consumption of the GSHP on a monthly basis for the period of study. These monthly totals are based on the mean of measurements taken every 5 seconds logged on 1 minute intervals. It is noted that power consumption data is not complete for the month of October 2011 due to logger connectivity issues. Power consumption information is missing between 12:00 AM and 7:59 PM October 1, 2011 and between 12:00 PM on October 24, 2011 and 11:59 PM on October 31, 2011. No actions were taken to represent this missing data. Presented data is strictly composed of measured results with the only known missing data as described.

Depicted in Figure 3.9 for reference, the monthly average shallow soil temperatures

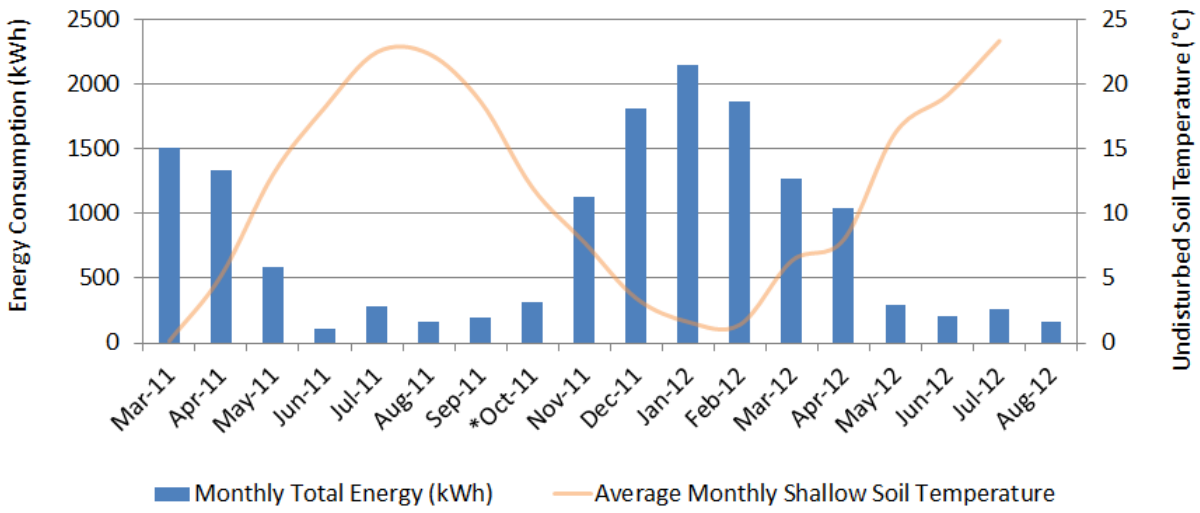

Figure 3.9: Total GSHP energy consumption by month (*12:00 am Oct. 1 to 7:59 pm Oct. 1 and 12:00 pm Oct. 24 to 11:59 pm Oct. 31)

are those that were measured by the off-site thermistor located 10 cm below the ground surface as shown in Figure 3.8. The energy consumption information was used to quantify the operation cost of the GSHP at the Elora Field Site.

The electric utility servicing the Robertson's home imposes the time of use (TOU) billing scheme defined by the Ontario Energy Board (OEB, 2012). The time of use rates schedules for the Summer and Winter billing periods are shown in Figure 3.10 (OEB, 2012). The values of these rates are summarized in Table 3.1 (OEB, 2012). These described time of use system rates, combined with the additional regulatory and delivery fees summarized in Table 3.2 and Table 3.3, were used to determine the exact cost to run the GSHP.

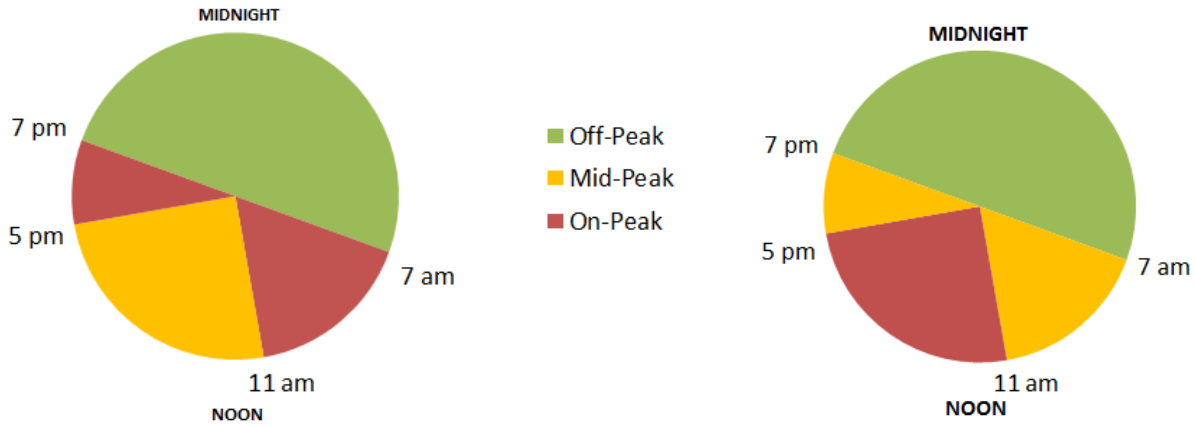

(a) (b)

Figure 3.10: Time of use rates in Ontario, Canada in a) Winter and b) Summer (OEB, 2012)

Table 3.1: Ontario electricity time of use rates (OEB, 2012)

Period	Rate ($/kWh)
Off-Peak	0.063
Mid-Peak	0.099
On-Peak	0.118

Using the amalgamated energy consumption data and the specified utility schedules, the GSHP total energy consumption data were decomposed into the various rate categories. This categorised energy consumption is shown in Figure 3.11. The average monthly shallow soil temperature is provided as reference. This categorised hourly energy consumption data and the described local utility rates were then used to calculate the actual operating costs of the system.

Table 3.2: Ontario electricity time of use delivery fees (OEB, 2012)

Description	Fee	Unit
Monthly Service Charge	14.80	$/month
Distribution Volumetric Rate	0.0153	$/kWh
Transmission Connection	0.0052	$/kWh
Transmission Network	0.0062	$/kWh

Table 3.3: Ontario electricity time of use regulatory fees (OEB, 2012)

Description	Fee ($)	Unit (¢/kWh)
Wholesale Market	0.0065	/kWh
Standard Supply Service Administration	0.25	/month
Debt Retirement Charge	0.007	/kWh

Figure 3.12 shows the monthly electricity costs associated with operating the GSHP at the Elora Field Site under the time of use billing system. The average monthly shallow soil temperature is provided as reference.

The time of use billing system was introduced with the implementation of smart meters in Ontario. However, for this billing system to be invoked the building must have had a smart meter installed. For those buildings that do not have a smart meter the traditional tiered billing system is imposed by the utility (OEB, 2012). The tiered billing system invokes a lower billing rate for a fixed quantity of energy use for each month and a higher billing rate for all additional energy use above this first tier. The tier structure and related billing rates are summarized after OEB (2012) in Table 3.4.

Using the collected power consumption data it was possible to assess the differences

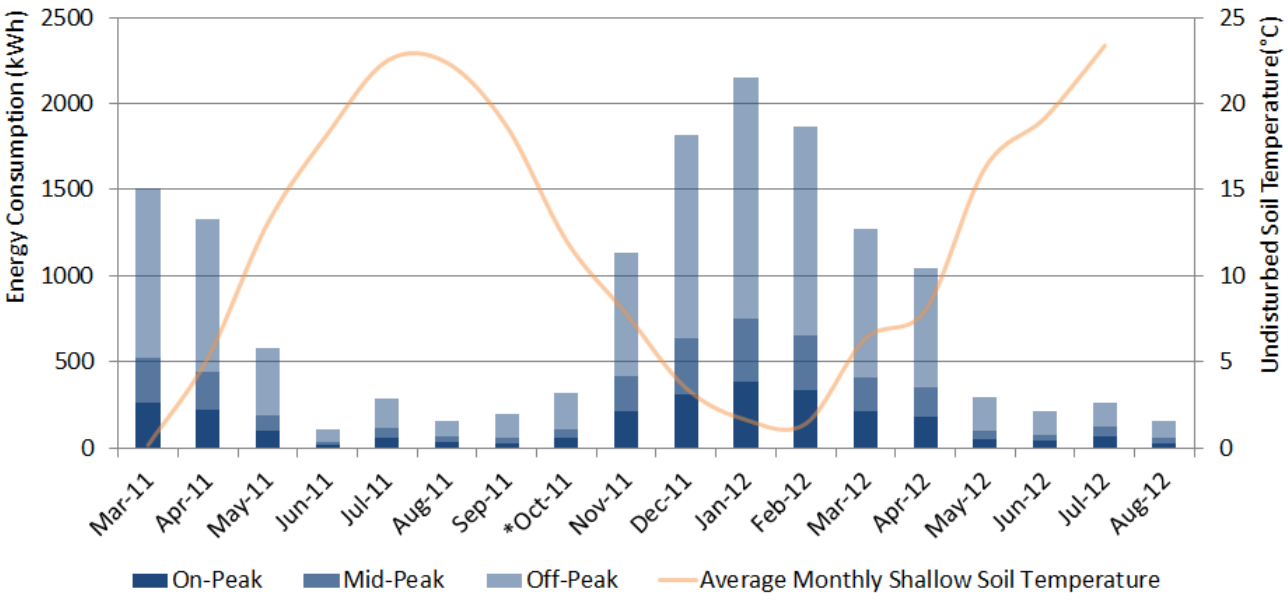

Figure 3.11: Categorised monthly energy consumption of the GSHP (*12:00 am Oct. 1 to 7:59 pm Oct. 1 and 12:00 pm Oct. 24 to 11:59 pm Oct. 31)

between the costs associated with running the Robertson's GSHP for the two billing types to asses the impact of the time of use billing scheme on GSHP operation costs. However, to adequately capture the potential costs associated with the tiered billing, two scenarios were investigated: a minimum cost, where it was assumed that all energy consumed by the GSHP was billed completely from the first tier until the quantity of the first tier was exceeded; and a maximum cost, where it was assumed that all energy consumed by the GSHP was billed completely from the second tier. These two scenarios were developed to provide a range of possible direct operating costs of the GSHP. The costs associated with

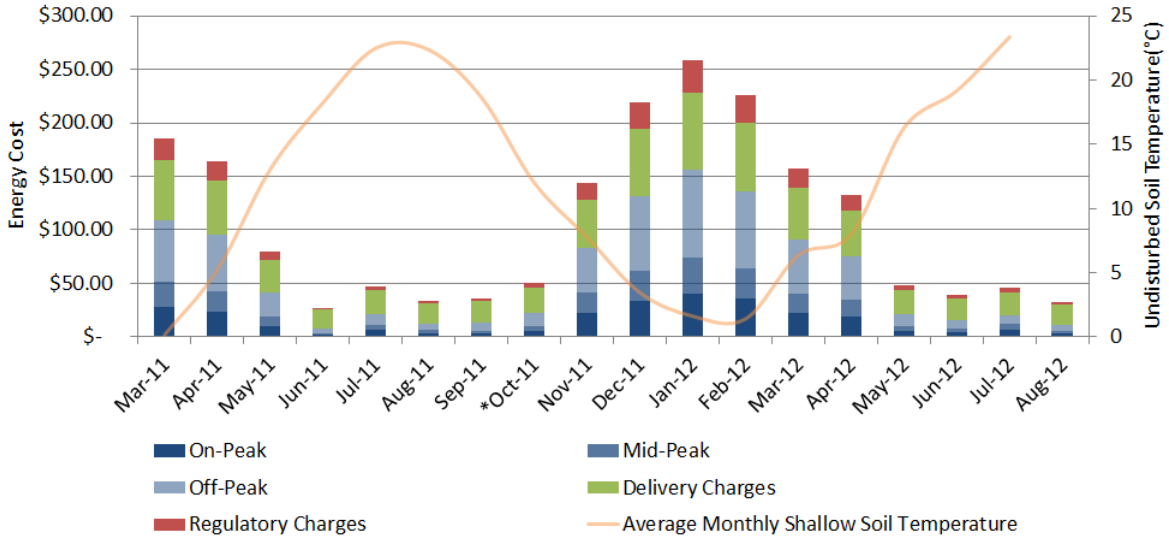

Figure 3.12: GSHP monthly operating costs (*12:00 am Oct. 1 to 7:59 pm Oct. 1 and 12:00 pm Oct. 24 to 11:59 pm Oct. 31)

Table 3.4: Ontario electricity tiered billing system rates (OEB, 2012)

Tier	Winter Fee ($/kWh)	Winter Range (kWh)	Summer Fee ($/kWh)	Summer Range (kWh)
1^{st} Tier	0.074	0-1,000	0.075	0-600
2^{nd} Tier	0.087	>1,000	0.088	>600

these minimum and maximum tiered billing schemes, including average monthly values for each scheme, are presented with the time of use billing scheme in Figure 3.13.

Figure 3.13 shows that the two types of billing schemes typically result in similar monthly operation costs. While the time of use scheme yielded a lower cost than the maximum tiered scheme for every month of the investigation, the assumption made in the calculation of this conservative maximum would not regularly be met.

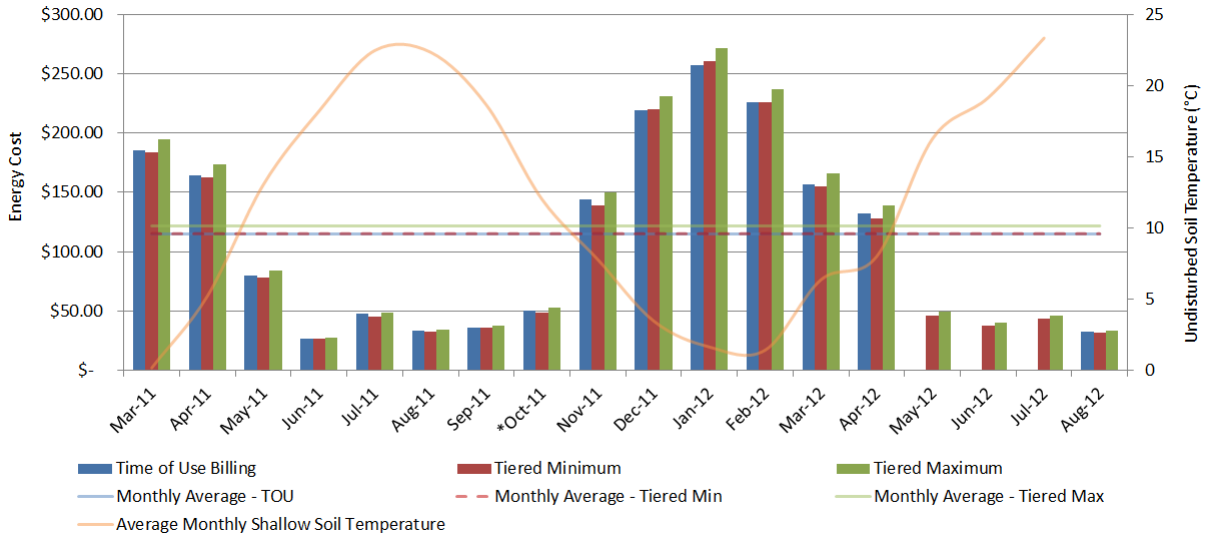

Figure 3.13: Comparison of maximum and minimum tiered billing schemes to TOU (*12:00 am Oct. 1 to 7:59 pm Oct. 1 and 12:00 pm Oct. 24 to 11:59 pm Oct. 31)

Table 3.5 summarizes the average annual cost of operating the GSHP for each billing scheme, where average annual cost is defined as 12 times the average monthly cost. While the time of use scheme tends to fall within the range of possible tiered billing scheme values, the differences between the two systems (considering the tiered minimum) are minor (<5%) and the type of billing scheme does not significantly affect the operation cost of the GSHP.

Table 3.5: Comparison of GSHP operation costs for different billing schemes

Billing Scheme	Average Annual Cost
Tiered minimum	$1,267
Time of use	$1,285
Tiered maximum	$1,345

Chapter 4

Model Development

4.1 Conceptual Model

A conceptual and numerical model was developed to help better understand the physical processes occurring between a GHX and the surrounding subsurface. Typically, in vertical GHXs, a U-tube shaped pipe (Figure 4.1a) is installed in a vertical borehole in an array of one or more boreholes. Horizontal GHXs are often installed in a similar configuration where the pipe runs parallel to the ground surface buried in a shallow trench (Figure 4.1b). This U-bend shape is the configuration around which the conceptual and mathematical models were developed.

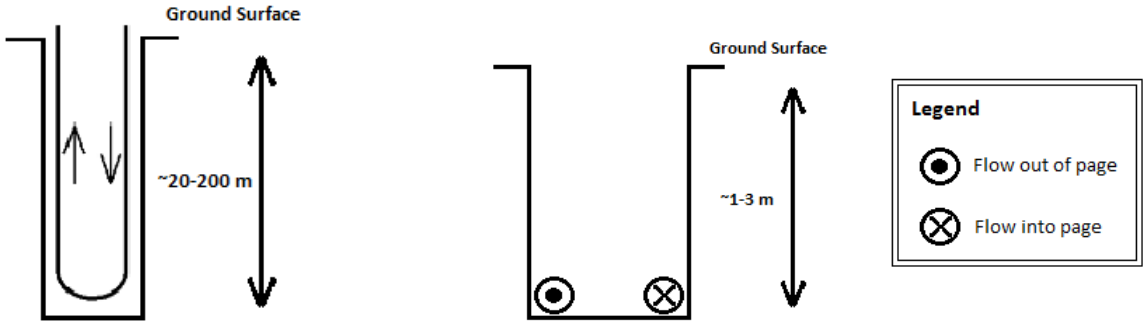

(a) (b)

Figure 4.1: Schematics of (a) vertical borehole with u-tube and (b) horizontal trench configurations

These systems function in both heating and cooling modes depending on the needs of the building being conditioned. While the developed model has the ability to simulate both heating and cooling modes, heating operation will be favoured during discussion since it is typically the dominant mode of operation for most buildings in Ontario.

As fluid circulates through a GHX, it extracts thermal energy from the subsurface, the magnitude of which is controlled by the difference in temperature between the subsurface and the fluid in the pipe. Since the dominant mode of heat transfer in these systems is thermal conduction, thermal convection and radiation are not considered in this model.

In a GHX, as the radial distance from the pipes increases, the temperature perturbation in the subsurface caused by the pipes decreases to zero at some distance. Beyond this radius

the far field temperature may be assumed constant (or independent of pipe effects).

The conceptual model used to represent the thermal energy transfer between the sub-surface and the GHX and between pipes in the GHX was developed based on a single U-tube shaped pipe in a cylindrical soil domain. The soil domain was characterized by two zones: the intermediate soil zone and the far field. The intermediate soil represents a cylinder with some radius measured from the centre of the U-tube and acts to connect the pipe to the far field, which is at a radius measured from the centre of the U-tube to some distance outside the intermediate soil. An effective thermal resistance was defined for: the material between each pipe and the intermediate soil, the material between the intermediate soil radius and the far field, and the material between the two adjacent pipes.

Figure 4.2a represents a cross section perpendicular to fluid flow, where: T_s [°C] is the temperature of the soil at the intermediate soil radius, r_s [m]; T_∞ [°C] is the far field temperature at the radius of influence, r_∞ [m]; and $T(x)$ and $T(L-x)$ [°C] represent the temperatures of the fluid in adjacent pipes, where L is the total length (into the page in Figure 4.2a) of the pipe [m]. Figure 4.2b is a cross section along the length of the pipes, perpendicular to that in Figure 4.2a and shows the relationship between the 2 pipes, the soil, and the far field, each connected by the effective thermal resistance between them. The main advantage of this model configuration is that the interactions between the 2 pipes are well defined, allowing for the analysis of the effects of these interactions.

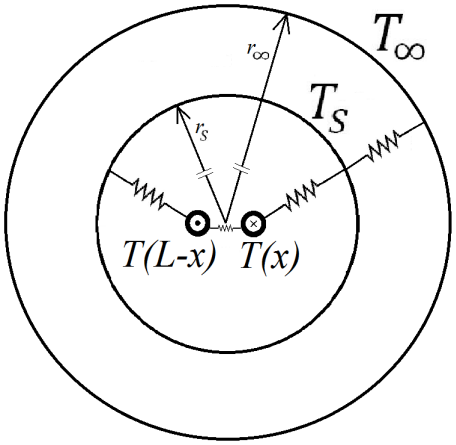

(a)

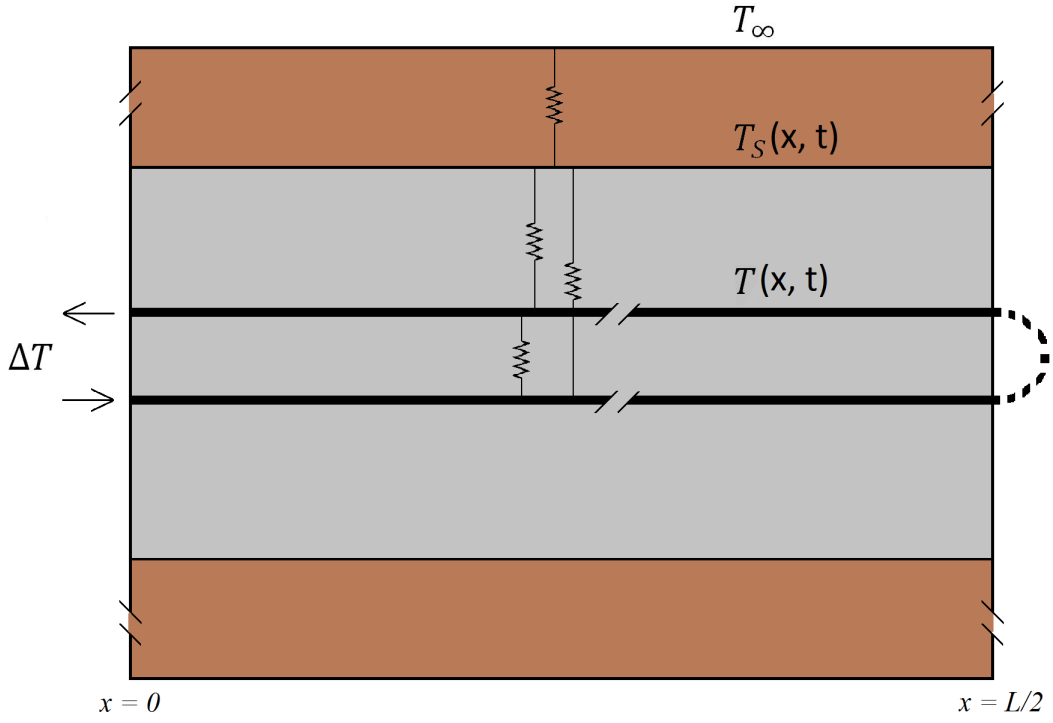

(b)

Figure 4.2: Cross sections of conceptual model: (a) perpendicular to flow and (b) parallel to flow, showing the intermediate soil radius and the far field radius - not to scale

As depicted in Figure 4.2b, the soil domain in this conceptual model is half the total pipe length, $L/2$. The U-bend in the pipe, which would be located at $L/2$, is not directly simulated in the model. The two adjacent pipes are represented by defining the thermal interactions between them and it is assumed in the model that fluid leaving the outgoing pipe immediately enters the incoming pipe. Therefore, since no discontinuity is present in this conceptualization, there would be no negative effect of not directly simulating the U-bend.

To represent the thermal energy change of the fluid caused by a heat pump, a change in temperature between the fluid flowing out of the loop and the fluid flowing into the loop was used as the forcing term. During periods when the system is idle, this boundary condition has a value of zero since the heat pump would not be operating. When the system is operating, this change in temperature has a non-zero value describing the amount of energy being extracted from, or rejected into, the fluid. The forcing term is the inlet boundary condition represented on the left in Figure 4.2b as ΔT and behaves as defined in Equation 4.1.

$$T_{in} = T_{out} + \Delta T \tag{4.1}$$

Where T_{in} is the temperature of the fluid flowing into the loop [°C]; T_{out} is the temperature of the fluid flowing out of the loop [°C]; and ΔT is the prescribed change in temperature

between the inlet and outlet temperatures, the primary forcing term in the developed model [°C].

Equation 4.1 is consistent with the physical operation of a heat pump. This boundary condition provides an internal energy sink, which is directly related to the amount of energy transferred from the fluid, defined in the model using Equation 4.2.

$$\Delta T = \frac{-P}{Q \cdot \rho_{fluid} c_{p_{fluid}}} \tag{4.2}$$

Where P is the total power (or energy per unit time) extracted by the loop [J/s]; Q is the volumetric flow rate of fluid through the heat pump [m^3/s]; and $\rho_{fluid} c_{p_{fluid}}$ is the volumetric heat capacity of the fluid circulating through the GHX [J/(m^3K)], where ρ_{fluid} is fluid density [kg/m^3] and $c_{p_{fluid}}$ is specific heat capacity of the fluid [J/(kgK)].

The expressions in Equation 4.1 and Equation 4.2 are defined such that the prescribed energy transfer from the fluid by the heat pump is positive during heat extraction, or heating mode. This convention ensures that a negative change in fluid temperature across the heat pump is experienced when the GSHP is operating in heating mode.

As the fluid circulates through the GHX in heating mode, it absorbs energy and its temperature rises. Given that the residence time of the fluid varies depending on the location along the pipe, there is an inherent temperature difference between adjacent pipes

that is a function of the distance along the pipe. The temperature difference between the pipes is greatest nearest the heat pump and decreases moving along the pipe toward the U-bend. This difference in temperature between adjacent pipes may, if not properly thermally insulted, results in the transfer of thermal energy from the warmer pipe to the cooler pipe. This heat transfer between adjacent pipes is controlled by the temperature difference between the fluid in the pipes and the effective thermal resistance between the pipes. The effective thermal resistance between adjacent pipes is represented in Figure 4.2.

The volumetric heat capacity (VHC) of a medium refers to the ability of that medium to store thermal energy in a unit volume. The VHC of the subsurface, which allows for the storage of thermal energy in the soil surrounding the GHX, is incorporated into the model as the intermediate soil zone (Figure 4.2). This intermediate radius acts as a thermal energy storage buffer between the pipes and the far field.

The described conceptual model was used as the basis of a mathematical model to simulate the operation of a GHX.

4.2 Mathematical Model

This section summarizes the developed mathematical model. Full derivations of all presented equations are provided in Appendix D.

To simulate the thermal processes in and around a ground heat exchanger, a one dimensional (1D) finite difference heat conduction model was developed. This model is based on two coupled differential equations defining the temperature in the fluid and the temperature in the surrounding soil at an intermediate radius away from the pipes, r_s. A differential equation representing the change in thermal energy flux in a fluid flowing through a pipe was derived based on a thermal energy balance in a cylindrical finite volume of fluid in a pipe (Figure 4.3). Both advective and dispersive fluxes in the pipe were considered, as well as conductive transfer through the pipe wall.

4.2.1 Control Volume

A cylindrical control volume, depicted in Figure 4.3, was used as the basis for the development of the mathematical model. In Figure 4.3, A_p is the cross sectional area of the inner pipe perpendicular to flow [m^2]; T is the fluid temperatures [°C] in the pipe; Δx is the length of the control volume [m]; ρ and c_p are the density [kg/m^3] and specific heat capacity [J/(kgK)] of the fluid, respectively; D is the dispersion coefficient of the flowing fluid in [m^2/s]; and Q_{source} is the thermal energy conduction through the pipe wall [J/sm]. The volume [m^3] of fluid in the control volume, $\forall$, is equal to $A_p \cdot \Delta x$.

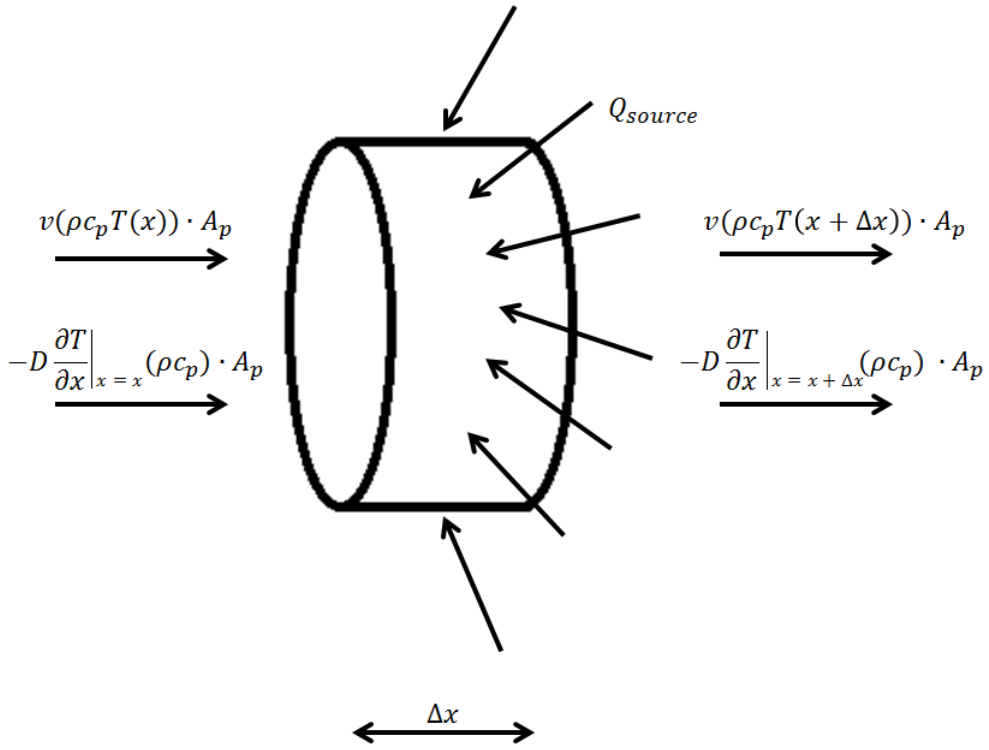

Figure 4.3: Control volume used for thermal energy balance

4.2.2 Governing Equations

From the energy balance flux, source, and sink terms depicted in Figure 4.3, assuming uniform flow and mixing across A_p and that Q_{source} may be represented using effective thermal resistances to the soil and adjacent pipe, an equation defining the transient temperature

of the fluid along the pipe was derived (Equation 4.3).

$$\frac{\partial T}{\partial t} = D\frac{\partial^2 T}{\partial x^2} - v\frac{\partial T}{\partial x} - \beta_1[T - T'] - \beta_2[T - T_s] \tag{4.3}$$

Where $T(x,t)$ is the temperature of the fluid in the pipe [°C]; t is time [s]; D is a dispersion coefficient describing the mechanical mixing and thermal diffusion of the fluid inside the pipe [m^2/s]; x is the coordinate describing distance along the pipe [m]; v is the mean fluid flow velocity within the pipe [m/s]; β_1 and β_2 are conductance terms [1/s] describing the heat transfer between the fluids in the two adjacent pipes and between the fluid in the pipe and the soil at the intermediate radius, respectively; $T'(x,t)$ is the fluid temperature in the pipe directly opposite the current location [°C]; and $T_s(x,t)$ is the soil temperature as a function of distance along the soil domain and time [°C]. Note that $T'(x,t) = T(L-x,t)$ is the fluid temperature in the adjacent pipe as a function of distance away from the end of the pipe and time [°C], where L is the total length of the pipe [m]. Also note that $T_s(x,t) = T_s(L-x,t)$ defines the soil at x and $L-x$ to be the same, due to U-tube shape of the pipe.

To describe the temperature in the soil, T_s in Figure 4.2, at the intermediate radius, r_s, an equation was developed in a similar manner to Equation 4.3. Equation 4.4 incorporates the radial, conductive heat transfer between both sections of the pipe and the soil and

between the soil and the far field to define the transient temperature of the soil at the intermediate radius.

$$\frac{\partial T_s}{\partial t} = -\beta_3[T_s - T)] - \beta_3[T_s - T'] - \beta_4[T_s - T_\infty] \tag{4.4}$$

Where β_3 and β_4 are conductance terms [1/s] describing the heat transfer between the fluid in the pipe and the soil at the intermediate radius and between the soil at the intermediate radius and the far field, respectively. Note that Equation 4.4 is effectively applied from $x = 0$ to $x = L/2$ since this is the length of the soil domain as depicted in Figure 4.2, while Equation 4.3 is applied from over the entire length of the pipe, $x = 0$ to $x = L$.

Equation 4.3 and Equation 4.4 are coupled through the heat transfer between both sections of pipe and the soil at the intermediate radius. Together these equations represent the mathematical model conceptualized in Figure 4.2 and describe the temperature inside the GHX and in the soil at the intermediate radius.

The conductance terms control the energy transfer between the two pipes (β_1), from the fluid in each pipe to the soil at the intermediate radius (β_2), from the soil at the intermediate radius to the fluid in each pipe (β_3), and between the intermediate soil and the far field (β_4). These parameters are inversely proportional to the properties of the

medium being investigated between the two bodies of interest, and are calculated as:

$$\begin{aligned}\beta_1 &= \frac{1}{R_p \rho c_p A_p} \\ \beta_2 &= \frac{1}{R_s \rho c_p A_p} \\ \beta_3 &= \frac{1}{R_s \rho_s c_{p_s} A_s} \\ \beta_4 &= \frac{1}{R_\infty \rho_s c_{p_s} A_\infty}\end{aligned} \tag{4.5}$$

where R_p is the effective thermal resistance between the 2 pipes [smK/J]; A_p is the cross sectional area inside the pipe perpendicular to fluid flow [m^2]; R_s is the effective thermal resistance between the fluid in the pipe and the soil at the intermediate radius [smK/J]; c_{p_s} is the specific heat capacity of the soil [J/(kgK)]; A_s is the cross sectional area perpendicular to fluid flow of the soil to the intermediate radius with the area of the pipes removed [m^2]; R_∞ is the effective thermal resistance between the soil at the intermediate radius and the far field [smK/J]; and A_∞ is the cross sectional area perpendicular to fluid flow of the annulus between the intermediate soil and the far field [m^2]. The effective thermal resistances are defined such that, for example, the thermal energy flux through the pipe wall may be represented simply as a temperature gradient across the pipe wall:

$$Q_{source} = \frac{T_{outer} - T_{inner}}{R_{eff}} \tag{4.6}$$

where Q_{source} is the thermal energy flux across the pipe wall [J/(sm)]; T_{outer} and T_{inner} represent the temperatures [°C] on the outside and inside of the pipe wall, respectively; and R_{eff} is the effective thermal resistance across the pipe wall [smK/J].

4.2.3 Initial Conditions

The initial conditions within the soil and the fluid inside the pipe were defined as everywhere equivalent to the far field soil temperature, T_∞, representing an undisturbed system at time zero. Equation 4.7 and Equation 4.8 define the initial conditions in the fluid and the soil, respectively.

$$T(x, 0) = T_\infty \tag{4.7}$$

$$T_s(x, 0) = T_\infty \tag{4.8}$$

4.2.4 Boundary Conditions

The heat pump operates such that it maintains a fixed change in temperature, ΔT, between the loop inlet and outlet temperatures. Therefore, while the heat pump is operating, the

inlet boundary condition is defined as:

$$T(0,t) = T(L,t) - \Delta T \tag{4.9}$$

where ΔT is an input to the model and represents the change in temperature provided by the heat pump [°C].

When the pump is not operating there is no advection of fluid through the system and it was assumed that there is no thermal energy transfer back into the heat pump from the pipe inlet. Therefore, the fluid flow velocity becomes zero, $v = 0$, and a no thermal energy flux condition is applied at the inlet, $x = 0$:

$$\frac{\partial T}{\partial x}\Big|_{x=0} = 0 \tag{4.10}$$

At the outlet of a GHX the fluid is fed directly into a heat pump. Therefore, to represent the fluid entering the heat pump as that fluid exiting the GHX outlet, an advective-only outflow condition (or "natural outflow" condition) is applied at the outlet, $x = L$ (Equation 4.11).

$$\frac{\partial T}{\partial x}\Big|_{x=L} = 0 \tag{4.11}$$

The boundary condition at the outlet, Equation 4.11, was used for all times.

4.2.5 In-Pipe Dispersion

The dispersion coefficient, D [m^2/s], in Equation 4.3 describes the influence of two processes: the mechanical mixing of the fluid in the pipe characterized by the longitudinal dispersion coefficient, D_L [m^2/s] and the thermal diffusivity, α [m^2/s], which is an intrinsic property. Thermal diffusivity is a function of the materials thermal conductivity, k [J/(smK)], specific heat capacity, c_p [J/(kgK)], and density, ρ [kg/m^3]:

$$\alpha = \frac{k}{c_p \rho} \tag{4.12}$$

and describes how quickly the material adjusts to its surrounding temperature. The dispersion coefficient is defined as:

$$D = D_L + \alpha \tag{4.13}$$

The longitudinal dispersion coefficient is a function of the in-pipe Reynold's number, Re, which is a unitless empirical value that characterizes the turbulence of a flowing fluid. For very turbulent flow rates (those with Reynolds numbers above 4×10^4) (Sittel et al., 1968) empirically defines the relationship between Reynolds number and the longitudinal dispersion coefficient for fluid flow through a pipe as:

$$D_L = 3.87 \times 10^{-5} Re^{0.764} \tag{4.14}$$

where D_L is defined in ft^2/s.

The Reynolds number of a fluid flowing through a pipe is dependent on the flow rate, cross sectional geometry of the pipe, and the properties of the fluid (Menon, 2005):

$$Re = \frac{QD_H}{\nu A_p} \tag{4.15}$$

where Q is the flow rate of the fluid in the pipe [m^3/s]; D_H is the inner pipe diameter [m]; and ν is the kinematic viscosity of the fluid [m^2/s]. The kinematic viscosity is equivalent to μ/ρ, where μ is the dynamic viscosity of the fluid [Pa·s] and ρ is the density of the fluid [kg/m^3] (Menon, 2005).

A base case calculation is described in Appendix E. This process was used in the developed model to estimate the dispersion coefficient for each simulation, where varying flow rates and temperatures were used.

4.2.6 Thermal Resistance

Specific thermal resistance [smK/J] is the reciprocal of thermal conductivity [J/(smK)] and is a measure of a materials ability to resist the flow of thermal energy when subjected to a thermal gradient. Specific thermal resistance is a material constant and is independent of the general shape of the material. Comparatively, the absolute thermal resistance, R^*

[sK/J], of a body defines the ability of a finite body to resist the flow of thermal energy and is dependent on the specific geometry of the body. With an absolute thermal resistance, energy flux, q [J/s], through a body due to a temperature gradient may be calculated as:

$$q = \frac{\Delta T}{R^*}$$

but, for the absolute thermal resistance for a unit length used here, referred to as effective thermal resistance, R [smK/J]:

$$R = R^* L$$

is equivalent to specific thermal resistance.

To estimate the effective thermal resistance between the fluids in each of the pipes, R_p, and between the fluid in the pipe and the soil, R_s, as used in Equation 4.5, the specific thermal resistances between each of these components were divided into sections and combined in series (Equation 4.16).

$$\begin{aligned} R_p &= R_{soil}^{pipes} + 2R_{pipe} \\ R_s &= R_{inter} + R_{pipe} \end{aligned} \tag{4.16}$$

Where R_{soil}^{pipes} is the effective thermal resistance of the medium (typically soil in the model)

between the two pipes [smK/J]; R_{pipe} is the effective thermal resistance of the pipe wall [smK/J]; and R_{inter} is the effective thermal resistance between either of the pipes and the soil at an intermediate radius [smK/J].

To estimate expressions for R_{soil}^{pipes} and R_{inter}, a solution presented by Yovanovich (1973) was used to quantify the absolute thermal resistance of the medium between 2 parallel, long cylinders as represented in Figure 4.4.

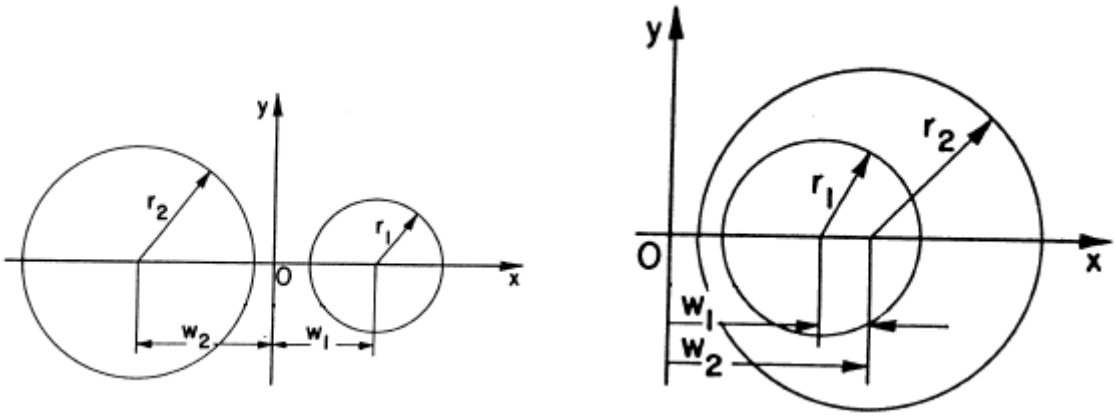

Figure 4.4: Bicylindrical system used by Yovanovich (1973) for thermal resistance derivation

Based on the dimensions in Figure 4.4 the absolute thermal resistance of the medium

between two cylinders of length L [m] was described by Yovanovich (1973) as:

$$R_{abs} = \frac{1}{2\pi kL}\left[ln\left\{\sqrt{\left(\frac{w_1}{r_1}\right)^2 - 1} + \left(\frac{w_1}{r_1}\right)\right\} \pm \left\{\sqrt{\left(\frac{w_2}{r_2}\right)^2 - 1} + \left(\frac{w_2}{r_2}\right)\right\}\right] \quad (4.17)$$

where k is the thermal conductivity of the medium between the cylinders [J/(smK)]; L is the length of the cylinders [m]; r_1 is the radius of cylinder 1 [m]; r_2 is the radius of cylinder 2 [m]; w_1 is the distance from the y-axis (Figure 4.4) to the centre of cylinder 1 [m]; w_2 is the distance from the y-axis to the centre of cylinder 2 [m]; and R_{abs} is defined as the absolute thermal resistance of the conducting material between the two parallel cylinders [sK/J].

In Equation 4.17, a negative sign describes the absolute thermal resistance of the medium between two cylinders on opposite sides of the y-axis (Figure 4.4a), as needed to estimate the effective resistance of the material between the pipes, R_{soil}^{pipes}. Normalizing by L, the appropriate parameters were substituted into Equation 4.17 to yield:

$$R_{soil}^{pipes} = \frac{1}{2\pi k_{soil}}\left[ln\left\{\sqrt{\left(\frac{w}{r_{1_o}}\right)^2 - 1} + \left(\frac{w}{r_{1_o}}\right)\right\} - \left\{\sqrt{\left(\frac{w}{r_{2_o}}\right)^2 - 1} + \left(\frac{w}{r_{2_o}}\right)\right\}\right] \quad (4.18)$$

where k_{soil} is the thermal conductivity of the soil between the pipes [J/(smK)]; w is equal to half the distance between the pipe centres [m], where $w = (w_1 + w_2)/2$; r_{1_o} is the outer radius of one pipe [m]; and r_{2_o} is the outer radius of the adjacent pipe [m].

A positive sign in Equation 4.17 describes the specific thermal resistance of the material between two cylinders on the same side of the y-axis (Figure 4.4b), as needed to estimate the effective thermal resistance of the material between each pipe and the soil at the intermediate radius, R_{inter}. Therefore, R_{inter} was estimated as:

$$R_{inter} = \frac{1}{2\pi k_{soil}} \left[ln \left\{ \sqrt{\left(\frac{w}{r_o}\right)^2 - 1} + \left(\frac{w}{r_o}\right) \right\} + \left\{ \sqrt{\left(\frac{w}{r_s}\right)^2 - 1} + \left(\frac{w}{r_s}\right) \right\} \right] \tag{4.19}$$

where r_o is the outer radius of the pipe of interest [m].

Equation 4.20 (Ingersoll et al., 1954) is a general form of Fourier's Law of heat transfer, defining the conductive heat flow through a thermally conductive medium.

$$q = -kA\frac{dT}{d\eta} \tag{4.20}$$

Where q is heat flow [J/s] perpendicular to cross sectional area, A [m^2]; k is the thermal conductivity of the medium [J/(smK)]; and $dT/d\eta$ is the temperature gradient in direction η [K/m]. The effective thermal resistance across the pipe wall was derived from this expression as:

$$R_{pipe} = \frac{ln(\frac{r_o}{r_i})}{2\pi k_{pipe}} \tag{4.21}$$

where r_i is the inner radius of the pipe [m] and k_{pipe} is the thermal conductivity of the pipe

material [J/(smK)].

Similarly, the effective thermal resistance of the annulus of soil between the intermediate radius and the far field was derived as:

$$R_{\infty} = \frac{ln(\frac{r_{\infty}}{r_s})}{2\pi k_{soil}} \tag{4.22}$$

where R_{∞} is the effective thermal resistance of the annulus of soil between the intermediate radius and the far field [smK/J]. Complete derivations of Equation 4.21 and Equation 4.22 are provided in Appendix D.

Equations 4.18, 4.19, and 4.21 were used to define the effective resistance terms, R_p and R_s, in Equation 4.16. The definitions presented for R_p, R_s, and R_{∞} were used to estimate the conductance terms β_1, β_2, β_3, and β_4 (Equation 4.5) utilized in Equation 4.3 and Equation 4.4.

4.2.7 Radius of Influence

In the system being simulated, the radius of influence, r_{∞}, defines the radial distance from the centre of the two pipes at which no effects from the GHX are observed. Beyond this distance, the temperature in the subsurface remains constant. This parameter is important as it is needed to define the specific thermal resistance to the far field (Equation 4.22) and it

describes the location of the Dirichlet type boundary condition, T_∞, at the outer boundary of the soil domain, r_∞. It was found that a radius of influence of 5 m was most appropriate (Appendix E). Therefore, the value of 5 m was maintained as the radius of influence for all investigations herein unless otherwise specified.

4.2.8 Intermediate Soil Radius

The sensitivity of the model to changes in the intermediate soil radius over a range of simulations was investigated (Appendix E). It was found that an intermediate soil radius of 1 m was most appropriate. Therefore, this value of 1 m was used for all investigations herein unless otherwise specified.

4.3 Finite Difference Approximation

To determine the solutions to Equation 4.3 and Equation 4.4, a finite difference approximation was employed using a Crank-Nicholson time stepping scheme. The derivation of the finite difference solution is detailed in Appendix D. To summarize, the solutions to Equation 4.3 and Equation 4.4 were defined as Equation 4.23 for $i = 1...2N$ and Equation 4.24 for $i = 1...N$, respectively. Here, i refers to the degree of freedom and 3N is the total

number of equations.

$$\begin{aligned} & T_{i-1}^{n+1}\left(-\frac{a}{2}\right)+T_{i}^{n+1}\left(\frac{1}{\Delta t}-\frac{b}{2}\right)+T_{i+1}^{n+1}\left(-\frac{c}{2}\right)+T_{2N-i+1}^{n+1}\left(-\frac{\beta_1}{2}\right)+T_{s_i}^{n+1}\left(-\frac{\beta_2}{2}\right) \\ = \; & T_{i-1}^{n}\left(\frac{a}{2}\right)+T_{i}^{n}\left(\frac{1}{\Delta t}+\frac{b}{2}\right)+T_{i+1}^{n}\left(\frac{c}{2}\right)+T_{2N-i+1}^{n}\left(\frac{\beta_1}{2}\right)+T_{s_i}^{n}\left(\frac{\beta_2}{2}\right) \end{aligned} \tag{4.23}$$

$$\begin{aligned} & T_{s_i}^{n+1}\left(\frac{1}{\Delta t}-\frac{d}{2}\right)+T_{i}^{n+1}\left(\frac{-\beta_3}{2}\right)+T_{2N-i+1}^{n+1}\left(\frac{-\beta_3}{2}\right) \\ & = T_{s_i}^{n}\left(\frac{1}{\Delta t}+\frac{d}{2}\right)+T_{i}^{n}\left(\frac{\beta_3}{2}\right)+T_{2N-i+1}^{n}\left(\frac{\beta_3}{2}\right)+T_{\infty}\left(\beta_4\right) \end{aligned} \tag{4.24}$$

Where:

$$\begin{aligned} a &= \frac{D}{\Delta x^2}+\frac{v}{2\Delta x} \\ b &= \frac{-2D}{\Delta x^2}-\beta_1-\beta_2 \\ c &= \frac{D}{\Delta x^2}-\frac{v}{2\Delta x} \\ d &= -\beta_3-\frac{\beta_4}{2} \end{aligned}$$

The temperatures in the fluid, $T_1 ... T_{2N}$, and in the soil, $T_{s_1} ... T_{s_N}$, are solved simultaneously in the model as a set of 3N equations, where N nodes are used to describe each of the supply pipe, return pipe, and soil at the intermediate radius. The system node distribution is represented in Figure D.2 on Page 175 in Appendix D.

Using this finite difference approximation the boundary conditions outlined in Equation 4.9, Equation 4.10, and Equation 4.11 were defined as Equation 4.25 for the change in temperature boundary at the inlet when the pump is on, Equation 4.26 for the no flux boundary at the inlet when the pump is off, and Equation 4.27 for the no flux boundary at the outlet for all times. Full derivations of all boundary conditions are provided in Appendix D.

$$\begin{aligned} & T_i^{n+1}\left(\frac{1}{\Delta t}-\frac{b}{2}\right)+T_{i+1}^{n+1}\left(-\frac{c}{2}\right) \\ +T_{2N-i+1}^{n+1}\left(-\frac{\beta_1}{2}\right)+T_{2N}^{n+1}\left(-\frac{a}{2}\right)+T_{s_i}^{n+1}\left(-\frac{\beta_2}{2}\right) &= T_i^n\left(\frac{1}{\Delta t}+\frac{b}{2}\right)+T_{i+1}^n\left(\frac{c}{2}\right)+T_{2N-i+1}^n\left(\frac{\beta_1}{2}\right) \\ & \quad +T_{2N}^n\left(\frac{a}{2}\right)+T_{s_i}^n\left(\frac{\beta_2}{2}\right)+\Delta T\,(a) \end{aligned} \tag{4.25}$$

$$\begin{aligned} & T_i^{n+1}\left(-\frac{a}{2}+\frac{1}{\Delta t}-\frac{b}{2}\right)+T_{i+1}^{n+1}\left(\frac{-c}{2}\right)+T_{2N-i+1}^{n+1}\left(-\frac{\beta_1}{2}\right)+T_{s_i}^{n+1}\left(-\frac{\beta_2}{2}\right) \\ & = T_i^n\left(\frac{a}{2}+\frac{1}{\Delta t}+\frac{b}{2}\right)+T_{i+1}^n\left(\frac{c}{2}\right)+T_{2N-i+1}^n\left(\frac{\beta_1}{2}\right)+T_{s_i}^n\left(\frac{\beta_2}{2}\right) \end{aligned} \tag{4.26}$$

$$\begin{aligned} & T_{i-1}^{n+1}\left(-\frac{a}{2}\right)+T_i^{n+1}\left(\frac{1}{\Delta t}-\frac{b}{2}-\frac{c}{2}\right)+T_{2N-i+1}^{n+1}\left(-\frac{\beta_1}{2}\right)+T_{s_i}^{n+1}\left(-\frac{\beta_2}{2}\right) \\ & = T_{i-1}^n\left(\frac{a}{2}\right)+T_i^n\left(\frac{1}{\Delta t}+\frac{b}{2}+\frac{c}{2}\right)+T_{2N-i+1}^n\left(\frac{\beta_1}{2}\right)+T_{s_i}^n\left(-\frac{\beta_2}{2}\right) \end{aligned} \tag{4.27}$$

4.4 Thermal Properties

4.4.1 Heat Exchange Fluid Properties

While the properties of water vary with temperature, the variation in thermal conductivity, k, and specific heat capacity, c_p, is not significant and for the purposes of the developed model they were assumed constant at values representing water at approximately 10°C. At 10°C, the thermal conductivity and specific heat capacity of water are approximately 0.6 J/(smK) and 4190 J/(kgK), respectively (Denny, 1993). However, the density of water varies significantly with temperature. Figure 4.5 was adapted after Denny (1993) and represents the density of water as a function of temperature. These properties of water were used for calculations in the model.

4.4.2 Bulk Soil Properties

The bulk soil thermal diffusivity, α in Equation 4.12, and thermal conductivity, k, at the Elora Field Site were approximated by Simms (2013) using the statistical parameter estimation technique of inverse modelling. The thermal diffusivity and thermal conductivity of the soil were approximately $6.01\times10^{-7}\text{m}^2/\text{s}$ and 1.20 J/(smK), respectively (Simms, 2013). These values were used as a basis upon which a range of soil thermal properties were simu-

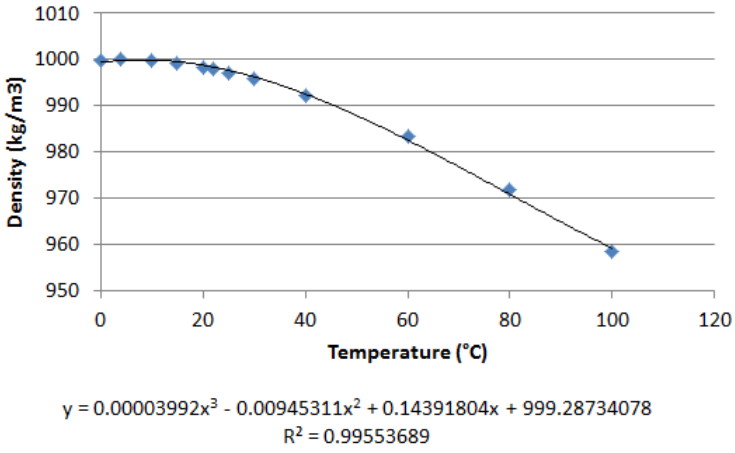

Figure 4.5: Density of water as a function of temperature (Denny, 1993)

lated for analyses using the developed finite difference model and the finite element model developed by Simms (2013).

4.5 Model Benchmarking

To verify the accuracy of the 1-D finite difference model, the model was compared to an existing analytical solution. The analytical model used to benchmark the simulated results was first described by van Genuchten and Alves (1982) as a method to solve the 1D convective-dispersive solute transport equation, which is similar in form to Equation 4.3 with $\beta_1 = 0$ and fixed boundary conditions.

The differential equation governing 1D convective-dispersive solute transport in an ideal column of porous medium is presented in Equation 4.28 (van Genuchten and Alves, 1982).

$$D\frac{\partial^2}{\partial x^2} - v\frac{\partial C}{\partial x} - R\frac{\partial C}{\partial t} = \mu C - \gamma \tag{4.28}$$

Where C is the concentration of the solution [kg/m^3]; D is the dispersion coefficient [m^2/s]; R is the retardation factor [-]; μ [1/s] and γ [kg/(m^{3}s] represent rate coefficients defining the decay of the solute in the aqueous and solid phases [kg/(m^{3}s]; x is distance [m]; and t is time [s] (van Genuchten and Alves, 1982).

Equation 4.28 has the general initial condition (van Genuchten and Alves, 1982):

$$C(x, 0) = f(x) \tag{4.29}$$

where $f(x)$ is a function describing the distribution of the solute in the column at time zero (van Genuchten and Alves, 1982). The boundary condition at the inlet to the column most relevant to the 1D conductive heat transfer model is (van Genuchten and Alves, 1982):

$$C(0, t) = g(t) \tag{4.30}$$

where $g(t)$ is a function describing the concentration type boundary condition at the inlet

(van Genuchten and Alves, 1982).

The boundary condition at the outlet of the column most relevant to the 1D conductive heat transfer model, assumes a semi-infinite soil column and is described in Equation 4.31 (van Genuchten and Alves, 1982).

$$\frac{\partial C}{\partial x}(\infty, t) = 0 \tag{4.31}$$

Based on these boundary conditions a solution to Equation 4.28 was presented by van Genuchten and Alves (1982) as Equation 4.32 (translated here to temperatures for consistency with the heat conduction model).

$$T(x,t) = T_s - \frac{T_s - T_{in}}{2}\left[e^{\frac{(u-v)x}{2\alpha}} erfc\left(\frac{z-vt}{2\sqrt{\alpha t}}\right) + e^{\frac{(u+v)x}{2\alpha}} erfc\left(\frac{z+vt}{2\sqrt{\alpha t}}\right)\right] \tag{4.32}$$

Where $T(x,t)$ is the temperature of the fluid in the pipe running along the x-axis [°C]; T_s is the constant temperature at the pipe outer wall [°C]; T_{in} is the fluid inlet temperature [°C]; u is the fluid flow velocity [m/s], assumed to be constant across the cross section of the pipe; and α is the thermal diffusivity of the fluid [m^2/s]. The parameters η and v are defined by van Genuchten and Alves (1982) as:

$$\eta = \frac{2b_{ig}}{r_i \rho c} \qquad \& \qquad v = u\sqrt{1 + \frac{4\eta\alpha}{u^2}}$$

Where b_{ig} is a thermal conductance term [J/(sm^{2}K)]; r_i is the pipe inner radius [m]; and ρc is the volumetric heat capacity of the fluid [J/(m^{3}K)].

Equation 4.32 was utilized by Nabi and Al-Khoury (2012b) to solve the temperature of a perfectly mixed fluid moving through a single, 1D pipe in contact with a medium at a constant temperature at it's outer surface.

4.5.1 Model Adjustments

In order to use Equation 4.32 as a benchmark for the developed model some modifications had to be made to match the model to the analytical solution. First, the analytical solution describes a single pipe model, while the finite difference model simulates two parallel, adjacent pipes. To remove the second pipe from the finite difference model the conductance term governing heat transfer between the pipes, β_1 in Equation 4.23, was set equal to zero. This modification acts to reset the finite difference model to a single pipe in a cylindrical soil domain.

Second, to impose a constant temperature in the soil at the pipe outer wall, all soil elements in the model were fixed at a temperature equal to that of the far field:

$$T_{s_i}(x,t) = T_\infty \tag{4.33}$$

Therefore, Equation 4.24, which defines the change in temperature in the soil over time, becomes homogeneous:

$$\frac{\partial T_{s_i}}{\partial t} = 0 \tag{4.34}$$

and the boundary condition at the outer radius of the pipe, r_o, was set equal to the background temperature, T_∞.

Finally, it was necessary to change the pipe inlet to a simpler Dirichlet boundary condition to impose a constant fluid inlet temperature, rather than a change in temperature between the inlet and outlet.

4.5.2 Benchmark Results

The modified finite difference model was compared to the analytical solution using two test cases. The first test case was the same used by Nabi and Al-Khoury (2012b). Table 4.1 summarizes the input parameters to the analytical solution defined in the first test case.

Figure 4.6 shows the temperatures and percent difference in temperatures of the fluid flowing through the pipe for the referenced analytical solution and the developed finite difference model for test case 1. The percent difference in temperature between the two

methods shown in Figure 4.6 was calculated at each node using:

$$\%\text{Difference} = \frac{T_{analytical} - T_{numerical}}{T_{analytical}} * 100\% \tag{4.35}$$

where $T_{analytical}$ and $T_{numerical}$ are the fluid temperatures [°C] calculated using the analytical method outlined by van Genuchten and Alves (1982) and the finite difference model developed herein, respectively.

Table 4.1: Analytical Solution Input Parameters - Test Case 1

Parameter	Magnitude	Units
Pipe Length	1	m
Simulation Time	1800	s
T_s	10	°C
T_{in}	50	°C
r_i	0.0131	m
ρc	4.1298×10^6	J/(m^{3}K)
α	9.2×10^{-8}	m^2/s
u	3.75×10^{-4}	m/s
$b_i g$	12	J/(sm^{2}K)
Model Δt	1	s
Pipe Nodes in Model	2000	–

Figure 4.6 shows that the temperatures calculated using each model seem to coincide for all nodes, giving evidence that the developed model is able to accurately simulate the heat transfer between a fluid circulating through a pipe and the surrounding subsurface. However, the test case presented in Table 4.1 is not completely relevant to the analyses that were conducted using the finite difference model because of the extreme temperature

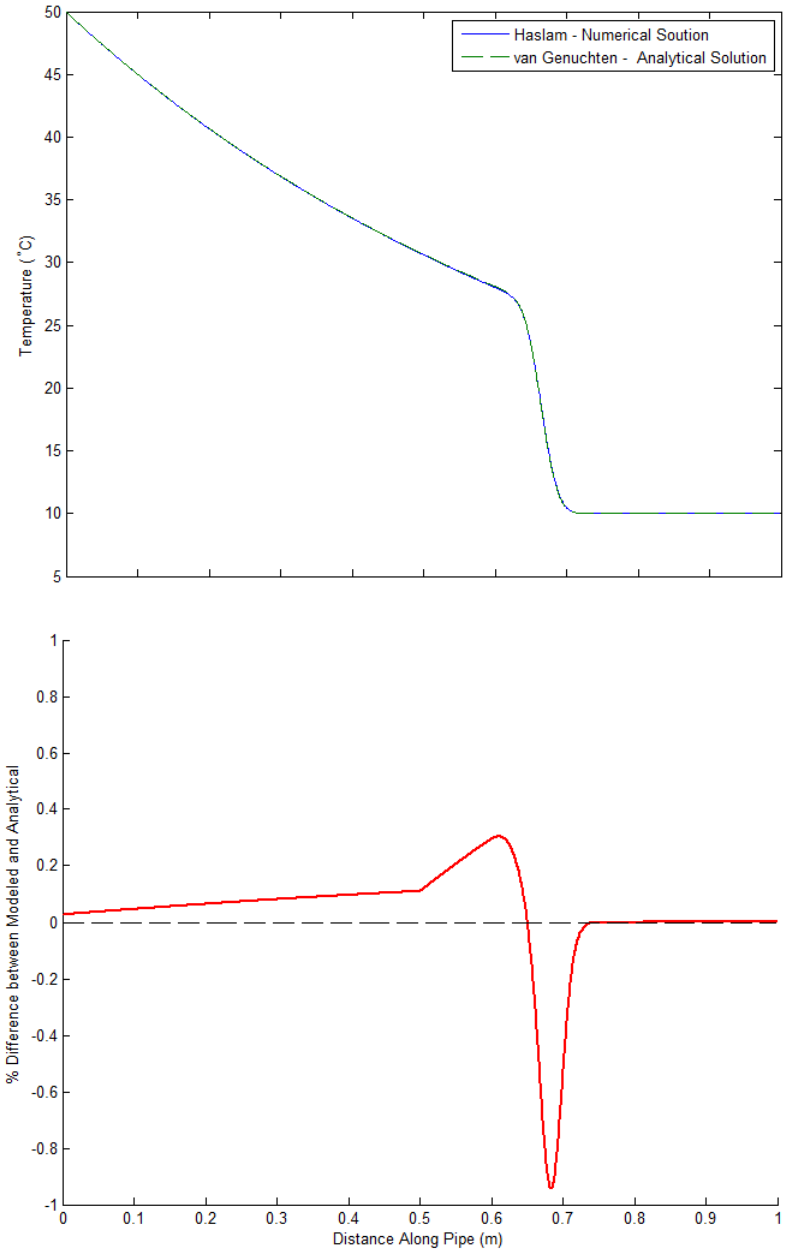

Figure 4.6: Comparison of fluid temperatures and percent difference in fluid temperatures along pipe for analytical and numerical models - test case 1

difference and the small pipe length. Therefore, a second test case was developed to more closely represent a typical GHX. For this test case all physical parameters were maintained as defined in Table 4.1 with changes to the pipe length, simulation time, fluid inlet temperature, and fluid flow velocity.

The parameters for the second test case were defined to represent a typical GHX of interest for the application of the finite difference model. The GHX at the Elora Test Site was taken as a basis for this test case. The Elora Field Site consists of a set of six 183 m (600 ft) loops with an approximate inner pipe radius of 0.013 m and a total flow rate of approximately 15 GPM. Therefore, a single loop consisting of a 183 m pipe was chosen with a fluid velocity, u in the analytical model, of 0.29 m/s. A simulation time of 1800 s was chosen to represent approximately three total pipe volumes through the system for these defined dimensions and flow velocity. An inlet temperature, T_{in}, of 6°C was chosen to represent a realistic temperature difference of 4°C between the inlet fluid and the surrounding soil. All other parameters for this test case were maintained as defined for test case 1.

The temperatures and percent difference in temperatures of the fluid along the pipe as simulated using the developed finite difference model and the analytical method proposed by van Genuchten and Alves (1982) for test case 2 are represented in Figure 4.7, where the percent difference in temperatures was calculated using Equation 4.35. The comparisons

in Figure 4.7 show that the solutions of both the numerical and analytical methods yield similar results for test case 2.

Based on the results of the comparisons for each test case, it is concluded that the developed finite difference model adequately solves (<1% error relative to the analytical solution) the mathematical problem statement used to represent the GHX and has the ability to simulate these systems.

4.6 System Performance

To accurately simulate the performance of the GSHP system as a whole, the function of a specific heat pump and fluid circulation pump were included in the model. The heat pump chosen was a variable speed equivalent of that installed at the Elora Field Site (Brodrecht, 2010), the ClimateMaster Tranquility ® 30 TE Series Model 072 (Cli, 2012). A variable speed fluid circulation pump was chosen to correspond with this heat pump. Two Stratos 1.25x3-25 circulation pumps from WILO (2010) were modelled in series (Brodrecht, 2010).

The COP of a heat pump is a function of the flow rate and the temperature of the fluid entering the heat pump. Using the specifications provided by the manufacturer (Cli, 2012), functions were developed to define the COP of the heat pump for all flow rates and temperatures within these specifications.

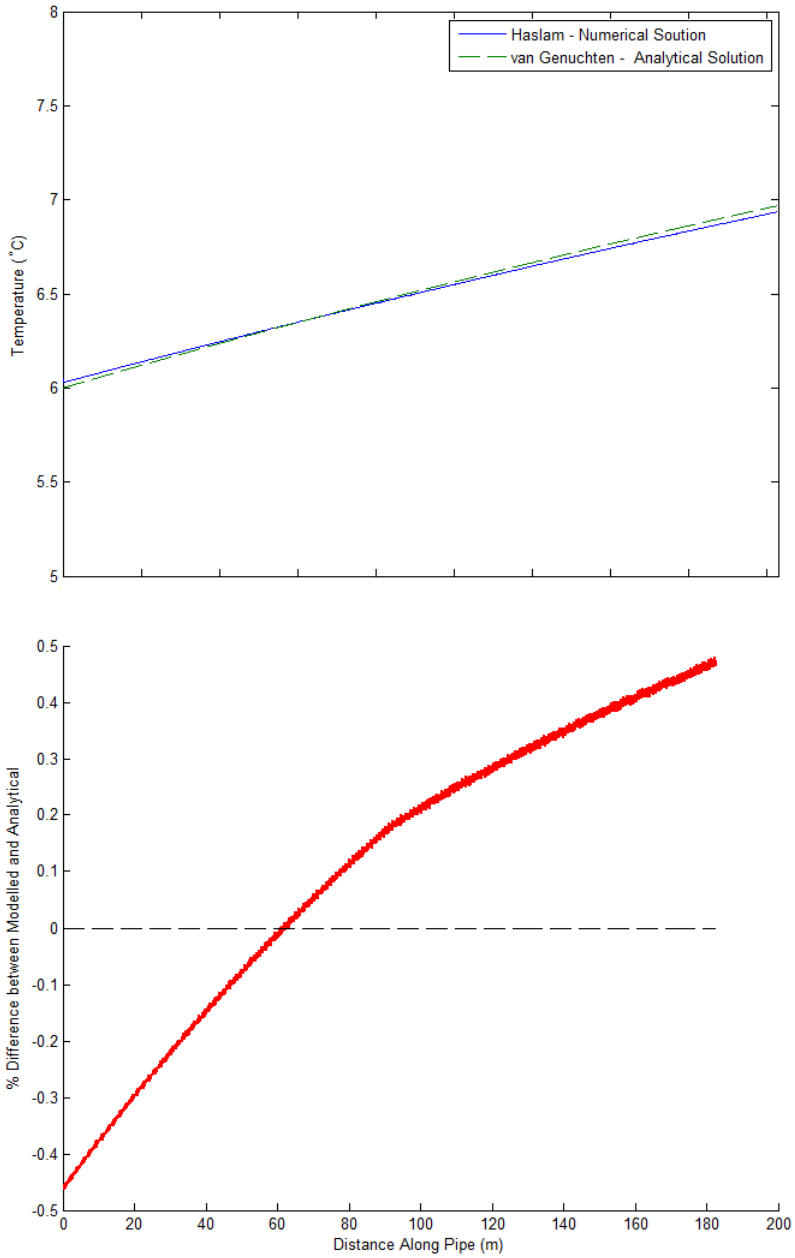

Figure 4.7: Comparison of fluid temperatures along pipe for analytical and numerical models - test case 2

To predict the COP of the entire system it was necessary to investigate the circulation pump input power. The power needed to operate the circulation pump is a function of flow rate and head loss through the system. Therefore, a function was developed in the model to utilize the circulation pump manufacturer's specifications (WILO, 2010) to define the pump power for the range of flow rates and system head losses within these specifications.

The total head loss through the system is a summation of the head loss through the heat pump and the head loss through the GHX due to friction between the flowing fluid and the pipe wall. To describe the head loss through the heat pump the manufacturer's specifications (Cli, 2012) were used to define a function in the model that estimates the heat pump head loss as a function of temperature and flow rate through the system. To quantify the head loss through the GHX, the method proposed by Moody (1944) was utilized:

$$h_f = f\frac{L}{D}\frac{v^2}{2g} \tag{4.36}$$

where h_f is head loss through the pipe due to friction [m]; f is an empirical parameter refered to as the Moody friction factor [-]; L is the length of the pipe [m]; D is the inner diameter of the pipe [m]; v is the average fluid flow velocity in the pipe [m/s]; and g is the acceleration due to gravity [m^2/s] (Moody, 1944).

The Moody friction factor is an empirical parameter based on the in-pipe Reynolds

number (Equation 4.15) and the relative roughness coefficient ϵ/D [-], which describes the roughness of the inside of the pipe, where ϵ represents the absolute roughness of the pipe material [m] (Moody, 1944).

The head loss through the GHX was combined with the head loss through the heat pump to describe the total head loss through the system, which was translated into circulation pump energy consumption during model simulation. Combining the circulation pump and heat pump energy consumption, the actual COP of the system was estimated based on:

$$COP = \frac{E_{extracted}}{E_{consumed}} \tag{4.37}$$

where $E_{extracted}$ is the total energy [J] extracted from the fluid for the length of the simulation and $E_{consumed}$ is the total energy [J] consumed by the system for the length of the simulation. This COP metric was used as the basis for all performance comparisons using the 1D finite difference model.

4.7 Sample Model Output

To illustrate the physical processes being modelled during simulation, an example model output is shown in Figure 4.8 in the form of fluid temperature along the pipe for increasing

times during the simulation of a single cycle of the GSHP, where t_R is the residence time in the pipe [s] and v is the mean fluid flow velocity [m/s].

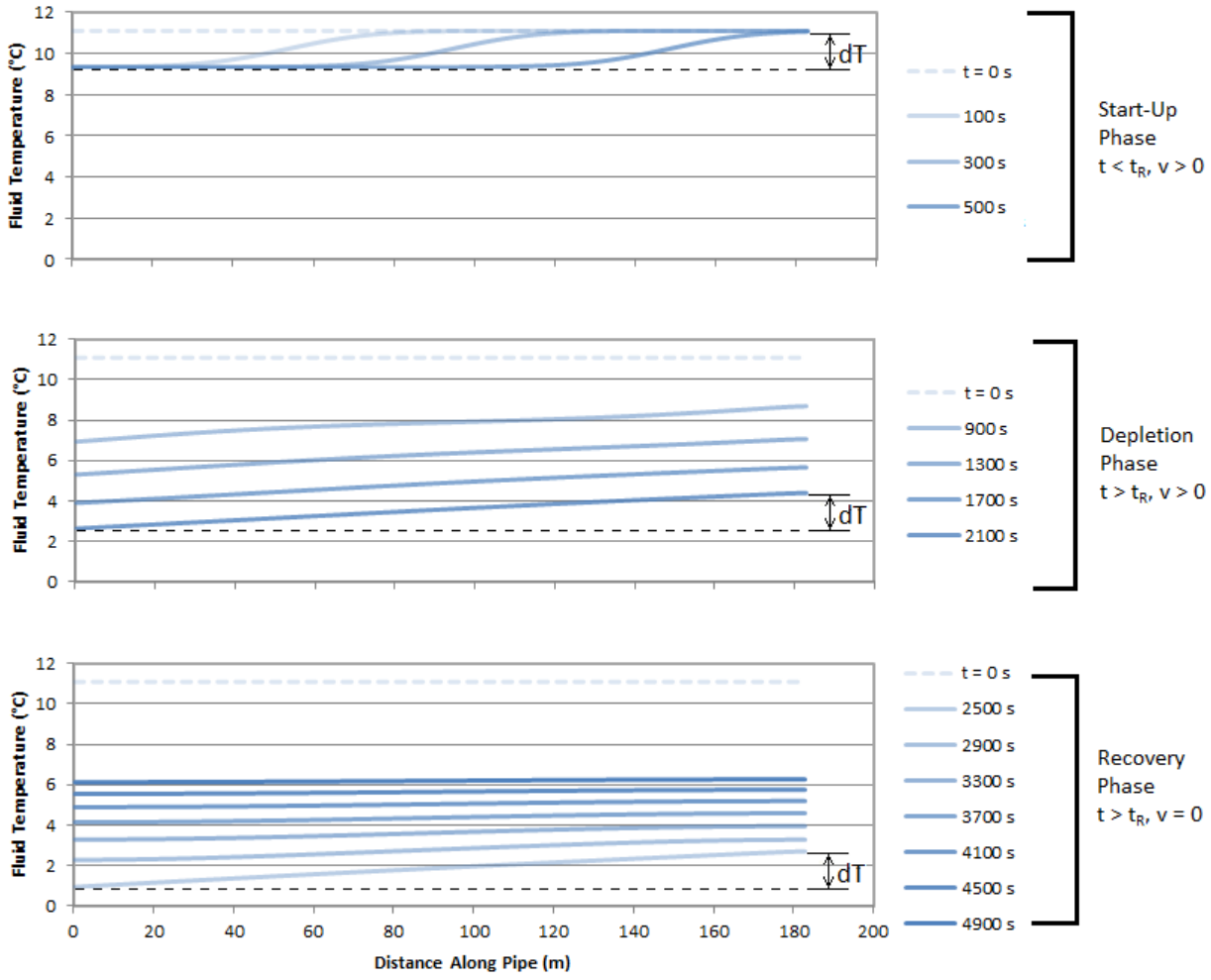

Figure 4.8: Three main phases of GSHP simulation - initial, depletion, and recovery

Figure 4.8 represents one pulse of fluid circulating through a ground loop with similar parameters as the system at the Elora Field Site during heating mode. Once the system

turns on, the fluid temperature at the inlet immediately decreases and the pulse, driven by the Dirichlet boundary condition at the inlet, circulates through the ground loop during the start-up phase. This temperature pulse disperses along the loop as the system enters the depletion phase. In the depletion phase the system is still operating and thermal energy is constantly being withdrawn from the circulating fluid, steadily depleting the temperature of the fluid. Once the system turns off, it enters the recovery phase where energy is no longer being extracted from the fluid and the fluid temperature begins to rise, approaching the temperature of the surrounding soil. The corresponding EWT, which is the fluid temperature at the outlet ($x = L$), and heat pump COP for this sample simulation are provided in Figure 4.9.

Figure 4.8 and Figure 4.9 show a single pulse travelling through the ground loop. However, in actual operation the system cycles frequently, following the basic pattern outlined in Figure 4.8 during each cycle with the average fluid temperature decreasing over time.

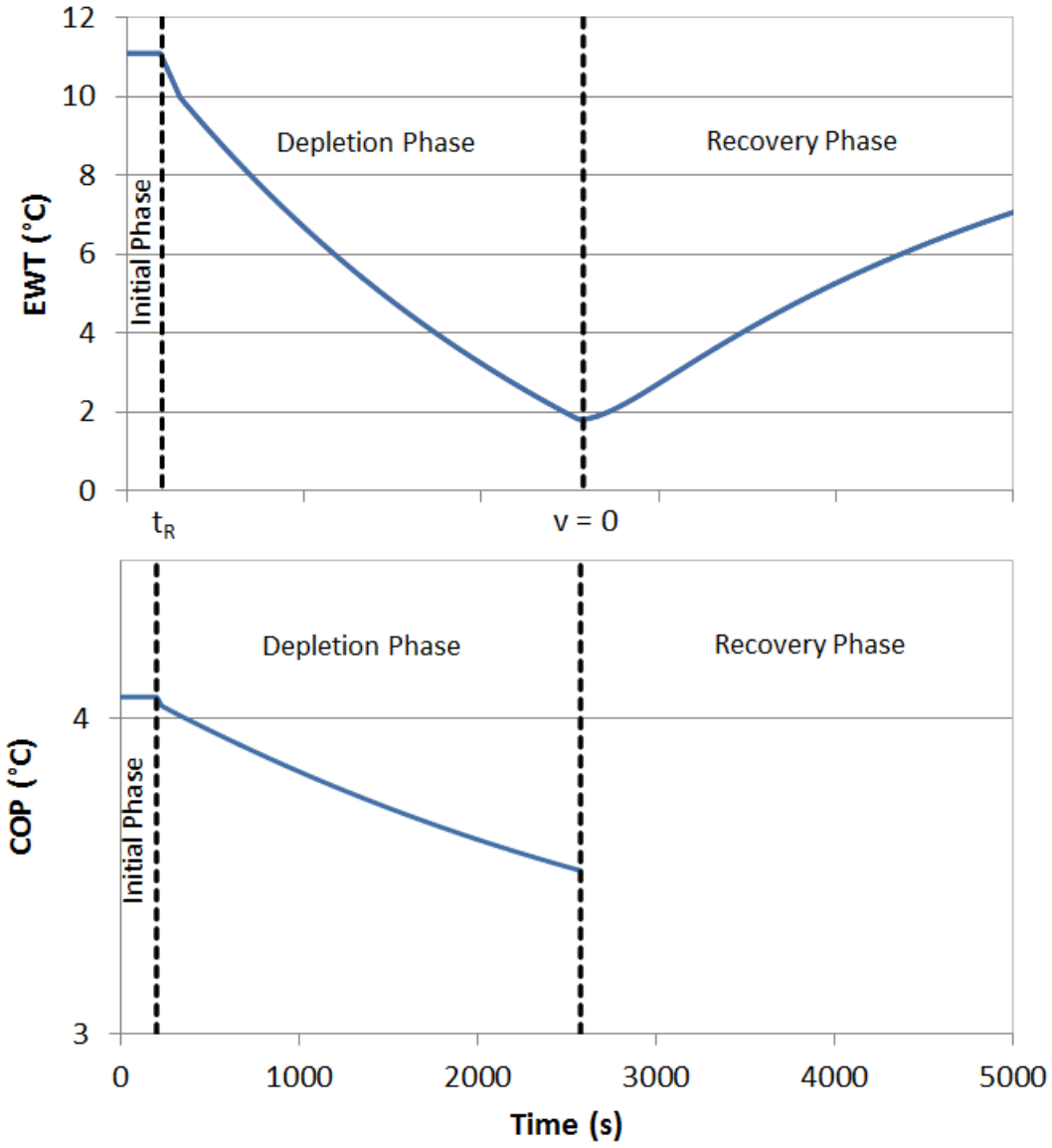

Figure 4.9: EWT and heat pump COP for initial, depletion, and recovery phases

Chapter 5

Model Application

The 1D finite difference model and Simms (2013) 3D finite element model were developed to investigate the function and performance of GSHPs, focusing upon the potential to improve the design and operation of such systems. A variety of test cases were developed, simulated, and analysed to attempt to: relate the behaviour of pulsed and steady state simulation of GSHPs; identify potential efficiencies in system operation, including pumping intensity and cycle frequency; and investigate the potential performance inefficiencies associated with the specification of GHX pipe spacing, pipe configuration, and pipe length.

5.1 Base Case Definition

To develop a starting point for investigations using model simulations, base case model realizations were developed for the 1D finite difference model and Simms (2013) 3D finite element model. The base cases were developed using the Elora Field Site as a reference and are detailed in Section 5.1.1 and Section 5.1.2.

5.1.1 1D Base Case

As installed, the GHX at the Elora Field Site consists of six 183 m loops. The model represented six identical 183 m pipes in U-tube shapes by simulating a single pipe and extending results to the full system by assuming that flow rates, fluid and soil temperatures, energy consumption and extraction, and dimensions were consistent for all six pipes. This assumption is valid since it represents a system composed of six identical U-tubes separated by distances large enough to ensure no interactions between adjacent U-tubes.

The pipes in the simulated U-tube were separated by 0.5 m and were surrounded by soil with homogeneous thermal properties: thermal conductivity, specific heat capacity, and bulk density. A variable speed heat pump and fluid circulation pump were simulated in all cases to analyse the performance of the system. Specific input parameters for the base case are provided in Table 5.1.

Table 5.1: Input parameters for 1D Finite Difference model

Parameter	Magnitude	Unit
Soil thermal conductivity	1.22	J/smK
Soil volumetric heat capacity	2.03	MJ/m^3K
Fluid volumetric flow rate in single U-tube	0.00016 [2.5]	m^3/s [GPM]
Fluid volumetric heat capacity	3.73	MJ/m^3K
In-pipe dispersion	0.032	m^2/s
Loop pipe inner diameter	0.021	m
Loop pipe outer diameter	0.027	m
Pipe thermal conductivity	0.4	J/(smK)
Average power extraction from fluid	3516 [1]	J/s [ton]
Heat pump and circulation pump cycles per day	24	[-]
Time step	2	s
Total number of nodes	900	[-]
Pipe length	183	m
Radius of influence, r_∞	5	m
Intermediate soil radius, r_s	1	m
Amount of time pump is on	70	%
Farfield temperature, T_∞	11.1	°C

5.1.2 3D Base Case

Parameters of the base case for the 3D FEM model are as defined in Table 5.1 with changes to the model boundary conditions, energy load requirements of the GHX, and element discretization. The sides and bottom of the soil domain were defined using no flux boundary conditions (Simms, 2013), rather than constant temperature as in the 1D model. The surface temperature was defined using the shallow soil temperature described in Chapter 3 for a one year period from December 2010 to December 2011. The energy requirements of the GHX were defined using the actual energy loads measured at the Elora

Field Site for the same period (Simms, 2013).

The base case realization for the 3D model used 6000 equal elements to represent each 183 m pipe. In all cases the lengths of pipe were parallel to the y-dimension and perpendicular to the x-dimension of the soil domain, while the z-dimension represented depth from the ground surface. Pipe segments were always centred in the x-dimension of the soil element in which they were passing through. A variable discretization was used in the soil domain to enhance model accuracy surrounding the GHX. The element dimensions increased from 0.05 m, 1.25 m, and 0.1 m near the pipes to 14.8 m, 10 m, and 24 m away from the pipes in the x-, y-, and z-directions, respectively. The soil domain consisted of 240, 91, and 46 elements representing a 62 m by 127.5 m by 74.7 m soil domain in the x-, y-, and z-directions, respectively. This pipe and soil discretization was used for all test cases.

5.2 Pump Schedule Optimization

One of the main advantages of the 1D finite difference model is its ability to model a dynamic system at fine temporal resolution. Therefore, it is possible to use the model to examine various pumping scenarios. In this section, a number of pump scheduling choices, including run time fraction and pump cycle frequency, are investigated to attempt

to identify potential efficiencies in GSHP operation. The run time fraction is the ratio of the time the heat pump and fluid circulation pump are operating to the total simulation time. The pump cycle frequency represents the number of pump cycles per unit of time, typically expressed as cycles per day, where a pump cycle is considered to be a duration of pump operation followed by a duration of no advection or heat pump operation.

5.2.1 Pumping Intensity

It was hypothesized that system COP was a function of pumping intensity since heat pump and circulation pump power consumption are dependent on the intensity at which these components are operating. By simulating variable speed heat pump and circulation pump operation in the 1D finite difference model, it was possible to investigate a range of pumping intensities to examine the effect on system performance. In this thesis, pumping intensity refers to the magnitude of the flow rate at which fluid is circulated through the GHX. It was expected that a system operating for a longer period at a lower pumping intensity would be more efficient than an equivalent system operating for shorter periods at higher intensities since, for example, the system (including the heat pump and circulation pump) consumes more than twice the power to operate at twice the intensity.

A test case was developed in which the total energy extracted from the fluid was maintained across simulations but the pumping intensity and run time fraction were modified.

By altering the pumping intensity and run time fraction simultaneously, the total energy extraction, which represents the heating load on the GHX, can be maintained while examining the effect of pump scheduling and intensity on system performance. All other parameters in this test case are as defined in the base case in Section 5.1.1.

Figure 5.1 represents three of the pumping schedules that were simulated using run time fractions of 100%, 70%, and 50%, in which each case was defined to represent an identical average power extraction of 3516 J/s. In total, six pump schedules were examined using run time fractions between 50% and 100%, which correspond to flow rates between 17.0 GPM and 8.5 GPM, to represent the range of allowable flow rates for the heat pump specified in Chapter 4. The turbulent, transitional, and laminar flow regimes are approximated in Figure 5.1 based on the fluid properties and pipe specifications of the base case (Section 5.1.1).

The pumping schedules were compared in terms of COP using 100 day simulations for a variety of pulsing cases, each extracting the same amount of total energy from the fluid. Five sets of simulations were conducted, each examining a multiple of the total power extraction used in the base case, 3516 J/s. This multiple ranged between 0.6 and 1.4. A summary of the overall system performance based on changes in pumping schedules for each energy extraction definition is depicted in Figure 5.2.

Since the total energy extraction from the fluid is fixed for each curve, the varying

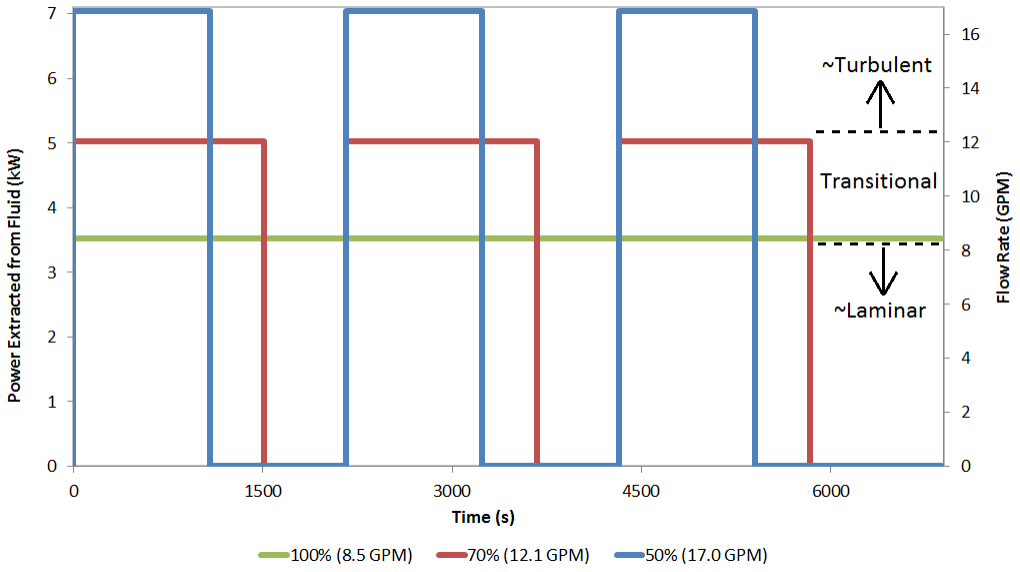

Figure 5.1: Simulated pump schedules with approximate flow regimes

performance of the system is solely dependent on the intensity at which it operates. The constant pumping case (run time fraction equal to 100%) yields the most efficient performance in all cases (Figure 5.2), even though the heat pump and circulation pump are operating continuously. The increase in performance as intensity decreases is attributed to the power consumption of the circulation pump and the moderated energy load on the subsurface. The relationship between circulation pump power and flow rate is not linear and more than twice the power is required to double the flow rate (Figure 5.3). Also, as the pumping intensity decreases, the instantaneous energy load on the subsurface is reduced, helping to maintain soil temperature over time. Therefore, as initially expected,

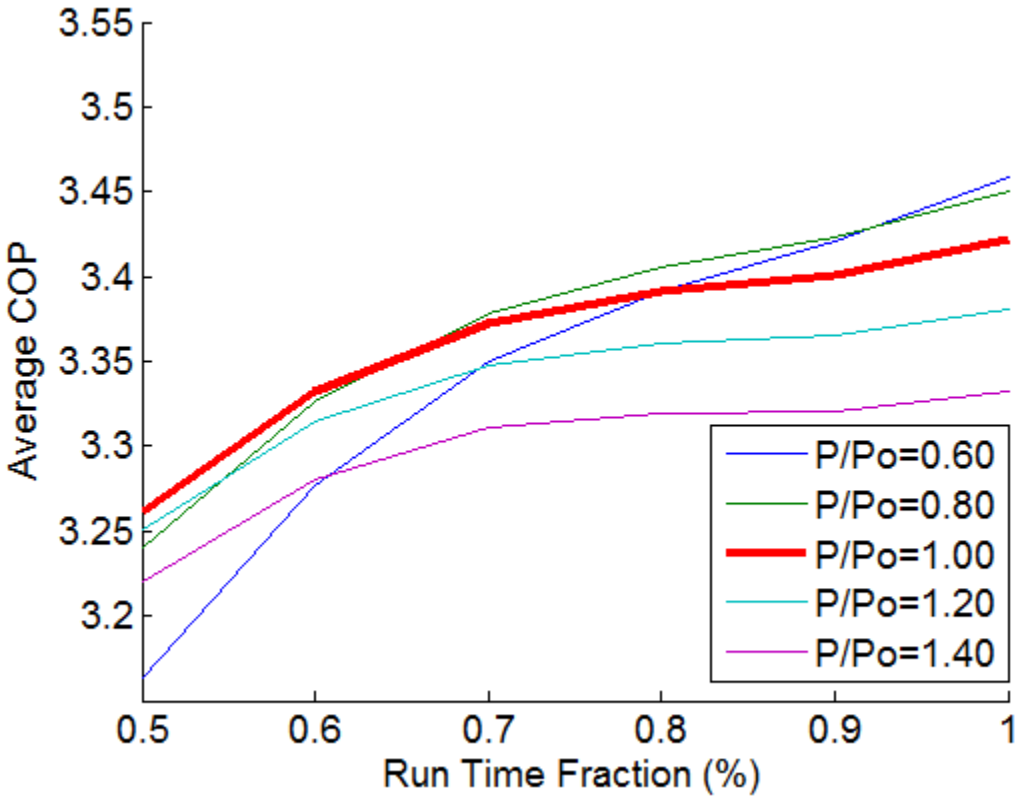

Figure 5.2: System COP related to run time fraction (P_O = 3516 J/s)

the constant pumping case at the minimum flow rate relevant to the selected heat pump yields the most efficient pumping schedule.

The test case described above shows how a GSHP can operate more effectively at lower flow rates and longer run times. However, in all cases it was assumed that the fluid was well mixed and its temperature was constant across the entire cross sectional area of the pipe, an assumption of fully turbulent flow. This assumption may not be valid for all

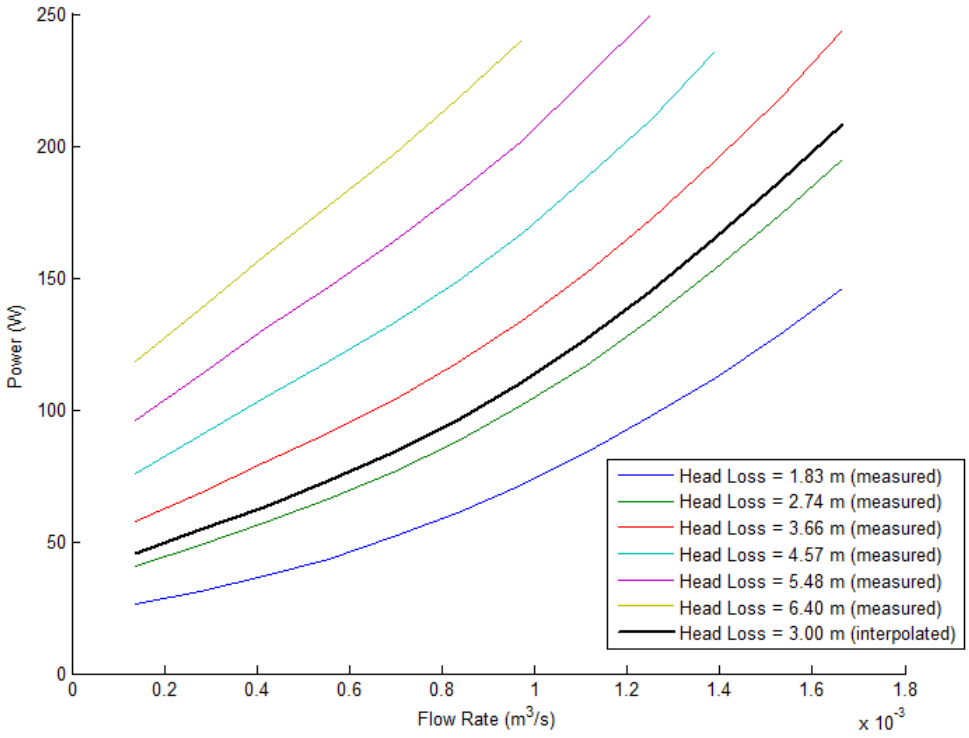

Figure 5.3: Circulation pump power as a function of flow rate for a range of head losses through the system - the measured values represent the manufacturer's performance specifications (WILO, 2010) and the interpolated values represent an example of those used by the model

cases since the minimum flow rates investigated yield Reynold's numbers in the laminar or transitional flow regimes for the simulated system. In cases where laminar flow exists, there would be reduced heat transfer between the fluid and the soil caused by the increase of the thermal resistance between them. Not accounting for this increased resistance to heat transfer would lead to over estimation of the performance of a system flowing in the

laminar regime. Section 5.2.2 describes a test case in which this increase in resistance was approximated.

5.2.2 Equivalent Resistance for Non-Turbulent Flow

The Nusselt number describes the ratio of radial heat transfer through a fully developed flowing fluid to purely conductive radial heat transfer of stagnant fluid in a pipe. Therefore, it was hypothesized that by relating the Nusselt number of the turbulent and non-turbulent cases, an equivalent effective thermal resistance to radial heat transfer through the fluid flowing in a pipe could be approximated to more accurately compare quasi-steady state (laminar flow) and pulsed (turbulent flow) pump operation. It was expected that this equivalent resistance would decrease the system COP for non-turbulent flows due to reduced heat transfer into the fluid in these cases. Equation 5.1 was developed to modify the effective thermal resistance across the pipe wall (as defined in Equation 4.21) in the 1D finite difference model to approximate the equivalent resistance due to the lack of mechanical mixing associated with non-turbulent flow.

$$R_{eq} = \frac{Nu_{max}}{Nu_{non-turbulent}} R_{pipe} \tag{5.1}$$

Where R_{eq} represents the equivalent effective thermal resistance across the pipe wall modified for non-turbulent flow [smK/J]; Nu_{max} is the Nusselt number [-] for the maximum flow rate considered in the model (17 GPM); and $Nu_{non-turbulent}$ is the Nusselt number [-] for a flow rate less than or equal to the maximum flow rate. Nu_{max} and $Nu_{non-turbulent}$ were approximated using the pipe characteristics defined in Section 5.1.1 and the method proposed by Churchill (1977). Churchill (1977) presented an empirical relationship for approximating the Nusselt number based on the Reynolds number of a fluid flowing through a smooth pipe. For Reynolds numbers below 2100, the expression simplifies to Equation 5.2 (Churchill, 1977).

$$Nu = 3.657 \left[1 + \left(\frac{RePrD/L}{7.60} \right)^{8/3} \right]^{1/8} \tag{5.2}$$

Where Pr is the Prandtl number [-], which is equivalent to the ratio of kinematic viscosity to thermal diffusivity ($Pr = \nu/\alpha$); D is the inner diameter of the pipe [m]; and L is the length of pipe [m] (Churchill, 1977).

For Reynolds numbers greater than 2100, the expression approximating the Nusselt number simplifies to Equation 5.3 (Churchill, 1977).

$$Nu = \left(\frac{1}{Nu_t^2} + \frac{1}{Nu_i^2} \right)^{-1/2} \tag{5.3}$$

Where Nu_t is an approximation of the Nusselt number for turbulent flows [-] and Nu_i is an approximation of the asymptote of the Nusselt number in transition to laminar flow (Churchill, 1977). Nu_t and Nu_i are approximated using Equation 5.4 and Equation 5.6, respectively.

$$Nu_t = Nu_0^0 + \frac{0.79Re\sqrt{f}Pr}{\left[1 + Pr^{4/5}\right]^{5/6}} \tag{5.4}$$

Where Nu_0^0 is the approximation of the asymptote of the Nusselt number [-] as $Pr \to 0$ and $Re \to 0$ and f is a dimensionless friction factor for the fluid flowing through a pipe approximated using Equation 5.5 (Churchill, 1977). The value of Nu_0^0 appropriate for this investigation was estimated to be 4.8 (Churchill, 1977).

$$f = \left(\frac{1}{\left[\left(\frac{8}{Re}\right)^{10} + \left(\frac{Re}{36500}\right)^{20} \right]^{1/2}} + \left(2.21ln\left[\frac{Re}{7}\right] \right)^{10} \right)^{-1/5} \tag{5.5}$$

$$Nu_i = Nu_{lc}e^{Re-2200)/730} \tag{5.6}$$

Where Nu_{lc} is the approximation of the Nusselt number [-] at Re = 2100, which is estimated using Equation 5.7 (Churchill, 1977).

$$Nu_{lc} = 3.657\left[1 + \left(\frac{276PrD}{L}\right)^{8/3}\right]^{1/8} \tag{5.7}$$

Equation 5.2 and Equation 5.3 are used to approximate the Nusselt numbers used in Equation 5.1 to calculate the modified effective thermal resistance across the pipe wall to account for non-turbulent flow. Using this equivalent effective thermal resistance relationship, simulations identical to those in Section 5.2.1 were conducted to more appropriately compare the quasi-steady state and pulsed pumping cases. For the system specified in Section 5.1.1, the minimum flow rate of 8.5 GPM yielded a Reynolds number of approximately 2050 and, using Equation 5.2, a Nusselt number of approximately 20. Comparatively, the maximum flow rate of 17.0 GPM yielded a Reynolds number of approximately 4150 and, using Equation 5.3, a Nusselt number of approximately 45. Therefore, the effective thermal resistance across the pipe wall would nowhere exceed approximately 2.25 times the unmodified case. The unmodified effective thermal resistance across the pipe wall for the base case is approximately 0.1 smK/J, which yields a maximum equivalent effective thermal resistance of 0.225 smK/J. Comparing this resistance to the base case effective thermal resistance between the pipe and the intermediate soil radius, R_{inter}, of approximately 0.563 smK/J, this modification of the thermal resistance across the pipe wall does not significantly impact the total effective thermal resistance between the fluid in the pipe and the soil, R_s, as defined in Equation 4.16. Therefore, it was expected that this modification to the thermal resistance across the pipe wall would not significantly effect the results for this test case, which are summarized in Figure 5.4.

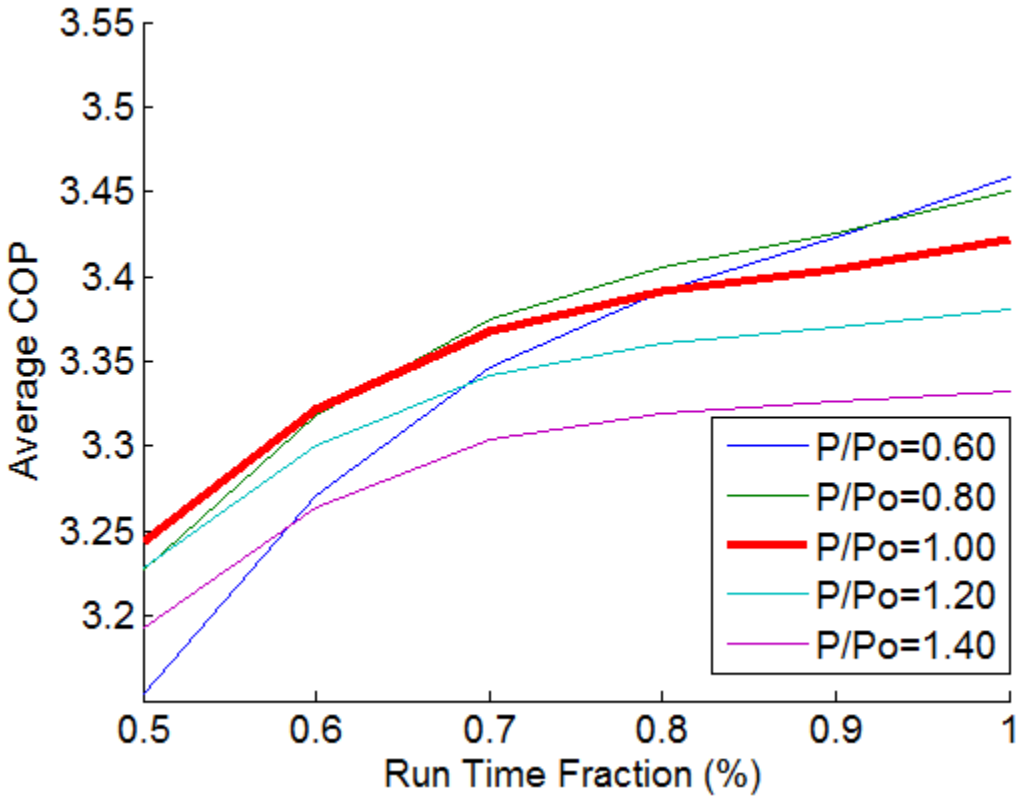

Figure 5.4: System COP related to run time fraction using equivalent effective thermal resistance for non-turbulent flow (P_O = 3516 J/s)

Based on the results (Figure 5.4) of this equivalent resistance test case, the effect of the reduced thermal transfer caused by non-turbulent flow reduces the system COP compared to the test case presented in Section 5.2.1, in which turbulent flow was assumed for all cases. However, the difference in COP for this equivalent resistance test case were everywhere less than 1%, which, as expected, is negligible. Therefore, by assuming that

this equivalent resistance technique (Equation 5.1) is appropriate, the effect of the increase in effective thermal resistance to radial heat transfer associated with non-turbulent flow is not significant in a U-tube shaped GSHP, suggesting that the conclusions made in Section 5.2.1 are reasonable and system performance increases with decreasing pumping intensity. Practically, these test cases show how a GSHP could operate marginally better (COP increases of ∼5%) by increasing run time fraction from 50% to 100% and decreasing flow rate from 17.0 GPM to 8.5 GPM for U-tube shaped GHXs, which is not a significant gain in performance. However, a full investigation into the effect of the increased thermal resistance and other potential mechanical issues associated with non-turbulent flow through the GHX was not within the scope of this research and further analyses should be completed to fully analyse the variations this may cause in simulated performance.

5.2.3 Cycle Frequency

While the differences in results observed between the test cases in Section 5.2.1, assuming completely turbulent flow in all cases, and in Section 5.2.2, using an equivalent effective thermal resistance for non-turbulent flow, were not significant (<1%), a full investigation into the effect of non-turbulent flow regimes is not within the scope of this research. Therefore, further analyses were conducted to attempt to identify system performance efficiencies through pump schedule optimization independent of pumping intensity.

It was hypothesized that COP was a function of pump cycle frequency because subsurface soil temperatures and, thus heat extraction efficiency, are dependent on the duration of pump operation. A test case in which pumping intensity is maintained while only pump cycle frequency is varied is described and analysed below to test this hypothesis with the expectation that an optimal frequency would provide a specific maximum COP. By maintaining pumping intensity at a higher flow rate and modifying pump schedules through pumping cycle duration and frequency, it was possible to eliminate the potential performance bias associated with low flow regimes. To ensure appropriate fluid flow in the pipe, a flow rate of 15 GPM (taken from the Elora Field Site) was simulated for all scenarios, yielding a Reynold's number of approximately 3655, which is in the transitional to turbulent flow regime and applicable for GSHP operation (ASHRAE, 2009).

A pumping cycle was considered to consist of a period of pumping followed by a similar or different duration of no pumping. To investigate the effects of pumping cycle frequency on COP, a test case was developed using the parameters defined in Section 5.1.1 and simulated using the 1D finite difference model. In this investigation the only variables changed were the number of pumping cycles per day and the duration of the cycles. The total operating time of the pump was consistent in all cases. Therefore, as cycle frequency was increased the, cycle duration was decreased along with the run time per cycle. The cycle frequency test case comprised a range of simulation durations (1 to 100 days) and run

time fractions (10% to 90%). These run time fractions could represent a range of realistic pumping schedules from shoulder season operation (spring and fall, where minimal heating capacity is required) at the lower run times to extreme operation (winter, where peak heating capacity is required) at longer run times. Figure 5.5 illustrates the relationship between system performance and cycle frequency for each of the 7 day simulations. Each curve in this figure represents a 7 day simulation for a unique run time fraction, where all other parameters are equal between curves. The run time fraction represents the percentage of total simulation time that the pump is operating and, in this test case, ranges from 10% to 90%. It is clear from the results summarized in Figure 5.5 that there are optimal cycle frequencies for each run time fraction. These maximum would correspond to the point at which the defined system is operating at maximum efficiency for the described power extraction.

To further investigate the mechanisms dictating the shape of the curves in Figure 5.5, a specific simulation was chosen for analysis. The 10% pump run time was isolated and evaluated using the 14 day simulation. Figure 5.6 shows the system COP of the cases with run time fraction equal to 10% and 50% (for comparison) for simulation durations between 1 day and 100 days.

Since the COP of these systems is a function of the temperature of the fluid entering the heat pump and flow rate, the entering water temperature (EWT) was recorded for all

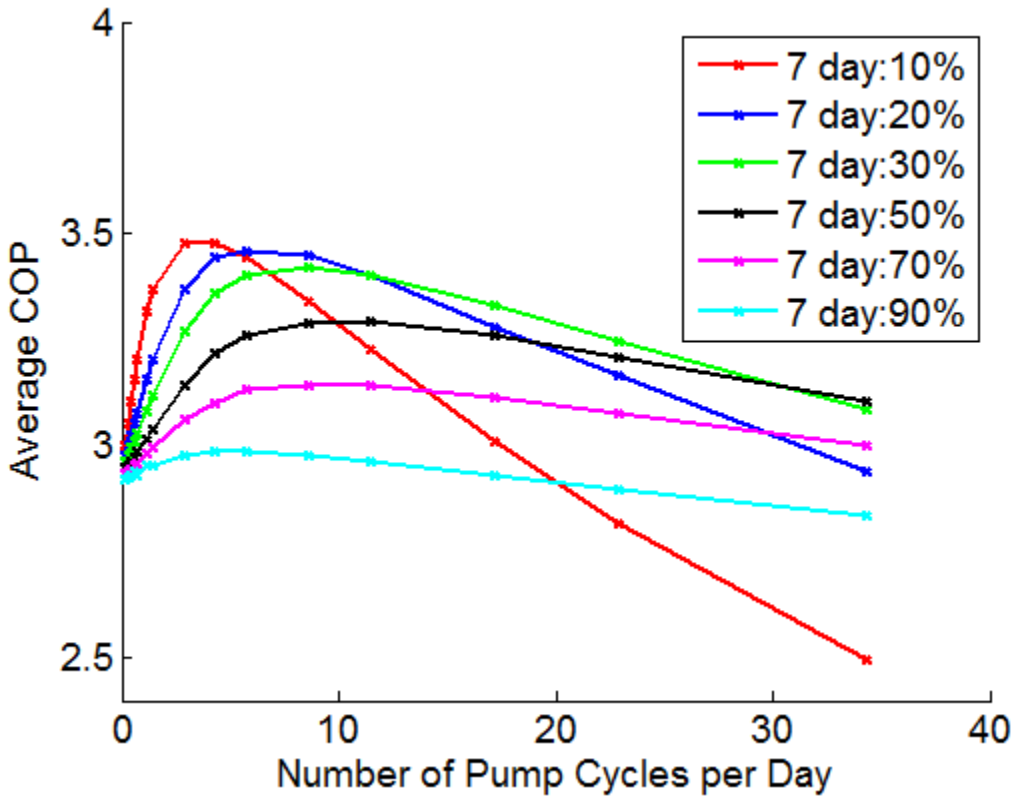

Figure 5.5: Cycle frequency test case: System performance as a function of cycle frequency for 7 day simulations and various run time fractions

time steps because flow rate was consistent across all simulations. In the model, the EWT is defined as the fluid temperature at the outlet, $T(L,t)$. This EWT was monitored for the four most optimally performing simulations in Figure 5.6 to investigate the mechanisms responsible for optimal performance. Figure 5.7 shows the EWT for the first day of these four simulations.

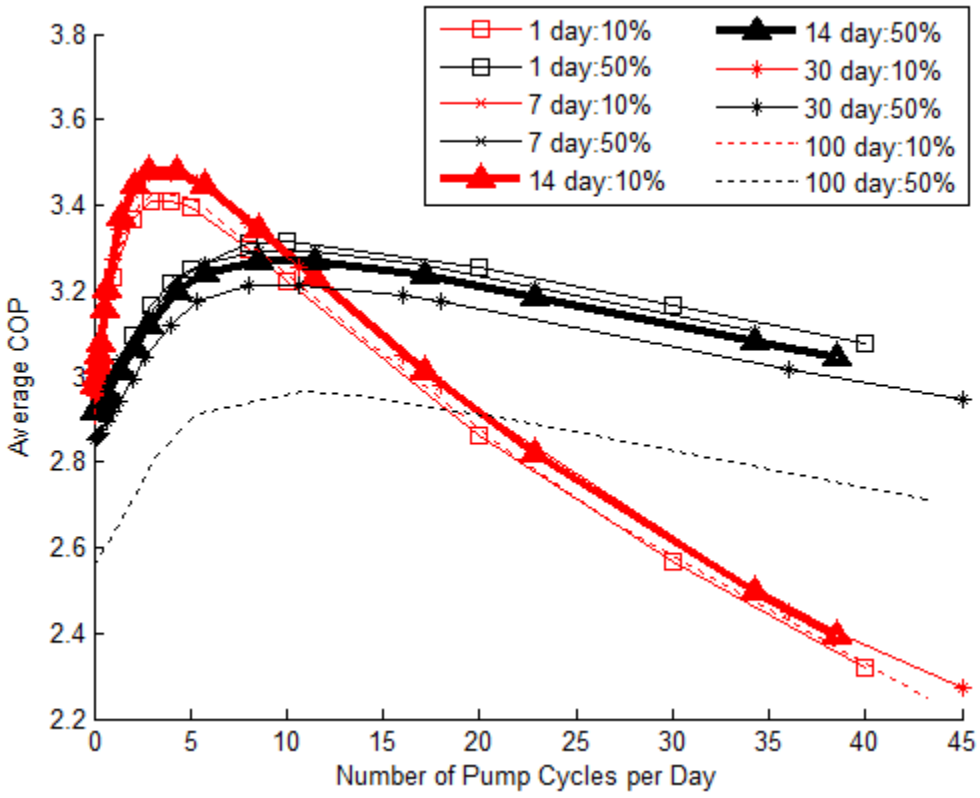

Figure 5.6: Cycle frequecny test case: Simulated performance as a function of cycle frequency for 10% and 50% run time fractions and a range of simulation lengths

For low cycle frequencies (e.g., 2.8 cycles/day in Figure 5.7), when the system turns on it reduces the fluid temperature considerably because of the relatively longer cycle runtime, which has a negative effect on COP. When the system turns off, the fluid temperature increases back to the soil background temperature. Since the fluid temperature has equilibrated to the soil temperature, there is no thermal gradient between the two and, thus no heat transfer occurring during this idle period. Therefore, it is concluded that when cycle

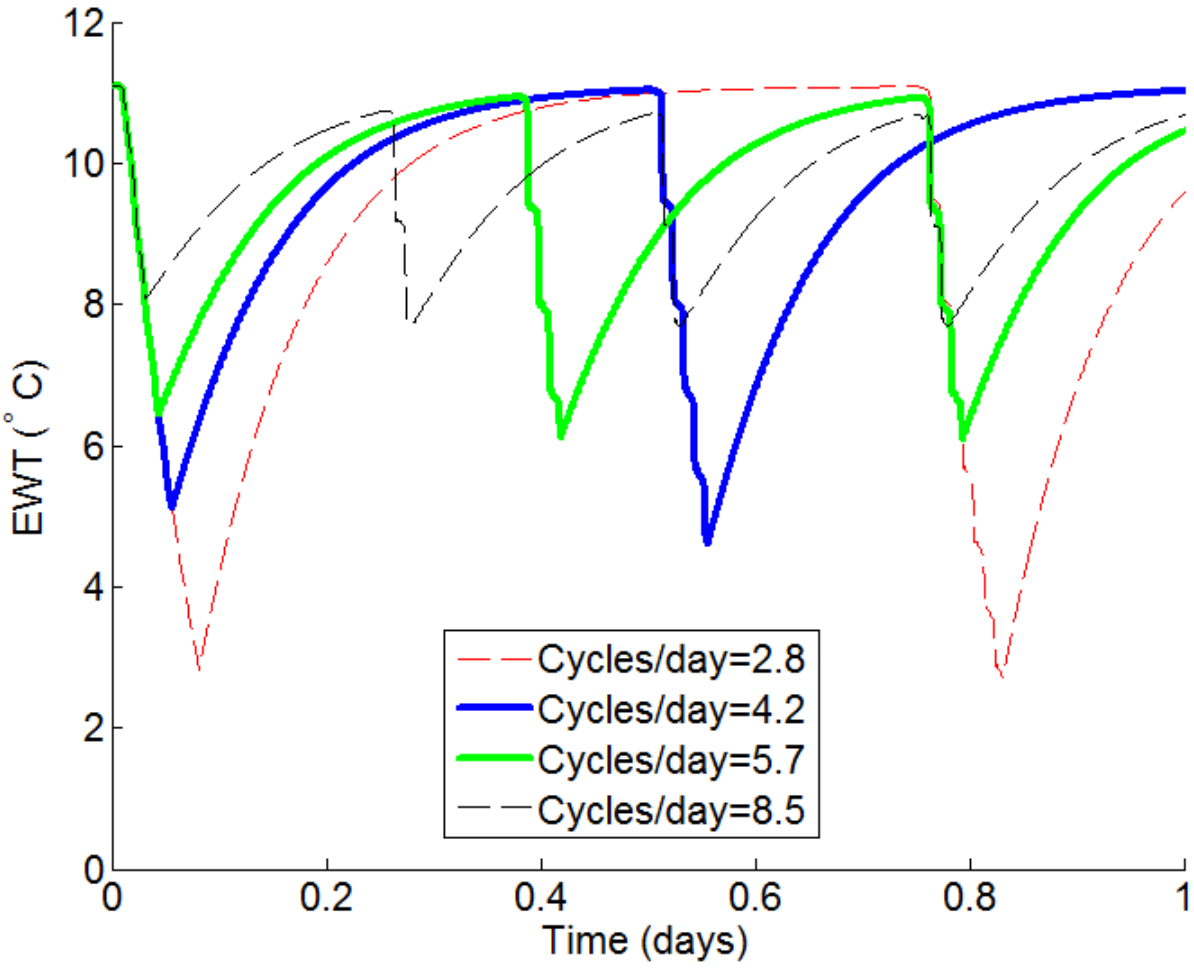

Figure 5.7: EWT of the four most optimally performing cycle frequency simulations

frequency is too low, cycle run times are too long, causing low fluid temperatures during operation, hindering performance. Then, when the pump is off, the system remains idle for too long, limiting heat transfer and reducing the potential energy extraction.

For higher cycle frequencies (e.g., 8.5 cycles/day in Figure 5.7), when the system turns on it does not significantly reduce the fluid temperature because of the relatively shorter pump runtime. However, when the system turns off, the fluid temperature does not completely return to the soil background temperature before the system turns back on, which acts to reduce the average fluid temperature over the simulation time, depleting long term system performance. Therefore, it is concluded that when cycle frequency is too high, fluid temperature reduces over time, depleting GSHP performance.

Finally, in the two optimal simulation cases, where cycle frequency is approximately 4.2 cycles/day and 5.7 cycles/day in Figure 5.7, the cycle length appears to be such that when the pump does turn off, the EWT rises to almost the background soil temperature before the pump turns back on. Therefore, there is always active heat transfer within the system. While the pump is on, energy is being extracted from the fluid and the soil surrounding the GHX. When the system is off, there is always a temperature difference and, thus heat transfer, between the fluid and the subsurface. It is concluded that the ideal scenario for the given system is one in which the cycle length is long enough to allow for almost full energy recovery of the fluid but still short enough to avoid periods of low energy transfer

between the GHX and the soil. It was expected that system performance would be a function of cycle length and this result of a optimum pump frequency is consistent with expectations.

5.2.4 Discussion

GSHP performance is a function of cycle frequency with an optimal performance existing in all cases analysed. For those simulations conducted, system COP varied by up to ∼30% when considering cycle frequency as the only variable, which could correspond to potential operating cost reductions. The variation in COP summarized in Figure 5.5 was found to be most significant during operation at lower pump run times, which represents shoulder season operation when energy demands are relatively lower. The system being examined (outlined in Section 5.1.1) represents a typical GSHP operating under a range of reasonable system loads. Therefore, the relationship observed between COP and pumping frequency could, with some confidence, be extended to most residential or light commercial GSHP applications. The conclusion is important since pump cycle frequency can significantly effect overall system performance. This conclusion identifies a method through which GSHP efficiency could be improved without substantial changes to design. Implementation of monitoring equipment to quantify system loads and EWTs would provide the information necessary to conduct a cycle frequency optimization exercise, either ensuring ideal

performance or providing insight into how the system could be more effectively operated. Considering the potential 30% variation in COP associated with changes in pump cycle frequency, this monitoring and optimization exercise could be beneficial in reducing GSHP operation costs for residential and light commercial applications. This improvement would act to further offset the high initial cost of the GHX installation, making these systems more economically attractive to consumers.

5.3 Transient and Steady State Pumping Behaviour

GSHPs typically function in a transient manner, with the heat pump and circulation pump turning off and on frequently during operation. This transient behaviour adds mathematical complexity when trying to simulate these systems using computational models. One simplification that can be made when modelling such systems is the quasi-steady state assumption, where the temperature distribution in the pipe is assumed to be in equilibrium with the soil at all times, instantly responding to fluid inflow temperatures. In the case of a GSHP, it could be assumed that instead of the system cycling off an on, it simply remains on continuously during the timescale of interest, operating at a lower intensity. This assumption would help to reduce the complexity of the mathematical equations governing the processes in a GSHP model and potentially reduce the required number of simulated

time steps, improving the efficiency of the model. Several test cases were developed to investigate the validity of such an assumption by comparing the outputs from a range of constant pumping simulations against a simulation in which the system is cycling in a transient manner for a variety of model realizations.

5.3.1 Sensitivity of System COP upon Pump Schedule and Soil Conductivity

The 1D finite difference model was employed to simulate the operation of a GSHP with constant and pulsed pumping schedules. The Elora Field Site operating in heating mode, as defined in the base case for the 1D model (Section 5.1.1), was used as the basis for this test case.

The constant pumping case was simulated by operating the circulation pump for 100% of the simulation time at a flow rate of 8.5 GPM. The temperature change boundary condition was defined using Equation 4.2 based on the fluid thermal properties and the specified power extracted from the fluid (Sec 5.1.1).

To represent an equivalent pulsed case, the circulation pump operated for 50% of the simulation time at a flow rate of 17.0 GPM with the same temperature change condition as the constant case. Therefore, the total energy extracted for the pulsed case was exactly

equivalent to the constant case. This test case was developed to examine the difference in performance associated with the quasi-steady state approximation across a range of soil thermal conductivities. It was expected that the variation in pumping intensity would result in differences between the two cases, with the quasi-steady state case yielding a higher COP, due to efficiencies related to lower pumping intensity.

This simulation was conducted for the pulsed and steady pumping cases for a range of 50 realizations in which the only parameter varied was the average thermal conductivity of the bulk soil medium in which the GHX was installed. The soil thermal conductivity was varied between 0.5 and 2.06 J/(smK) to represent a range of realistic soil conditions. Figure 5.8 presents the results of this investigation as a function of system performance characterized by COP.

Figure 5.8 shows how the performance of the constant and pulsed pumping cases relate. The constant pumping case tends to yield a larger system COP (by between ∼6% and ∼9%) for all soil thermal conductivities investigated, which can be attributed to the increased fluid residence time in the pipe and the lower energy cost associated with the lower flow rate. The increased residence time allows for extended thermal energy transfer from the surrounding subsurface, while the lower pumping energy reduces the overall power consumption, both processes increasing average COP. However, it is noted that the shape and magnitude of the curves in Figure 5.8 are similar, suggesting that these pumping

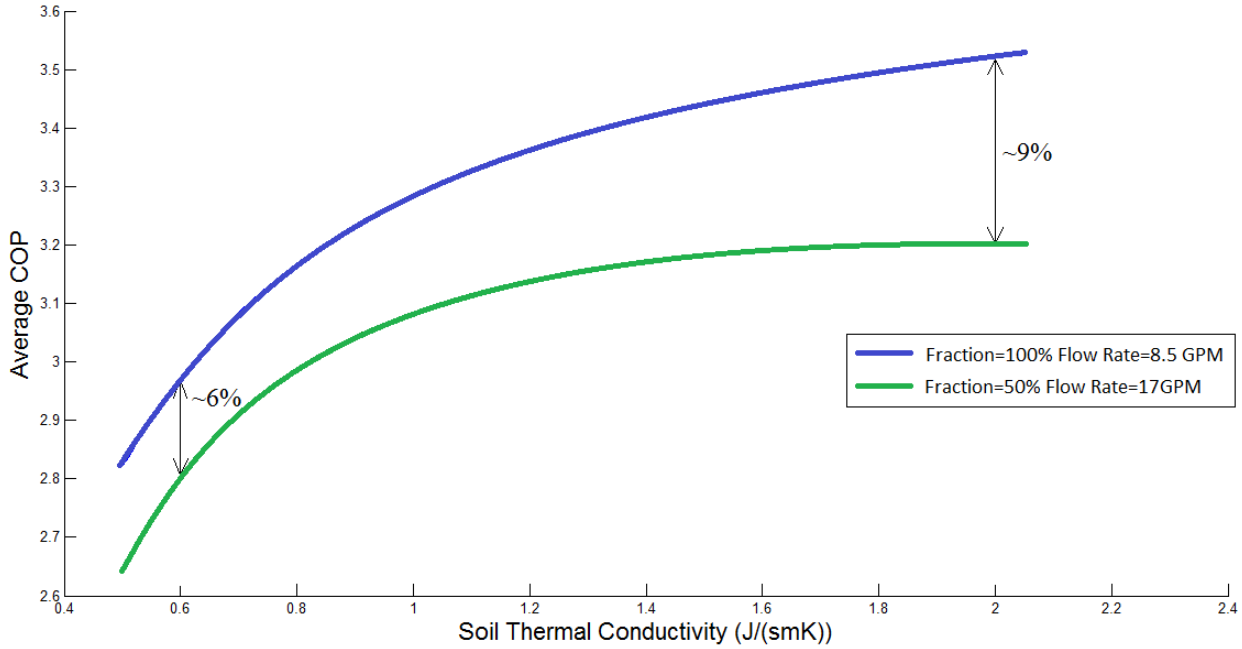

Figure 5.8: Average COP for a range of soil thermal conductivities - comparison between pulsed and steady state

schemes are comparable and that the constant case can represent a system similar to the transient case. Within a range of realistic soil thermal conductivities, for a typical U-tube GHX, the quasi-steady state approximation over estimates COP by between ∼6% and ∼9% for an extreme transient case of the modelled system (pump operation at maximum flow rate for 50% of simulation duration).

5.3.2 Equivalence of Transient and Steady State Pumping

The test case presented in Section 5.3.1 investigated the effect of the quasi-steady state approximation on system COP for a range of soil thermal conductivities. To enhance this investigation to further understand the differences in COP seen in Figure 5.8, the transient base case from Section 5.3.1 was compared to a range of constant pumping cases to identify and quantify potential sources of the difference between transient and quasi-steady state simulation and attempt to relate the two cases. These constant pumping cases were defined as described in Section 5.1.1 with the power extraction parameter varied between 2766 and 4266 J/s.

It was hypothesized that a relationship exists between the behaviour of the transient and quasi-steady state cases. The author expected that, when comparing these cases, variations in simulated fluid temperature and thermal energy flux into the fluid caused the COP differences observed in 5.3.1 since these are the main factors in the calculation of COP. Therefore, these factors were investigated to attempt to identify the relationship between transient and quasi-steady state operation and investigate the validity of this quasi-steady state approximation as it relates to analyses of system performance (COP).

The differences in fluid temperature between the pulsed and constant cases were examined by comparing the average fluid temperature over the entire 100 day simulation along

the total length of the pipe (Figure 5.7 (a)). The differences in energy flux into the fluid along the pipe were analysed in two ways: the cumulative thermal energy change in the fluid (Figure 5.7 (b)), to investigate energy flux as a function of distance along the pipe; and the total change in energy at each node along the pipe (Figure 5.7 (c)), to investigate the overall energy extracted from the subsurface. Finally, the average system COP was compared to investigate the relationship between system performance of the pulsed and steady cases (Figure 5.7 (d)).

Figure 5.7 summarizes the results of the comparison between a range of constant pumping cases and a pulsed case for a simulation duration of 100 days. Here, P/P_O represents the average power extracted from the fluid for a specific trial normalized by the average power extracted for the base case, where $P_0 = 3516$ J/s for the base case. The average temperature of the fluid in each node (Figure 5.7 (a)) represents the temperature in the fluid at each time step averaged over the entire duration of the simulation.

The change in thermal energy in the fluid was quantified by calculating the energy change in the fluid caused by external sources: the adjacent pipe and the surrounding soil. These energy fluxes were calculated using:

$$\Delta E_{fluid} = \frac{\Delta T_{fluid}^{source}}{R_{eff}^{source}} \Delta x \Delta t \tag{5.8}$$

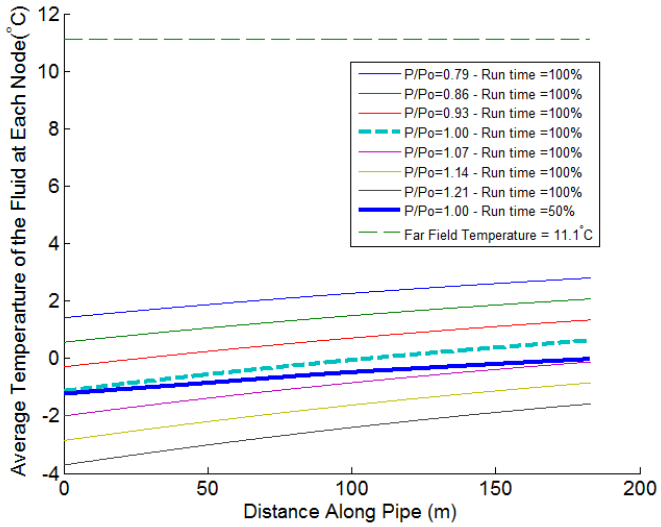

(a) Average temperature of the fluid in each element - 100 day simulation

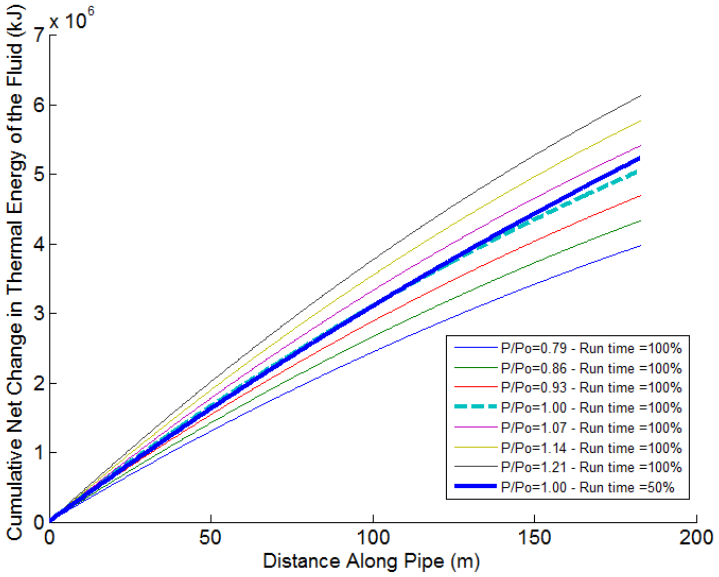

(b) Cumulative energy change of the fluid in each element - 100 day simulation

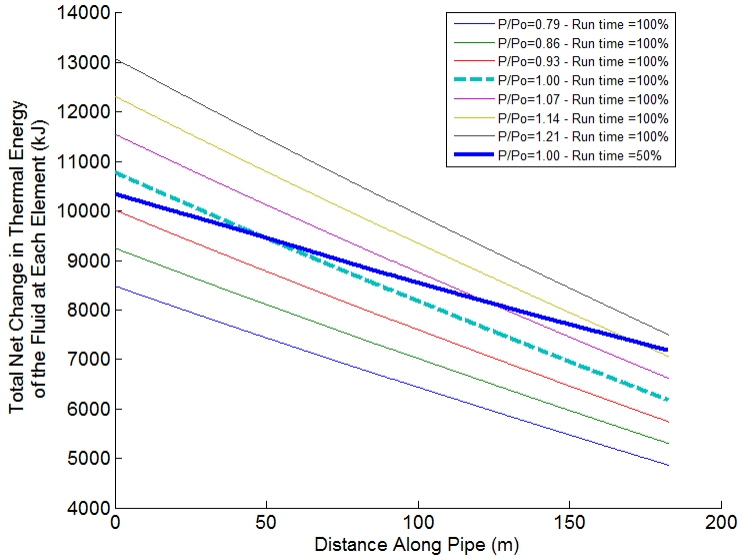

(c) Total energy change of the fluid in each element - 100 day simulation

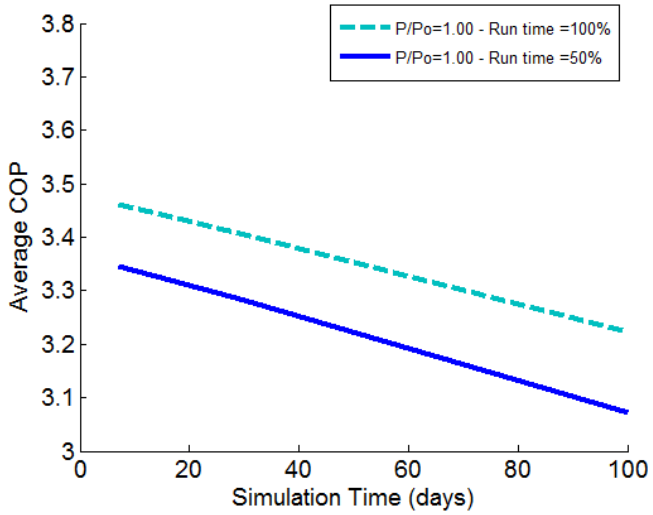

(d) COP for 1 day, 7 day, 14 day, 30 day, and 100 day simulation durations

Figure 5.7: Comparison between pulsed and constant pumping cases

where ΔE_{fluid} is the change in energy in the fluid due to external sources [J]; $\Delta T_{fluid}^{source}$ is the change in temperature between the external source and the fluid in the pipe [°C]; and R_{eff}^{source} is the effective thermal resistance between the external source and the fluid in the pipe [smK/J], as defined in Chapter 4.

The cumulative energy change of the fluid in each element (Figure 5.7 (b)) represents the summation along the length of the pipe of the total change in energy in the fluid for the duration of the simulation, while the total energy change of the fluid in each element (Figure 5.7 (c)) represents the total change in thermal energy at each point in the pipe for the duration of the simulation.

The reduction in COP with increasing simulation duration summarized in Figure 5.7 (d) is caused by the reduced soil temperature associated with extended energy extraction. As the simulation progresses, the soil temperature decreases due to prolonged energy extraction, reducing the energy available in the soil to be transferred to the fluid, thus reducing the temperature of the fluid. As the fluid temperature decreases, the system must perform more work to extract the defined energy, reducing system COP over time.

Based on the simulated average fluid temperature, thermal energy, and COP summarized in Figure 5.7, the pulsed case shows similarities to the constant cases. The magnitude and the trends of all curves are comparable and, except when considering COP, the single pulsed case is seen to fall inside the range of realistic constant pumping cases for the sim-

ulation duration of 100 days. Identical simulations were conducted for 30 day, 14 day, 7 day, and 1 day durations. Results from these simulations are presented in Appendix F and show comparable relationships to those in Figure 5.7. These similarities suggest that there is a strong relationship between the fluid temperature and change in energy simulated for the pulsed and constant pumping cases, as initially hypothesized. These differences are everywhere within ∼10% for all cases simulated and account for the changes observed in COP between the transient and quasi-steady state cases summarized in Section 5.3.1. The observed differences in COP between the steady state case and the equivalent pulsed case were approximately ≤5%, with the constant case estimating a larger COP than the pulsed case. Therefore, the use of a constant pumping approximation, as in Simms (2013) 3D FEM model, will lead to slight over prediction of system performance, which is attributed to the decreased power consumption and instantaneous energy demand on the subsurface associated with the lower pumping intensity (flow rate) in the constant case.

Since the differences in COP observed for the constant case are consistent across the range of scenarios that were simulated, it is concluded that this quasi-steady state approximation is valid for cases that use the COP as a relative performance metric. This conclusion helps to justify the use of this approximation by authors such as Simms (2013) and validates the use of the 3D finite element model in this thesis.

5.4 Configuration Optimization

A major GHX design variable that was expected to have an effect on GSHP performance was the configuration of the ground loop. Three specific aspects of GHX configuration were investigated: pipe spacing, pipe layout, and pipe length.

5.4.1 Pipe Spacing

The conductive transfer of thermal energy between two points is proportional to the magnitude of the temperature difference between the points. In a GHX, the largest temperature difference between two adjacent pipes will occur in the header trench near the heat pump, where the supply and return pipes converge. The subsurface temperature data collected from the Elora Field Site suggest that some efficiency may be lost in the system due to the proximity of the adjacent supply and return pipes in the header trench. Figure 3.6, a snapshot in time of temperature along the Elora Field Site header trench cross section during heating mode, shows how the temperature anywhere between these two pipes does not return to the background soil temperature. Since the temperature between the pipes does rise above that in the supply pipe, it is concluded that no thermal energy is being transferred between the pipes at this particular moment in time. However, the supply pipe is affecting the temperature of the subsurface in the header trench in the vicinity of the

return pipe.

Since the developed finite difference model directly accounts for heat transfer between two pipes, it was used to display the effect of the loss of efficiency between the supply and return pipes in a header trench. Figure 5.8, which represents two simulations after 3600 seconds of continuous pumping, illustrates the effect that the effective thermal resistance between the fluid in the pipes has on fluid temperature, since this thermal resistance is the only parameter changed. While this test case uses the parameters defined in Section 5.1.1, the thermal dispersion, pump run time, and thermal resistance between the pipes were exaggerated to emphasize the interactions between the pipes. However, the mathematical definitions and physical processes in the model are respected.

The differences in thermal resistance used to develop Figure 5.8 could represent changes in any of the parameters that define the thermal resistance between the pipes, including the distance between the pipes. As the distance between the pipes decreases, the resistance to heat transfer decreases, increasing the thermal energy transfer between the pipes. This increase in pipe interactions acts to decrease the fluid temperature at the end of the pipe for the low thermal resistance simulation shown in Figure 5.8. These results illustrate how a decrease in thermal resistance between the pipes (e.g., decreased pipe spacing) can lead to lower system COP due to decreased operating temperatures attributed to the loss of energy caused by the interactions between the pipes.

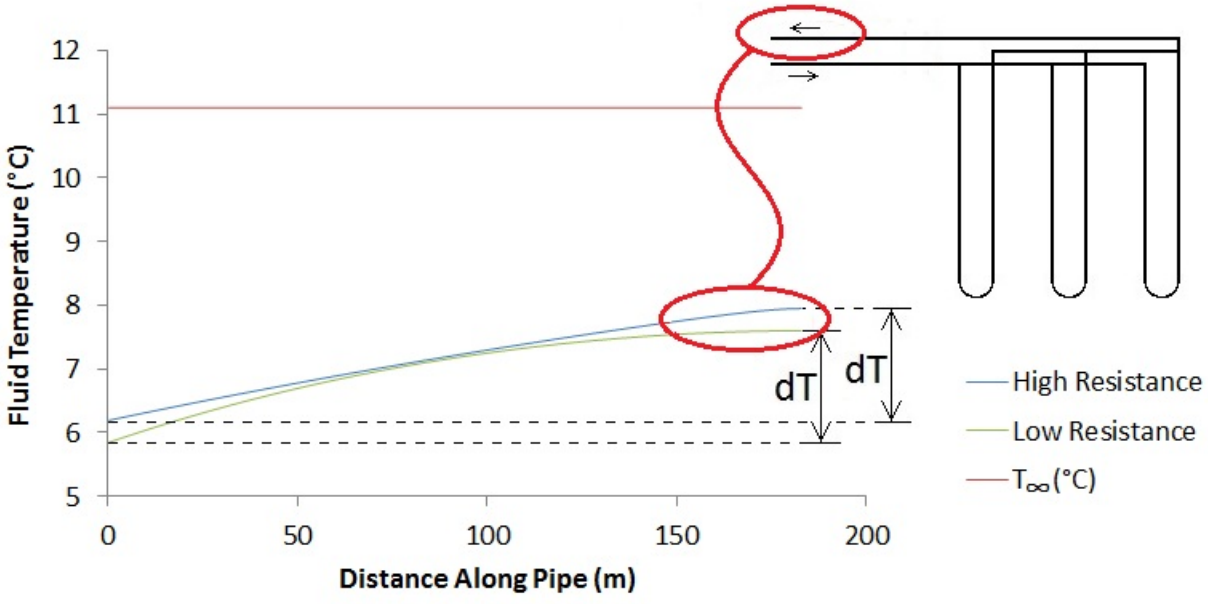

Figure 5.8: Fluid temperature along the pipe after continuous pumping

Simms (2013) FEM model was employed to further investigate the effect of header pipe spacing on GSHP performance. A test case was developed in which a single, 183 m (600 ft) rabbit loop with a 30 m header trench (30 m supply and return pipes) was simulated with varying header pipe spacing. All other parameters were as defined in Section 5.1.2. Figure 5.9 is a schematic of this pipe configuration.

In this base case (Figure 5.9), each of the header pipes are connected to the loop by a 0.5 m pipe. For this test case, the loop configuration will be referred to as "the loop" and the combination of the header pipes and the pipes connecting the header pipes to the loop will be referred to as "the header pipes". The dimensions of the loop remained

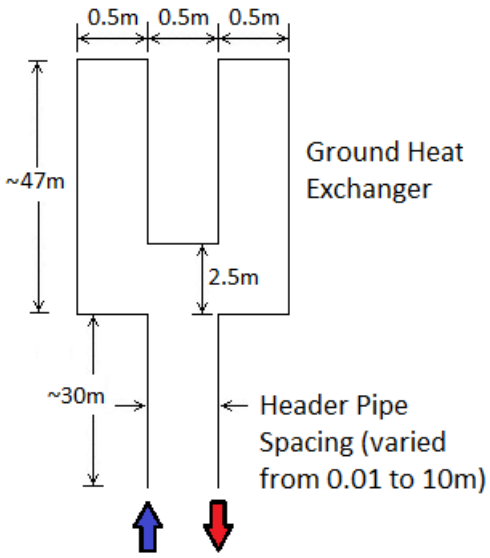

Figure 5.9: Configuration including rabbit loop for header trench investigation in which the header pipe spacing varied from 0.01 to 10 m - not to scale

constant for all investigations, while only its position relative to the soil domain changed. The combined total length of the header pipes was maintained at 61 m. Therefore, as the header pipe spacing was changed the header pipe length was altered accordingly. In all cases the header trench terminated at the edge of the modelled domain and all pipes were located in the centre (in the x-dimension) of the soil elements they intersected. The performance of this configuration was analysed for various header pipe spacings ranging from 0.01 m to 10 m.

The performance of these systems was compared using the COP of the heat pump, which was defined as a function of EWT using the manufacturer's specification's for the

the ClimateMaster Tranquility ® 27 (TT) Series Model 072 (Cli, 2010), the heat pump installed at the Elora Test Site. Simms (2013) model outputs the average heat pump COP for the entire simulation based on the EWT determined by the model. The COP provided by Simms (2013) model was equivalent to heat pump COP rather than total system COP. Therefore, this performance metric is higher than that associated with the 1D finite difference model since circulation pump energy was not incorporated. However, since pumping intensity was always maintained at a constant flow rate, this heat pump COP offers a valid performance metric for the relative comparisons conducted using the 3D model. In each model realization, the system was simulated for a period of 1 year with the system loads and the surface boundary conditions defined as in Section 5.1.2. The results of the header pipe spacing simulations are summarized in Figure 5.10 for the base case with soil thermal conductivity, k_{soil}, equal to 1.22 J/(smK) and a range of realistic soil thermal conductivities between 0.25 and 2.50 J/(smK).

Figure 5.10 illustrates that the performance of the simulated GSHP is dependent on the spacing of the supply and return pipes in the header trench. However, the magnitude of the variation in performance is small ($\leq$2.5% in all cases) and much more strongly dependent on the soil thermal conductivity, which is the homogeneous thermal conductivity of the entire soil domain being simulated. It is noted that the effect of pipe spacing in the header trench on performance is more significant for the low thermal conductivity case, which

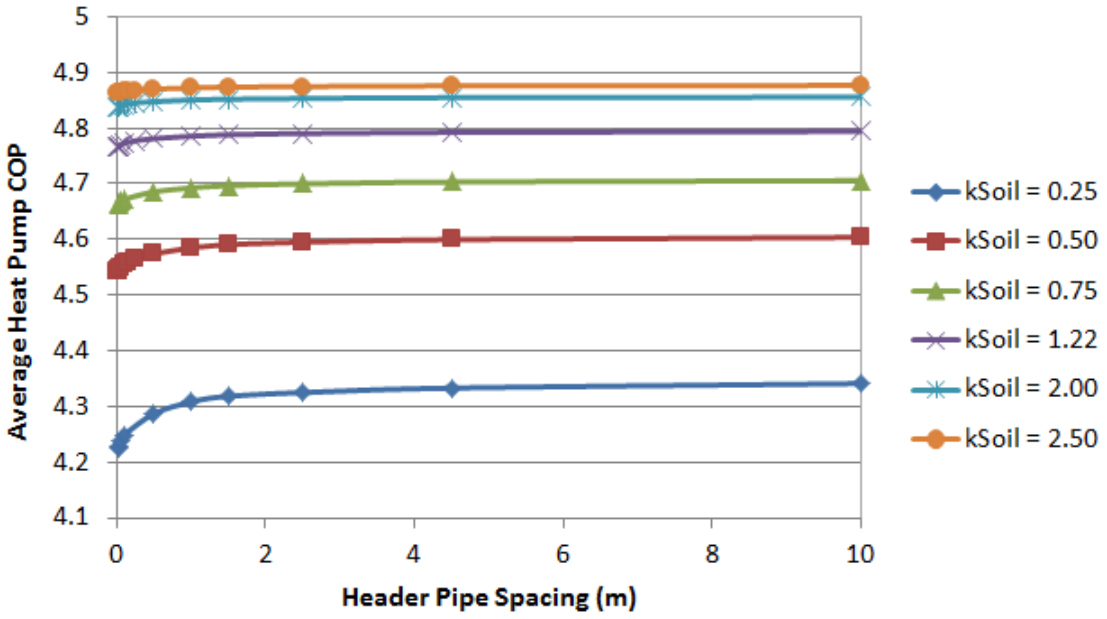

Figure 5.10: COP as a function of header pipe spacing for the single rabbit loop configuration depicted in Figure 5.9 in soils with various bulk thermal conductivities

may not be intuitive. It may be expected that as thermal conductivity increases, the heat transfer between the supply and return pipes would increase, reducing the performance of the system. However, since the thermal conductivity is increasing everywhere in the domain, it also acts to increase the size of the effective thermal reservoir that the GHX is accessing, which would improve the performance of the system significantly more than pipe interactions may degrade performance. Figure 5.10 does show that header pipe spacing has an effect on GSHP performance and that this effect is exaggerated in soils with low thermal conductivities. In the case of a soil thermal conductivity of 0.25 J/(smK) an increase in

header pipe spacing from 5 cm to 1 m resulted in an increase in heat pump COP of approximately 2.5%. This difference is negligible given the uncertainties and assumptions used in the model.

5.4.2 Two Parallel Pipes

It was hypothesized that the differences in performance due to changes in header pipe spacing illustrated in Section 5.4.1 were buffered by the large GHX being simulated. Therefore, to isolate the effect of pipe interactions on system performance, a test case was developed also using Simms (2013) 3D model to simulate two identical lengths of parallel pipes with an imaginary disconnect replacing the U-bend (Figure 5.11). The imaginary disconnect acts to eliminate any bias that may be associated with simulating this connection for a variety of pipe spacings. Since the FEM model assumes that the fluid flows continuously from the outlet of one pipe to the inlet of the other, the total length of the pipe is completely independent of the space between them.

The simulated pipe configuration represented in Figure 5.11 consisted of two identical, parallel 91.5 m lengths of pipe for a total of 183 m of pipe in a homogeneous soil domain. This configuration was simulated for a range of pipe spacings between 0.05 m and 10 m for a low, average, and high soil thermal conductivity (Figure 5.12).

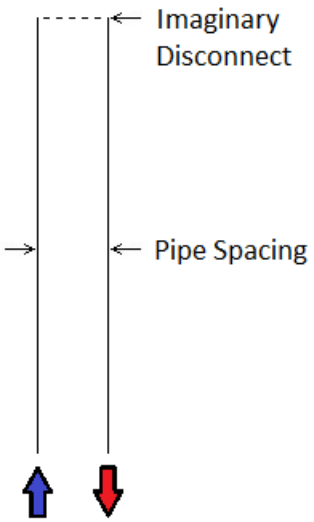

Figure 5.11: Schematic of 2 parallel pipes test case

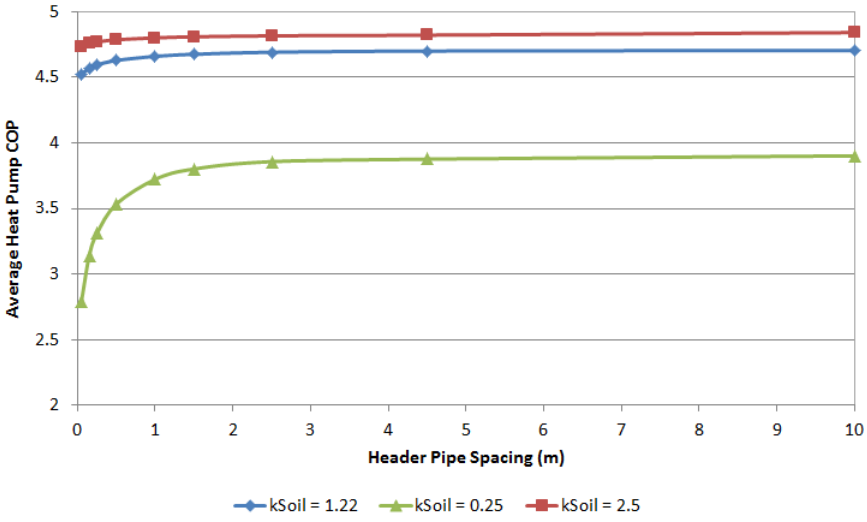

Figure 5.12: COP as a function of parallel pipe spacing

Figure 5.12 illustrates how pipe spacing in the two parallel pipe test case has a more significant impact on performance than in the rabbit loop with header trench test case (Section 5.4.1). Similar to that previous test case, the effect of pipe spacing is much more significant for the low soil thermal conductivity.

The results of the header spacing and two parallel pipes test cases show that pipe spacing has an effect on overall system performance. As pipe spacing increases the heat pump COP of the simulated system increases. The magnitude of these effects is related to the soil thermal conductivity and are most significant in systems within a soil of low thermal conductivity. Therefore, when installing a GHX in a U-bend shape, it is necessary to adequately characterize the soil thermal properties and, for low soil thermal conductivity cases, adequately separate the pipes to maintain system performance. For the low thermal conductivity case investigated, a decrease in performance of approximately 25% was observed when decreasing the pipe spacing from 100 cm to 5 cm. This change in spacing represents the difference between a trenched GHX with pipe spacing of 1 m (a standard excavator bucket width) and a horizontally bored U-tube shaped GHX (minimal pipe spacing), suggesting that this change in system configuration could reduce operation costs by up to 25% when installed in low thermal conductivity soils.

5.4.3 GHX Layout

In practice, GHXs are installed in a variety of configurations as described in Chapter 2. It was expected that pipe configuration, independent of pipe length, would have only a small impact on system performance but no substantial information exists on the topic. Therefore, a test case was developed using Simms (2013) model to investigate the effects of pipe layout on system performance by simulating systems in which the configuration of the pipe is the only variable. Figure 5.13 is a schematic of the 6 configurations that were investigated. In all simulations, two identical pipes of 183 m (600 ft) were considered and all pipe spacings were 0.5 m. All other parameters were as defined in Section 5.1.2. Each simulation had a duration of 1 year and used the system loads and shallow soil temperatures summarized in Section 5.1.2. Since two loops were considered in each case and all adjacent pipes were spaced 0.5 m apart, configurations (a), (b), and (c) were simulated in a trench 3.5 m wide and approximately 50 m long, while configurations (d), (e), and (f) were simulated in a trench 1.5 m wide and approximately 90 m long.

The GHX layout test case was simulated for homogeneous soil thermal conductivities of 1.22, 0.25, and 2.5 J/(smK). Figure 5.14 illustrates how system performance is a function of GHX configuration. In all cases, the longer, more narrow trenches performed better than the shorter, wider trenches by up to 3% for the low soil thermal conductivity case. The

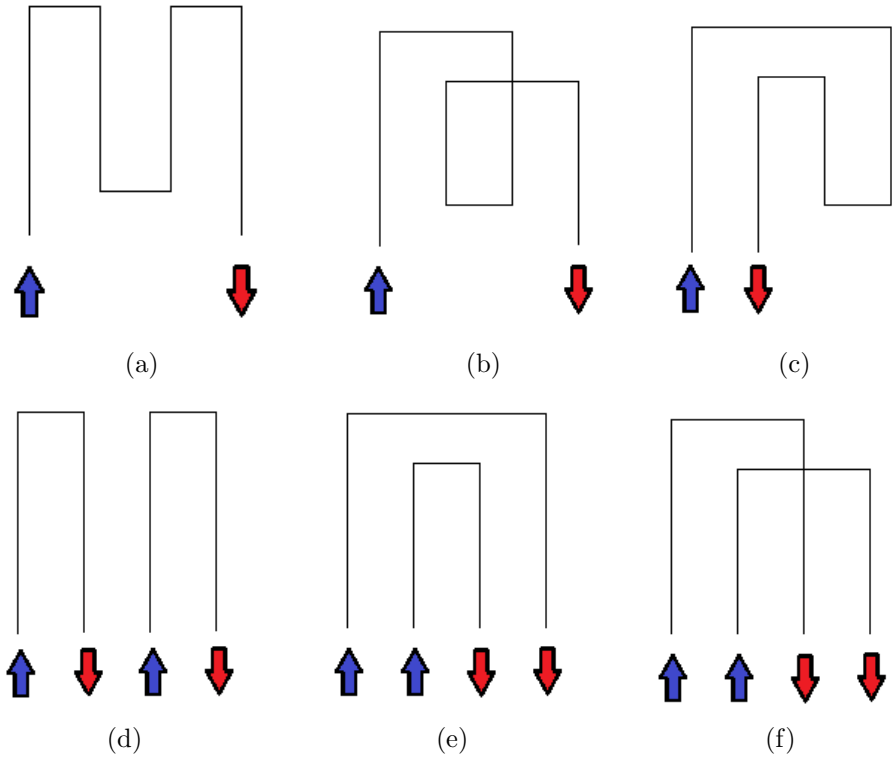

Figure 5.13: Pipe configurations investigated using Simms (2013) FEM model: (a) "rabbit loop", (b) spiral loop, (c) "floppy rabbit loop", (d) side-by-side loops, (e) overlapping loops, and (f) cross over loops - not to scale

decreased performance of the wider trenches is likely a result of these trenches having eight adjacent pipes, rather than four adjacent pipes as in the longer trench, because the heat transfer from the soil domain to the inner pipes would be limited, depleting the efficiency of the system. Based on this test case, it is concluded that longer trenches perform better than wider, shorter trenches with identical pipe spacing when all other parameters are equal. This difference in performance is most significant in soils of low thermal conductivity.

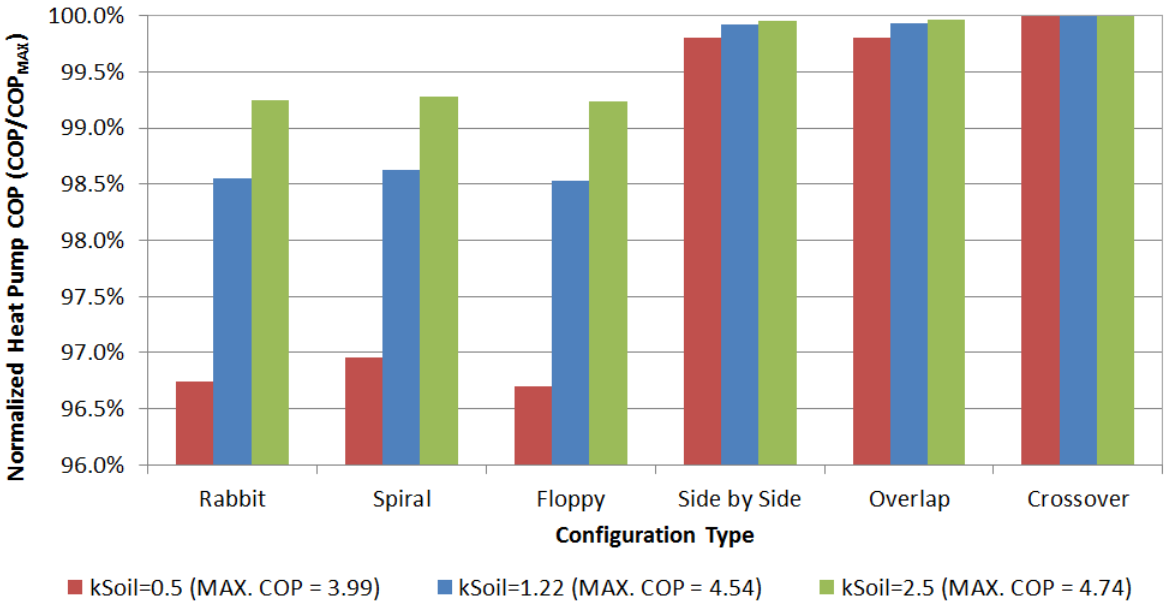

Figure 5.14: Performance based on GHX configuration - identical pipe spacing

The differences in performance based on the GHX configuration independent of trench shape are negligible. The crossover loop performed <0.5% better than the side-by-side and overlapping loops, and the spiral loop performed <0.5% better than the rabbit and floppy loops in all cases.

To investigate when shorter, wider trenches may provide increased performance, the simulations for configurations (a), (b), and (c) were duplicated using a spacing of 3 m between the 2 loops while no changes were made to configurations (d), (e), and (f) (Figure 5.15).

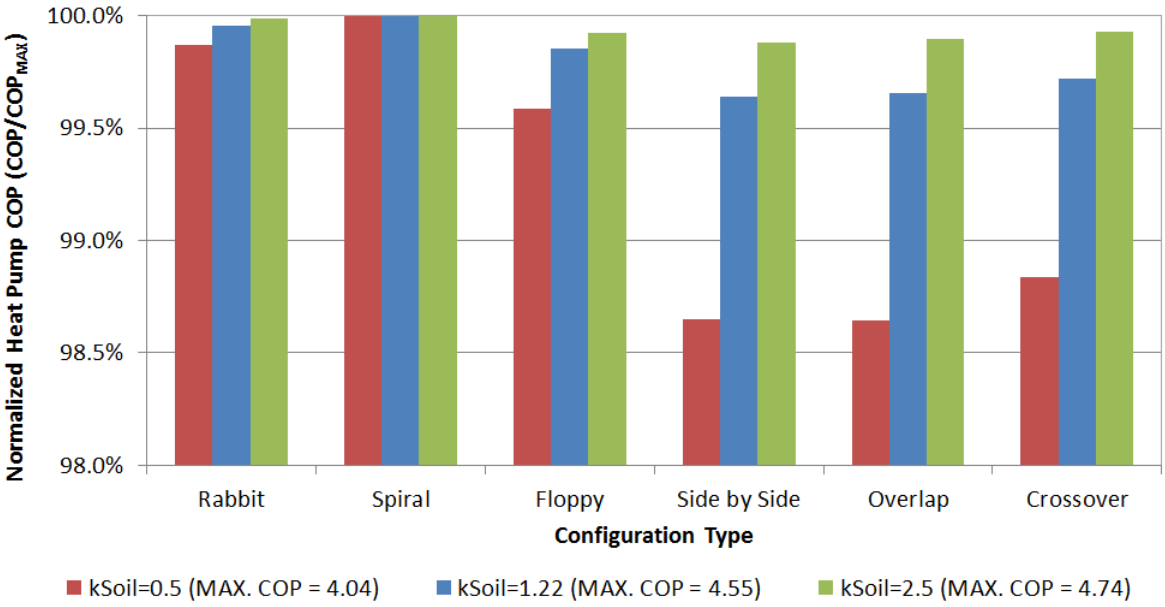

Figure 5.15: Performance based on GHX configuration - varying pipe spacing

Figure 5.15 shows how increasing the spacing between the loops in the shorter, wider trench increases the performance of these systems by approximately 1.5% relative to the longer, more narrow trenches. This result suggests that system performance is mildly improved through increased spacing of adjacent loops.

The relationships between pipe configurations and system performance could be used practically to determine the most ideal configuration for a GHX depending on the land area available for installation; however, no significant efficiencies in GHX layout were identified.

5.4.4 Loop Length

The most significant variable in GHX design is the length of pipe that is installed. A typical design rule of thumb is to assume that 183 m (600 ft) of installed pipe would provide 1 ton (3516 J/s) of heating capacity. However, this rule of thumb may not meet the design requirements in all scenarios and could possibly result in the over or under design of the GHX. Therefore, a test case was developed to investigate the effect of changing pipe length on the performance of the GSHP and analyse the validity of this rule of thumb. It was expected that increasing loop length would increase COP to a point at which pumping losses become more significant than the increased heat transfer associated with the additional pipe. It was expected that COP would decrease with increasing GHX length.

Since the developed 1D finite difference model takes into account the power consumption of the fluid circulation pump, it was utilized for this test case. This power consumption is dependent on the friction losses through the system which are a function of the length of the pipe, the volumetric flow rate, and the physical properties of the fluid. The finite difference model was employed to simulate a range of realizations in which the only variable was the pipe length. All other model parameters were as described in Section 5.1.1. This test case was simulated for 100 days using total pipe lengths from 90 m to over 400 m in a U-tube configuration. Figure 5.16 summarizes the heat pump, circulation pump, and total

energy consumption of the system on the primary vertical axis and average system COP on the secondary vertical axis, and shows how system performance is a function of loop length.

Heat pump and total system energy consumption tend to decrease with increasing GHX length for the range of loop lengths investigated. This trend is associated with the increase in EWT to the heat pump with increasing loop length. Greater loop lengths provide more thermal energy transfer from the subsurface to the fluid, increasing the fluid temperature and reducing the energy required by the heat pump to extract the defined energy difference from the fluid.

Comparatively, as GHX length increases, the circulation pump energy tends to decrease initially then begins to increase with loop length. This trend is caused by the initial reduction in head loss through the system as the average fluid temperature in the pipe rises with increasing loop length. The fluid temperature rise reduces the fluid density and viscosity, thus reducing its resistance to flow and the frictional head losses through the GHX and the heat pump. However, as the loop length increases further, the head loss associated with the additional pipe increases the energy required to maintain the specified flow rate.

As initially expected, simulations showed that heat pump and total system COP increased with loop length, while circulation energy consumption increased with longer

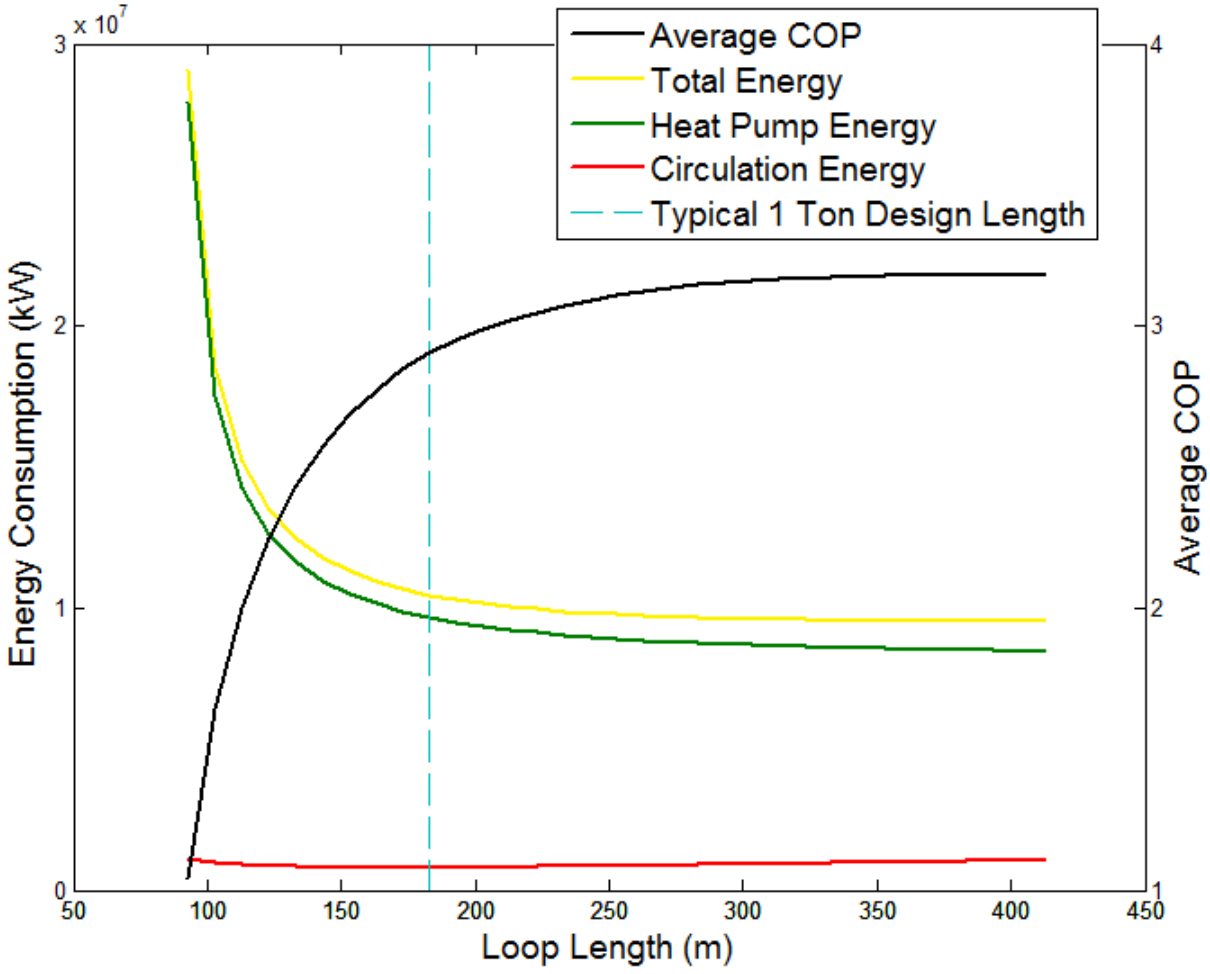

Figure 5.16: Performance of U-bend configuration as a function of total pipe length

GHXs. However, since the circulation pump energy consumption was significantly smaller than that of the heat pump, which was not expected for extremely large GHX lengths, this effect was negligible within the range of loop lengths investigated.

The vertical line representing the typical 1 ton design length in Figure 5.16 denotes the common assumption that 183 m (600 ft) of pipe will provide 1 ton (3516 J/s) of heating capacity. The results show how the total system energy consumption for GHXs beyond this typical design length tends to plateau, suggesting that performance is not significantly enhanced with increased loop length. This conclusion agrees with the typical design length since increases in performance (COP) are marginal beyond this loop length (<10% for length increase from 183 m to 413 m), suggesting that additional pipe is not required to meet this energy demand for the system being investigated. Below this length, reduction in system performance became significant. Therefore, GSHP design optimization becomes a trade off between the additional installation cost of larger ground loops or increased operating costs associated with shorter loops. The findings of this test case agree with typical current design practice but only in the basic case examined. It would not be valid to extend these findings to cases of extreme soil thermal conductivities or irregular GHX configurations.

Chapter 6

Conclusions

The investigations conducted in this thesis help to improve the understanding of GSHP operations. Some conclusions help to support existing practices in the industry, while others help to advance it for a range of GHX designs. These systems offer an efficient technology for heating and cooling applications and expanding the understanding of their operation has an integral role in increasing their utility.

Two main research objectives were addressed to identify potential design efficiencies: in-depth monitoring of a fully function residential GSHP and a comprehensive simulation of these systems using computational models.

A fully functioning residential GSHP was monitored for insight into system operation

and performance at the Elora Field Site. An array of temperature sensors were installed in the subsurface on and surrounding the GHX to investigate temperature changes due to system operation. Power monitoring equipment and temperature sensors were installed on the system inside the residence to quantify system energy loads and total operating costs. Specific temperature measurements and power consumption data were presented and provided motivation for further analyses using numerical computer models. The data analysed, including system operating costs and basic subsurface temperature profiles, were in line with initial expectations. The resolution of the subsurface temperature data was insufficient to establish detailed energy flux estimates or conduct extensive loop configuration performance comparisons.

The total power consumption of the GSHP at the Elora Field Site was directly measured and operating costs were calculated using two different electric utility billing schemes: the time of use billing scheme and the tiered billing scheme. A comparison of these two billing schemes concluded that the time of use billing scheme yielded an average annual cost within 5% of that using the tiered billing scheme. Therefore, the implementation of the time of use billing scheme does not significantly effect the operating costs of this GSHP. Since costs associated with this billing scheme are a function of the time of energy consumption, this conclusion could be extended to other systems with similar occupant schedules in comparable climates.

In Section 5.4, a 3D finite element model developed by Simms (2013) was employed to investigate the effects of GHX configuration on system performance. Test cases were simulated using this model to investigate the effect of pipe spacing and GHX layout on system performance. It was concluded that performance was only nominally a function of pipe spacing and variations in performance were most significant in simulations with low thermal conductivities. When considering a single 183 m ground loop with a 30 m header trench, increases in header pipe spacing from 5 cm to 10 m increased heat pump COP by approximately 2.5% for the extreme low soil thermal conductivity case investigated, which is not a significant improvement related to the implications on system installation associated with this spacing increase. However, when considering a U-tube shaped configuration, increases in pipe spacing from 5 cm to 1 m resulted in an increase in heat pump COP of approximately 25% for the extreme low soil thermal conductivity case investigated. Since operation costs are directly related to heat pump COP, this performance improvement is significant when comparing horizontally bored GHXs (minimal pipe spacing) to potential trenched GHXs in which spacing could be up to 1 m using existing excavating equipment.

To investigate the effect of pipe layout on system performance, the 3D finite element model developed by Simms (2013) was employed to simulate a test case in which the pipe configuration was the only variable. A group of six GHX configurations were investigated. It was found that longer trenches performed better than shorter, wider trenches, which was

attributed to reduced pipe interactions in the longer trenches. However, the differences in performance between all configurations were within ∼3.5% for all simulations, spanning a range of reasonable soil thermal conductivities. In all of the longer trench cases, the configuration referred to as the cross over loop (see Figure 5.13) had the highest system performance by a negligible amount (<0.3%), which was attributed to the minor variations in model output.

In Chapter 4, a 1D finite difference heat conduction model of a U-tube pipe configuration was presented. The model was used to investigate the potential optimization of system performance through pumping intensity, the differences between transient and steady state simulation of GSHPs, and the effect of total loop length on overall system performance.

Comparisons between the transient and steady state simulations concluded that, in the case of a U-tube shaped GHX operating under a range of reasonable energy loads, it is appropriate to simulate the pulsed operation of a GSHP using an equivalent steady state approximation. This result helps to justify the quasi-steady state assumption that is sometimes made when simulating these systems using numerical modelling techniques, as is done by Simms (2013) and in the configuration test cases described above. However, the system COP for the steady state case would be overestimated by up to approximately 10% for the range of reasonable flow rates and soil thermal conductivities investigated.

To attempt to identify performance efficiencies through pump schedule optimization,

the effect of pump cycle frequency was investigated. System performance was shown to be a function of cycle frequency. For the range of cycle frequencies, system loads, and simulation times investigated, system COP varied by up to ∼30% when considering cycle frequency as the only variable. The variation in COP was found to be most significant during operation at lower pump run times, which would represent shoulder season operation when energy demands are relatively lower. Since a typical GSHP operating under a range of reasonable system loads was simulated, this relationship could, with some confidence, be extended to most residential or light commercial GSHP applications. The conclusion is important since pump cycle frequency can significantly effect overall system performance, identifying a method through which system efficiency could be improved without substantial changes to design. System monitoring could be implemented to optimize pump scheduling and maximize system performance after installation.

Finally, the 1D finite difference model was used to investigate the effect of total pipe length on overall system performance by analysing energy consumption and average COP in heating mode with a constant energy demand of 3516 J/s. Pipe length is the primary design variable and the one most likely controlling potential GHX over design. As initially expected, simulations showed that heat pump and total system COP increased with loop length. This increase in COP is caused by the improved heat pump efficiency resulting from the increase in fluid temperature with loop length. The circulation pump energy

consumption initially decreased as loop length increased for the same reason but, for larger loops, the circulation pump energy consumption increased due to the additional head loss through the system. However, the circulation pump energy consumption was significantly smaller than that of the heat pump and this effect was negligible within the range of loop lengths investigated. Therefore, larger loop lengths may be beneficial for GSHP operation since improved heat pump performance is observed with small increases in fluid pumping costs.

The GHX length analysis compared the average COP of each simulation to a typical design length of 183 m (600 ft) per ton (3516 J/s) of heating capacity. It was concluded that this design rule of thumb is reasonable since improvements in COP were marginal beyond this loop length (<10% for length increase from 183 m to 413 m). Below this length, reduction in system performance became significant. Therefore, GSHP design optimization becomes a trade off between the additional installation cost of larger ground loops or increased operating costs associated with shorter loops.

Existing design standards for residential and light commercial GHX applications are unlikely to be dramatically improved upon via changes in configuration or pipe spacing. However, system monitoring could lead to, or at least ensure, optimal GSHP operation through improved pump scheduling.

6.1 Recommendations for Future Work

The developed 1D finite difference model could be employed to conduct additional analyses to further enhance our understanding of GHX design and GSHP operation beyond this thesis. For example, the cycle frequency optimization exercise summarized in Chapter 5 was conducted using this model for a single heat pump and fluid circulation pump combination. This investigation could be extended to any heat pump and circulation pump combination by inputting the manufacturer's specifications into the model and executing similar simulations to provide insight into maximized operating efficiency of the specified systems. The model could also be used to investigate the sensitivity of U-tube shaped GSHP performance to various design parameters, including pipe wall thickness or thermal conductivity, U-tube pipe spacing, heat exchange fluid thermal properties, or pipe diameter. These parameters could be altered within the model to assess how the system reacts to such changes, perhaps offering insight into potential design efficiencies.

In Chapter 3 the Elora Field Site and the associated monitoring data were introduced and summarized. A large quantity of temperature and power consumption data were collected at the field site but an extensive analysis of these data has not been completed. These data could be used to investigate various aspects of this system. The power consumption data could be combined with the temperature data from the supply and return

pipes inside the residence to calculate COP, quantifying the efficiency of the system during heating and cooling operation. The subsurface temperature data could be analysed to quantify temperature profiles around the GHX and estimate the magnitude of thermal energy transfer, giving insight into the way in which heat transmits through the soil. The temperature data could be further analysed to conduct a comparison between the different loop configurations at the field site. It is hypothesized that the slinky loop may not perform as well as the other configurations since the same length of pipe would be extracting energy from, or rejecting energy into, a relatively smaller volume of soil. Analysing the temperatures on the supply and return pipes to each loop and the temperature profile along the trenches would provide preliminary insight for such an investigation.

References

R. Al-Koury and P. G. Bonnier. Efficient finite element formulation for geothermal heating systems. part ii: Transient. *International Journal for Numerical Methods in Engineering*, 67:725–745, 2006.

R. Al-Koury, P. G. Bonnier, and R. B. J. Brinkgreve. Efficient finite element formulation for geothermal heating systems. part i: Steady state. *International Journal for Numerical Methods in Engineering*, 63:988–1013, 2005.

ASHRAE. *2007 ASHRAE Handbook - Heating, Ventilation, and Air-Conditioning Applications*. American Society of Heating, Refrigeration and Air-Conditioning Engineers, Inc., Atlanta, GA, USA, 2007.

ASHRAE. *2009 ASHRAE Handbook - Fundamentals*. American Society of Heating, Refrigeration and Air-Conditioning Engineers, Inc., Atlanta, GA, USA, 2009.

A. Baudoin. *Stockage intersaisonnier de chaleur dans le sol par batterie d'échangeurs baïonnette verticaux: Modèle de prédimensionnement*. PhD thesis, Reims University, France, 1988.

M. Bernier, A. Chala, and P. Pinel. Long-term ground-temperature changes in geo-exchange systems. *ASHRAE Transactions*, 114(2):342–350, 2008.

David J. Brodrecht. Personal communication, 2010. David Brodrecht is the Manager of Geothermal Applications at NextEnergy Inc.

H. S. Carslaw and J. C. Jaeger. *Conduction of Heat in Solids*. Oxford University Press, Oxford, United Kingdom, 1947.

Stuart W. Churchill. Comprehensive correlating equations for heat, mass and momentum transfer in fully developed flow in smooth tubes. *Ind. Eng. Chem., Fundam.*, 16(1): 109–116, 1977.

Tranquility® 27 (TT) Series IOM - Installation, operation & Maintenance Instructions. ClimateMaster® Geothermal Heat Pump Systems, USA, 2010.

Tranquility® 30 Digital (TE) Series IOM - Installation, operation & Maintenance Instructions. ClimateMaster® Geothermal Heat Pump Systems, USA, 2012.

COMSOL Multiphyics User's Guide. COMSOL AB: COMSOL, Stockholm, Sweden, 2008.

CSA. *CAN/CSA-C448 Series-02: Design and Installation of Earth Energy Systems*. Canadian Standards Association, Canada, 2009.

CSA. *CAN/CSA-F280-12 Determining the required capacity of residential space heating and cooling appliances*. Canadian Standards Association, Canada, 2012.

Mark W. Denny. *Modern Hydronic Heating: For Residential and Light Commercial Buildings*. Princeton University Press, Princeton, NJ, USA, 1993.

H.-J. G. Diersch, D. Bauer, W. Heidemann, W. Rühaak, and P. Schätzl. Finite element modelling of borehole heat exchanger systems: Part 1. fundamentals. *Computers and Geosciences*, 37(8):1122–1135, 2011a.

H.-J. G. Diersch, D. Bauer, W. Heidemann, W. Rühaak, and P. Schätzl. Finite element modelling of borehole heat exchanger systems: Part 2. numerical simulation. *Computers and Geosciences*, 37(8):1136–1147, 2011b.

P. Eskilson. *Thermal analysis of heat extraction boreholes*. PhD thesis, University of Lund, Lund, Sweden, 1987.

P. Eskilson and J. Claesson. Simulation model for thermally interacting heat extraction boreholes. *Numerical Heat Transfer*, 13(2):149–165, 1988.

Jose Etcheverry, Paul Gipe, William Kemp, roger Samson, Martijn Vis, Bill Eggerton, Rob McMonagle, Sarah Marchildon, and Dale Marshall. *Smart Generation: Power Ontario with Renewable Energy*. The David Suzuki Foundation, Vancouver, B.C., Canada, 2004.

Pier-Olivier Fontaine, Denis Marcotte, Philippe Paquier, and Denis Thibodeau. Modeling of horizontal geoexchange systems for building heating and permafrost stabilization. *Geothermics*, 40(3):211–220, 2011.

Ground Loop Design™ Premier 2010 User's Manual. Gaia Geothermal, USA, 2010.

M. He, S. Rees, and L. Shao. Simulation of a domestic ground source heat pump system using a transient numerical borehole heat exchanger model. *Journal of Building Performance Simulation*, 4(2):141–155, 2011.

G. Hellström. *Ground Heat StorageThermal Analyses of Duct Storage Systems*. PhD thesis, University of Lund, Lund, Sweden, 1991.

Patrick J. Hughes. Geothermal (ground-source) heat pumps: Market status, barriers to adoption, and actions to overcome barriers. Technical report, Oakrdige National Laboratory, 2008.

IGSHPA. *Closed-Loop Geothermal Systems - Slinky Installation Guide*. International Ground Source Heat Pump Association, Stillwater, OK, USA, 1994.

L. R. Ingersoll and H. J. Plass. Theory of the ground pipe heat source for the heat pump. *Heating, Piping and Air Conditioning*, 20(7):119–122, 1948.

L. R. Ingersoll, O. J. Zobel, and A. C. Ingersoll. *Heat Conduction*. The University of Wisconsin Press, Madison, WI, USA, 1954.

Stephen P. Kavanaugh and Kevin Rafferty. *Ground-Source Heat Pumps - Design of Geothermal Systems for Commercial and Institutional Buildings*. American Society of Heating, Refrigeration and Air-Conditioning Engineers, Inc., Atlanta, GA, USA, 1997.

Application Guide (AG 31-008): Geothermal Heat Pump Design Manual. McQuay® Air Conditioning, 2002. $Retrieved on May 20, 2011 from http://www.mcquay.com/$.

V. C. Mei and C. J. Emerson. New approach for analysis of ground-coil design for applied heat pump systems. *ASHRAE Transactions*, 91(2B):1216–1226, 1985.

E. Shashi Menon. *Gas Pipeline Hydraulics*. CRC Press - Taylor and Francis Group, Boca Raton, FL, USA, 2005.

Lewis F. Moody. Friction factors for pipe flow. In *The American Society of Mechanical Engineers Semi-Annual Meeting*, Pittsburgh, PA, USA, June 1944.

Norman K. Muraya. *Numerical Modelling of the Transient Thermal Interference of Vertical U-Tube Heat Exchangers*. PhD thesis, Texas A&M University, 1994.

M. Nabi and R. Al-Khoury. An efficient finite volume model for shallow geothermal systems - part i: Model formulation. *Computers and Geosciences*, 49:290–296, 2012a.

M. Nabi and R. Al-Khoury. An efficient finite volume model for shallow geothermal systems - part ii: Verification, validation and grid convergence. *Computers and Geosciences*, 49: 297–307, 2012b.

National Resources Canada: NRCan. Heating and cooling with a heat pump: Ground-source heat pumps (earth-energy systems). Website, 2009. $Retrieved on May 26, 2011 from http://oee.nrcan.gc.ca/$.

OEB. Electricity prices. Webpage, Ontario Energy Board, 2012. http://www.ontarioenergyboard.ca/OEB/Consumers/Electricity/Electricity+Prices, Accessed 28 November, 2012.

Oklahoma State University: OSU. *Closed-Loop/Ground-Source Heat Pump Systems: Installation Guide*. International Ground Source Heat Pump Association, Stillwater, OK, USA, 1988.

Oklahoma State University: OSU. *Ground Source Heat Pump Residential and Light Commercial: Design and Installation Guide*. International Ground Source Heat Pump Association, Stillwater, OK, USA, 2009.

Mikael Philippe, Michel Bernier, Dominique Marchio, and Simon Lopez. A semi-analytical model for serpentine horizontal ground heat exchangers. *HVAC&R Research*, 17(6): 1044–1058, 2011.

M. Phillipe, M. Bernier, and D. Marchio. Sizing calculation spreadsheet: Vertical geothermal borefields. *ASHRAE Journal*, 52(7):20–28, 2010.

J. Raymond, R. Therrien, and L. Gosselin. Borehole temperature evolution during thermal response tests. *Geothermics*, 40(1):69–78, 2011.

S. J. Rees, J. D. Spitler, Z. Deng, C. D. Orio, and C. N. Johnson. A study of geothermal heat pump and standing column well performance. *ASHRAE Transactions*, 110(1):3–13, 2004.

John Siegenthaler. *Air and Water: The Biology and Physics of Life's Media*. Delmar Learning, Clifton Park, NY, USA, 2 edition, 2004.

Richard B. Simms. The effects of soil heterogeneity on the performance of horizontal ground loop heat exchangers. Master's thesis, The University of Waterloo, Waterloo, ON, Canada, 2013.

C. N. Jr. Sittel, W. D. Threadgill, and K. B. Schnelle Jr. Longitudinal dispersion for turbulent flow in pipes. *I&EC Fundamentals*, 7(1):39–43, 1968.

Jeffrey D. Spitler and James Cullin. Misconceptions regarding design of ground-source heat pump systems. In *Proceedings of the World Renewable Energy Congress*, Glasgow, Scotland, July 2008.

J. S. Steinhart and J. R. Hart. Calibration curves for thermistors. *Deep-Sea Research*, 15: 497–503, 1968.

James W. Stevens. Coupled conduction and intermittent convective heat transfer from a buried pipe. *Heat Transfer Engineering*, 23(4):34–43, 2002.

M. Th. van Genuchten and W. J. Alves. Analytical solutions of the one-dimensional convective-dispersive solute transport equation. Technical Bulletin 1661, U.S. Department of Agriculture, 1982.

WaterFurnace. Waterfurnace® energy analysis. Spreadsheet, n.d.

VSX Vogel Software GMBH WILO. Software, 2010. Wilo-Select used to asses circulation pump power requirements.

S. D. Wood, B. W. Mangum, J. J. Filliben, and S. B. Tillett. Investigation of the stability of thermistors. *J Res Natl Bur Stand (US)*, 83(3):247–263, 1978.

C. Yavuzturk, J. D. Spitler, and S. J. Rees. A transient two-dimensional finite volume model for the simulation of vertical u-tube ground heat exchangers. *ASHRAE Transactions*, 105(2):465–474, 1999.

M. M. Yovanovich. A general expression for predicting conduction shape factors. In *AIAA 11th Aerospace Sciences Meeting*, Washington, D.C., USA, January 1973.

APPENDICES

Appendix A

CSA 448 Multiple Measure Method

This appendix outlines the procedure, referred to as the Multiple Measure Method, defined by the Canadian Standards Association (CSA, 2009) for the design of GHX systems in Canada. To follow the CSA (2009) guidelines the designer must complete the seven step process referred to as the Multiple Measure Method.

Step 1,2,3 - Residential Load Calculation and Gains Factor

The designer must first complete a heating and cooling load calculation in an acceptable manner and is referred to the method defined by CSA (2012) as an example of an acceptable load calculation procedure.

A gains factor is a coefficient describing the building thermal energy gains due to internal and solar heat gains. This gains factor is defined based on basic quantifications of building windows, occupancy, base electrical use, and construction quality. The gains factor is used to determine the heating correction factor, Cd, as described in the *ASHRAE Handbook - Fundamentals* (ASHRAE, 2009). Cd is determined using the gains factor and the annual degree days for the specific GHX design. CSA (2009) includes a table of Cd values as functions of degree days and the gains factor.

Step 4 - Determining the System Balance Point by Degree Days

CSA (2009) requires that a GHX provide 95% of the required heating load for a building. This requirement is based on experience designing these systems in Canada. This step involves estimating the minimum outdoor air temperature at which a back-up heating system is required for a maximum of 5% of the heating load, the system balance point. The system balance point is a function of the annual heating degree days and the heat loss for the specific GHX design as described in the *ASHRAE Handbook - Fundamentals* (ASHRAE, 2009). The heat loss is a function of the building envelop and is determined during an energy audit for the building.

Step 5 - Heat Pump Heating Capacity and Entering Water Temperature Correction for Closed Loop Systems

The GSHP heat capacity is a quantification of the heating capacity of the subsurface in a specific location. This parameter is estimated based on the heat loss, Cd factor, system balance point, and the temperature difference, which is a measure of the design temperature heat loss in a specific location as defined in the *ASHRAE Handbook - Fundamentals* (ASHRAE, 2009).

The minimum entering water temperature (EWT) of the fluid that will be entering the heat pump is approximated by CSA (2009) as a difference from the average soil temperature and is dependent on the relative soil moisture. In Canada, the difference between the average soil temperature and the minimum EWT is approximated as 10°C, 11°C, and 14°C for wet soils, damp soils, and dry soils, respectively (CSA, 2009).

Step 6 - Selecting an Appropriate Ground Heat Exchanger

To identify minimum GHX length, the heat pump manufacturer's specifications must first be examined to determine a unit that will provide the necessary heating capacity of the system given the minimum EWT determined in Step 5. Once a heat pump with the required heating capacity is identified, the minimum required GHX length is based on

the nominal cooling capacity of this heat pump. The nominal cooling capacity [W] is the maximum total thermal energy that an air conditioner can remove from the air in a unit of time and is defined by the heat pump manufacturer. CSA (2009) defines the required loop length for specific GHX configurations based on pipe length per unit of cooling capacity. Therefore, total GHX length is determined using the nominal cooling capacity of the selected heat pump and the tables provided by CSA (2009), which are only appropriate for Canadian applications where annual heating requirements are greater than annual cooling requirements. The sources of these tables in CSA (2009) are not described in detail.

Step 7 - Correcting for Soil Type

To this point in the design process, the type of soil has not been considered. CSA (2009) defines a soil type correction factor to account for the variation in thermal properties of different soils. This correction factor is based on specific soil type and GHX configuration. It appears to the author that these factors are based on empirical data. The soil type correction factor is applied to the GHX minimum length calculation, increasing or decreasing the required GHX length. For horizontal GHX applications, the soil type correction factor ranges from 0.95 for wet sand to 3.9 for dray sand.

The Canadian standard for GHX design is an example of guidelines used in the in-

dustry. The summary was meant to provide insight into the techniques and some of the requirements of GHX design. The investigations that follow attempt to further the understanding of GHX interactions with the intention of providing insight into the optimization of their operation and design.

Appendix B

GeoDesigner® Design Report

Project Information

Prepared For:
Peter and Jane Robertson
1 Some St.
Elora, ON

Notes:

Prepared By:
University of Waterloo
200 University Avenue W.
Waterloo, CAN N2L 3G1
519-888-4567 x. 3117

Notes:

Design Data

Heating Load:	45,000	Btu/Hr	Heating Setpoint:	72	Deg F
Htg Load Temp Diff:	65	Deg F	Cooling Setpoint:	75	Deg F
Cooling Load:	30,000	Btu/Hr	Begin Cooling At:	70	Deg F
Clg Load Temp Diff:	25	Deg F	Hot Water Setpoint:	130	Deg F
Sensible Cooling:	26,400	Btu/Hr	Hot Water Users:	2	
			Continuous Fan:	Yes	
Reference City:	Waterloo-Wellington, CAN-ON				
Winter Design:	-2	Deg F	Annual Heating:	109.0	Million Btu
Summer Design:	84	Deg F	Annual Cooling:	12.8	Million Btu
Bldg Balance Temp:	62	Deg F	Annual Water Heating:	12.1	Million Btu
Avg Internal Gains:	7,179	Btu/Hr	Daily Hot Water Use:	40	Gallons

Estimated Operating Cost Summary

System	Heating Cost	Cooling Cost	Hot Water Cost	Constant Fan	Total Cost	Per Month
TT 072 Vspd / Horz 4 pipe - 0.75"	$1,146	$49	$239	$74	$1,508	$126
18 SEER - Twin Compressor - R22 System	$1,470	$112	$209	$260	$2,052	$171
Gas-80%-Ignitor-Induced System	$1,582	$147	$209	$336	$2,275	$190

Comments:
UW Test Location

1
elora_test_site.ged

Utility Cost	Rate	Summer	Winter
Electric - Geothermal	$/kwh	.110	.110
Electric - Heat Pump	$/kwh	.110	.110
Electric - Furnace	$/kwh	.110	.110
Natural Gas	$/therm	1.00	1.00
Propane	$/gallon	3.50	3.50
Fuel Oil	$/gallon	3.50	3.50

Due to the variability of weather, system installation, and living habits this analysis is to be considered an estimate.

12/7/12

System Comparison Graph

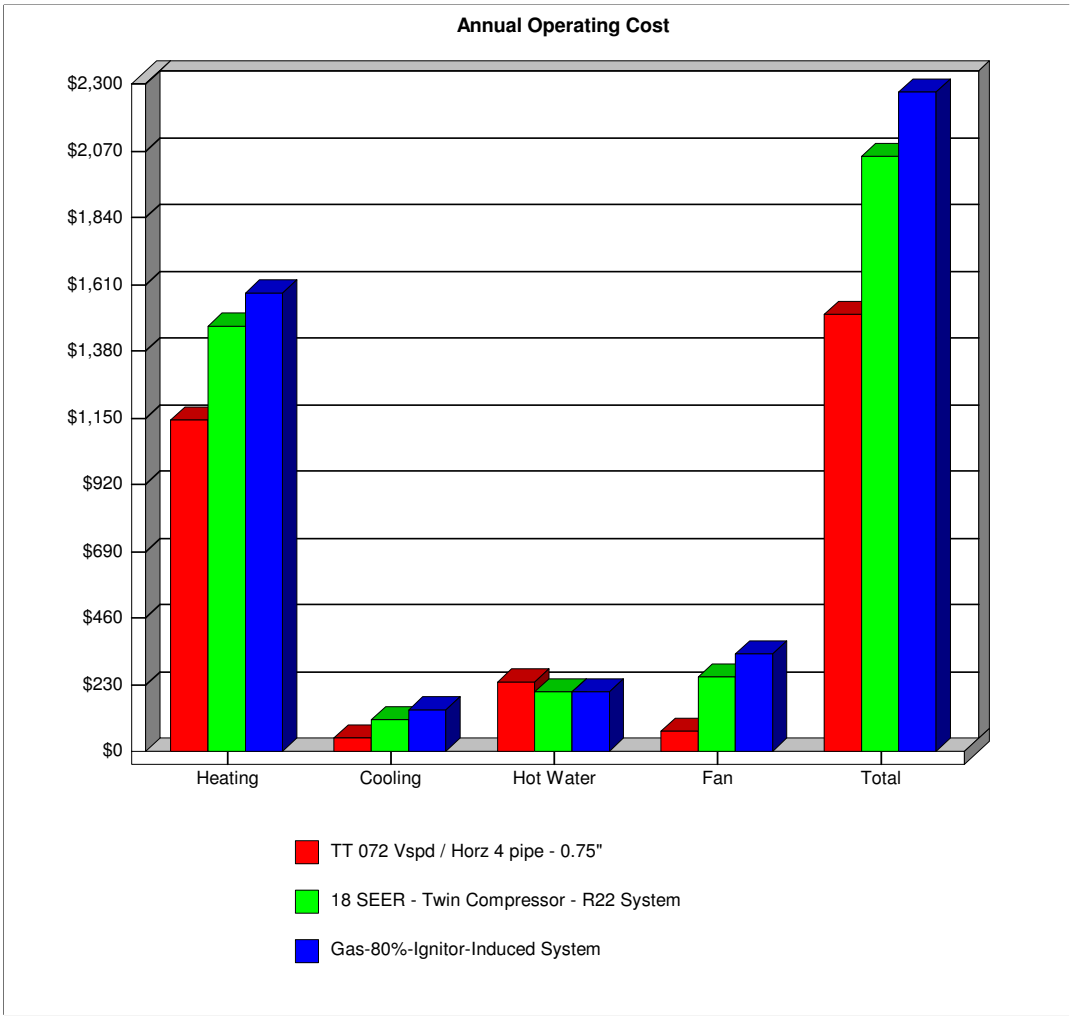

System Summary

TT 072 Vspd / Horz 4 pipe - 0.75"

ClimateMaster Unit

Series:	Tranquility 27 - EarthPure	
Model:	72	
Style:	Two Stage - Var. Speed	
Hot Water Generator:	Yes	
Heating Run Time:	2,474	Hours
Cooling Run Time:	210	Hours
Heating Stage 1:	99	% of Htg
Cooling Stage 1:	100	% of Clg

Geothermal Source

Source Type:	Horizontal Closed Loop	
Soil Type:	0.75 - Damp Silt/Clay	
Pipe Type:	3/4" IPS PE SDR 11	
Pipe Configuration:	4 Pipes in Trench	
Avg Pipe Depth:	5	Feet
Trench Length:	915	Feet
Min Freeze Protect:	10	Deg F
Max Source-Cooling:	66	Deg F
Avg Source-Cooling:	56	Deg F
Avg Source-Heating:	40	Deg F
Min Source-Heating:	30	Deg F
Deep Earth Temp:	50.1	Deg F
Surface Swing:	22.6	Deg F
Swing Time Lag:	39	Days
Soil Conductivity:	0.75	
Soil Diffusivity:	0.60	
Loop Conductivity:	3.03	

Auxiliary Heat

Type:	Electric Resistance	
Style:	Duct Heater	
Auxiliary Required:	0	Kw
Optional Emergency:	14	Kw
Efficiency:	100	%
Aux Balance Point:	N/A	Deg F

Water Heater

Type:	Electric Storage Water Heater	
Style:	Standard Efficiency	
Efficiency:	88.0	%

Heating

Tranquility 27 - EarthPure		
Electrical Use:	10,420	Kwh
Average Efficiency:	3.07	COP
Annual Contribution:	100	%
Annual Cost:	$1,146	
Electric Resistance		
Electrical Use:	1	Kwh
Average Efficiency:	100	%
Annual Contribution:	0	%
Annual Cost:	$0	
Annual Heating Cost:		$1,146

Cooling

Tranquility 27 - EarthPure		
Electrical Use:	447	Kwh
Average Efficiency:	28.7	EER
Annual Cooling Cost:		$49

Water Heating

Geothermal Hot Water Generator		
Electrical Use:	665	Kwh
Average Efficiency:	3.36	COP
Annual Contribution:	63	%
Annual Cost:	$73	
Electric Storage Water Heater		
Electrical Use:	1,505	Kwh
Average Efficiency:	88	%
Annual Contribution:	37	%
Annual Cost:	$166	
Annual Water Heating Cost:		$239

Continuous Fan

Electrical Use:	668	Kwh
Annual Continuous Fan Cost:		$74

Total Annual Operating Cost: $1,508

Due to the variability of weather, system installation, and living habits this analysis is to be considered an estimate.

12/7/12

Temperature Bin Analysis

TT 072 Vspd / Horz 4 pipe - 0.75"

Outdoor Air Temp	Annual Weather Hours	Space Load Btu/Hr	Hot Water Load Btu/Hr	Geo Source Temp	Htg - Clg Capacity Btu/Hr	H.W. Gen Capacity Btu/Hr	Geo Run Time	Geo Operating Cost	Aux Heating Cost	Aux Hot Water Cost
112										
107										
102										
97										
92	5	22,697	1,387	61	59,798	3,653	38%	$0.70		
87	69	18,133	1,387	59	60,263	3,503	30%	$7.56		$0.84
82	228	13,569	1,387	57	60,726	3,249	22%	$18.25		$5.52
77	436	9,005	1,387	55	61,189	2,994	15%	$22.62		$15.11
72	615	7,179	1,387	55	61,374	2,892	12%			$23.61
67	705		1,387							$35.80
62	705		1,387							$35.80
57	672	-3,205	1,387	45	45,973	4,779	7%	$24.45		$25.93
52	637	-6,667	1,387	44	45,304	4,742	15%	$48.43		$16.07
47	586	-10,128	1,387	43	44,637	4,705	23%	$68.01		$6.85
42	590	-13,590	1,387	42	44,145	4,504	31%	$91.96		
37	724	-17,052	1,387	42	44,406	3,611	38%	$139.43		
32	762	-20,513	1,387	41	44,387	3,000	46%	$174.93	$0.01	
27	618	-23,975	1,387	40	44,203	2,557	54%	$164.90	$0.01	
22	464	-27,436	1,387	39	43,916	2,219	62%	$141.22	$0.01	
17	367	-30,898	1,387	38	43,558	1,955	71%	$125.58	$0.01	
12	260	-34,359	1,387	37	43,151	1,741	80%	$98.87	$0.01	
7	160	-37,821	1,387	37	42,709	1,566	89%	$66.98	$0.01	
2	91	-41,282	1,387	36	42,240	1,419	98%	$41.61		
-3	43	-44,744	1,387	35	44,744	1,387	100%	$21.20		
-8	17	-48,205	1,387	34	48,205	1,387	100%	$8.98		
-13	5	-51,667	1,387	33	51,667	1,387	100%	$2.82		
-18	1	-55,128	1,387	33	54,541	1,387	100%		$0.02	
-23										
-28										
-33										
	8760							$1,269	$0	$166

12/7/12

Bin Analysis Graph

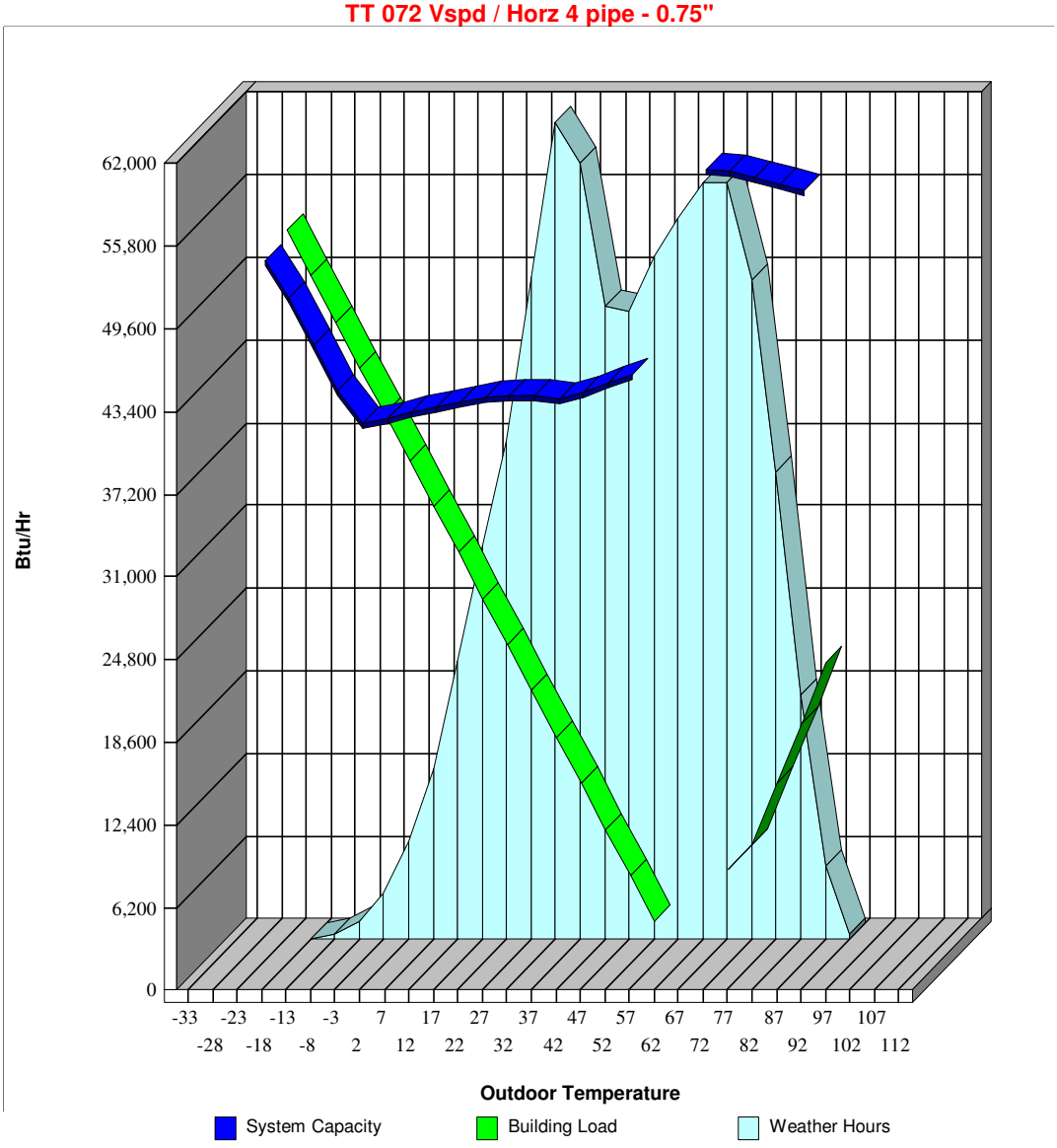

12/7/12

System Summary

18 SEER - Twin Compressor - R22 System

Heat Pump

Type:	Heat Pump - Split	
Style:	18 SEER - 2stg - R22	
95 F Cool Capacity:	34,200	Btu/Hr
95 F Cool Efficiency:	10.0	EER
47 F Heat Capacity:	33,840	Btu/Hr
47 F Heat Efficiency:	3.28	COP
17 F Heat Capacity:	19,440	Btu/Hr
17 F Heat Efficiency:	2.25	COP
Heat Cut-off Temp:	35	Deg F
Indoor Coil Match:	Standard	
Outdoor Coil Rating:	Average	
95 F Low Cool Cap:	19,015	Btu/Hr
95 F Low Cool Eff:	12.9	EER
47 F Low Heat Cap:	18,875	Btu/Hr
47 F Low Heat Eff:	3.57	COP
17 F Low Heat Cap:	9,588	Btu/Hr
17 F Low Heat Eff:	2.09	COP
Heating Run Time:	2,104	Hours
Cooling Run Time:	734	Hours

Auxiliary Heat

Type:	Gas Furnace	
Style:	Ignitor-Induced Draft	
Input Capacity:	100,000	Btu/Hr
Output Capacity:	81,000	Btu/Hr
Efficiency:	80	AFUE

Water Heater

Type:	Gas Storage Water Heater	
Style:	Standard Efficiency	
Efficiency:	58.0	%

Heating

Heat Pump - Split

Electrical Use:	3,576	Kwh
Average Efficiency:	2.68	COP
Annual Contribution:	30	%
Annual Cost:	$393	

Gas Furnace

Fuel Use:	992	Therms
Electrical Use:	774	Kwh
Average Efficiency:	77	%
Annual Contribution:	70	%
Annual Cost:	$1,077	

Annual Heating Cost: $1,470

Cooling

Heat Pump - Split

Electrical Use:	1,017	Kwh
Average Efficiency:	12.6	EER

Annual Cooling Cost: $112

Water Heating

Gas Storage Water Heater

Fuel Use:	209	Therms
Average Efficiency:	58	%

Annual Water Heating Cost: $209

Continuous Fan

Electrical Use:	2,367	Kwh

Annual Continuous Fan Cost: $260

Total Annual Operating Cost: $2,052

Due to the variability of weather, system installation, and living habits this analysis is to be considered an estimate.

12/7/12

Temperature Bin Analysis

18 SEER - Twin Compressor - R22 System

Outdoor Air Temp	Annual Weather Hours	Space Load Btu/Hr	Hot Water Load Btu/Hr	Heating Capacity Btu/Hr	Heating Run Time	Cooling Capacity Btu/Hr	Cooling Run Time	Heat Pump Operating Cost	Aux Heating Cost	Water Heating Cost
112										
107										
102										
97										
92	5	22,697	1,387			22,697	100%	$1.26		$0.12
87	69	18,133	1,387			18,814	97%	$11.03		$1.65
82	228	13,569	1,387			19,318	76%	$27.32		$5.45
77	436	9,005	1,387			19,821	53%	$34.73		$10.42
72	615	7,179	1,387			20,325	42%	$37.56		$14.70
67	705		1,387							$16.85
62	705		1,387							$16.85
57	672	-3,205	1,387	20,423	20%			$23.26		$16.07
52	637	-6,667	1,387	18,875	42%			$45.70		$15.23
47	586	-10,128	1,387	16,288	69%			$67.02		$14.01
42	590	-13,590	1,387	14,050	98%			$93.66		$14.11
37	724	-17,052	1,387	17,052	100%			$163.76		$17.31
32	762	-20,513	1,387						$221.89	$18.22
27	618	-23,975	1,387						$209.78	$14.77
22	464	-27,436	1,387						$179.80	$11.09
17	367	-30,898	1,387						$159.77	$8.77
12	260	-34,359	1,387						$125.59	$6.22
7	160	-37,821	1,387						$84.89	$3.83
2	91	-41,282	1,387						$52.59	$2.18
-3	43	-44,744	1,387						$26.88	$1.03
-8	17	-48,205	1,387						$11.43	$0.41
-13	5	-51,667	1,387						$3.60	$0.12
-18	1	-55,128	1,387						$0.77	$0.02
-23										
-28										
-33										
	8760							$505	$1,077	$209

12/7/12

Bin Analysis Graph

18 SEER - Twin Compressor - R22 System

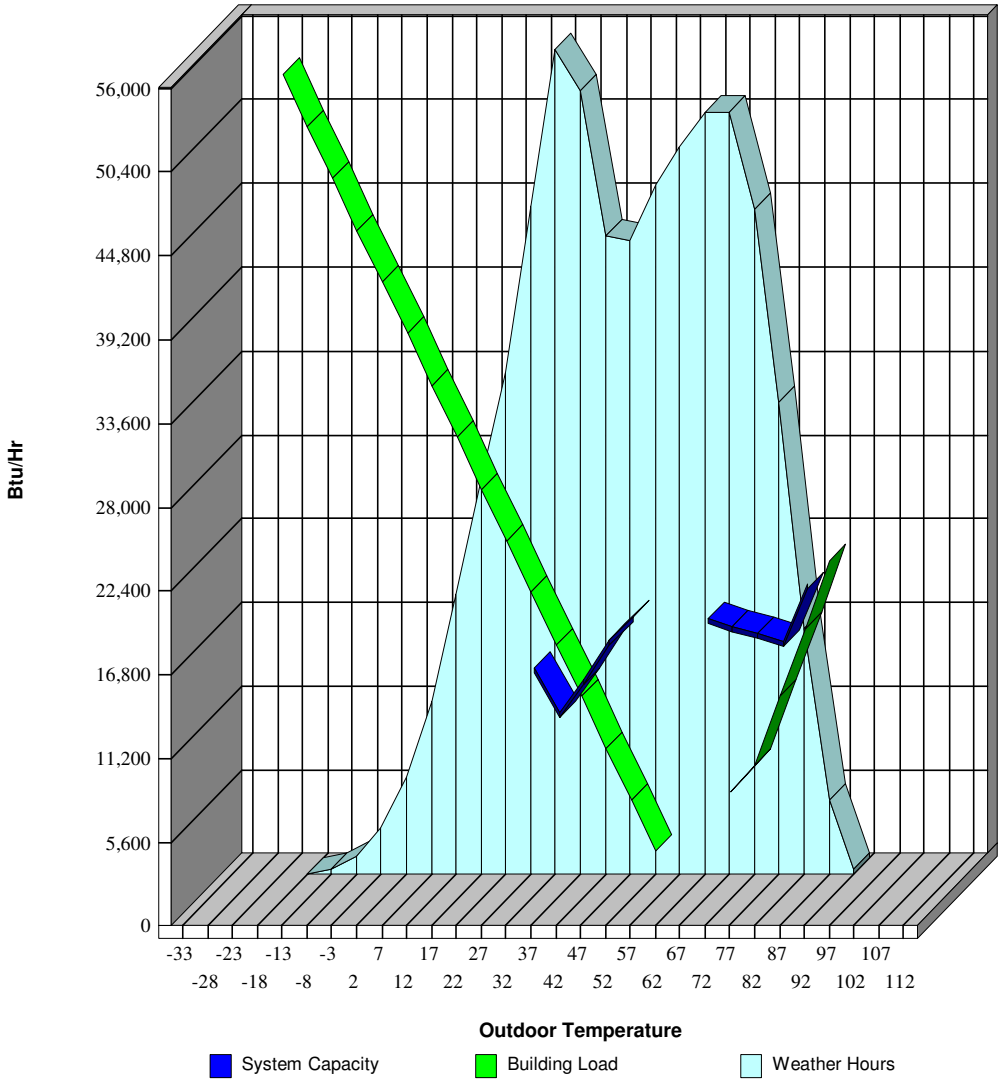

12/7/12

System Summary

Gas-80%-Ignitor-Induced System

Air Conditioner

Type:	Air Conditioner - Split	
Style:	12 SEER - R410a	
95 F Cool Capacity:	35,280	Btu/Hr
95 F Cool Efficiency:	10.3	EER
Indoor Coil Match:	Standard	
Outdoor Coil Rating:	Average	
Run Time:	424	Hours

Heating System

Type:	Gas Furnace	
Style:	Ignitor-Induced Draft	
Input Capacity:	71,886	Btu/Hr
Output Capacity:	58,228	Btu/Hr
Efficiency:	80.0	AFUE
Run Time:	1966	Hours

Water Heater

Type:	Gas Storage Water Heater	
Style:	Standard Efficiency	
Efficiency:	58.0	%

Heating

Gas Furnace

Fuel Use:	1,414	Therms
Electrical Use:	1,534	Kwh
Average Efficiency:	77	%
Annual Heating Cost:		$1,582

Cooling

Air Conditioner - Split

Electrical Use:	1,333	Kwh
Average Efficiency:	9.6	EER
Annual Cooling Cost:		$147

Water Heating

Gas Storage Water Heater

Fuel Use:	209	Therms
Average Efficiency:	58	%
Annual Water Heating Cost:		$209

Continuous Fan

Electrical Use:	3,057	Kwh
Annual Continuous Fan Cost:		$336

Total Annual Operating Cost: $2,275

Due to the variability of weather, system installation, and living habits this analysis is to be considered an estimate.

12/7/12

Temperature Bin Analysis

Gas-80%-Ignitor-Induced System

Outdoor Air Temp	Annual Weather Hours	Space Load Btu/Hr	Hot Water Load Btu/Hr	Furnace Capacity Btu/Hr	Furnace Run Time	A/C Capacity Btu/Hr	A/C Run Time	Furnace Operating Cost	A/C Operating Cost	Water Heating Cost
112										
107										
102										
97										
92	5	22,697	1,387			33,872	73%		$1.48	$0.12
87	69	18,133	1,387			34,878	59%		$15.71	$1.65
82	228	13,569	1,387			35,883	45%		$37.20	$5.45
77	436	9,005	1,387			36,889	30%		$45.08	$10.42
72	615	7,179	1,387			37,894	24%		$47.13	$14.70
67	705		1,387							$16.85
62	705		1,387							$16.85
57	672	-3,205	1,387	58,228	6%			$31.95		$16.07
52	637	-6,667	1,387	58,228	12%			$62.73		$15.23
47	586	-10,128	1,387	58,228	19%			$87.31		$14.01
42	590	-13,590	1,387	58,228	25%			$117.48		$14.11
37	724	-17,052	1,387	58,228	31%			$180.23		$17.31
32	762	-20,513	1,387	58,228	37%			$227.41		$18.22
27	618	-23,975	1,387	58,228	43%			$214.86		$14.77
22	464	-27,436	1,387	58,228	49%			$184.06		$11.09
17	367	-30,898	1,387	58,228	55%			$163.50		$8.77
12	260	-34,359	1,387	58,228	61%			$128.48		$6.22
7	160	-37,821	1,387	58,228	67%			$86.82		$3.83
2	91	-41,282	1,387	58,228	73%			$53.79		$2.18
-3	43	-44,744	1,387	58,228	79%			$27.49		$1.03
-8	17	-48,205	1,387	58,228	85%			$11.69		$0.41
-13	5	-51,667	1,387	58,228	91%			$3.68		$0.12
-18	1	-55,128	1,387	58,228	97%			$0.78		$0.02
-23										
-28										
-33										
	8760							$1,582	$147	$209

12/7/12

Bin Analysis Graph

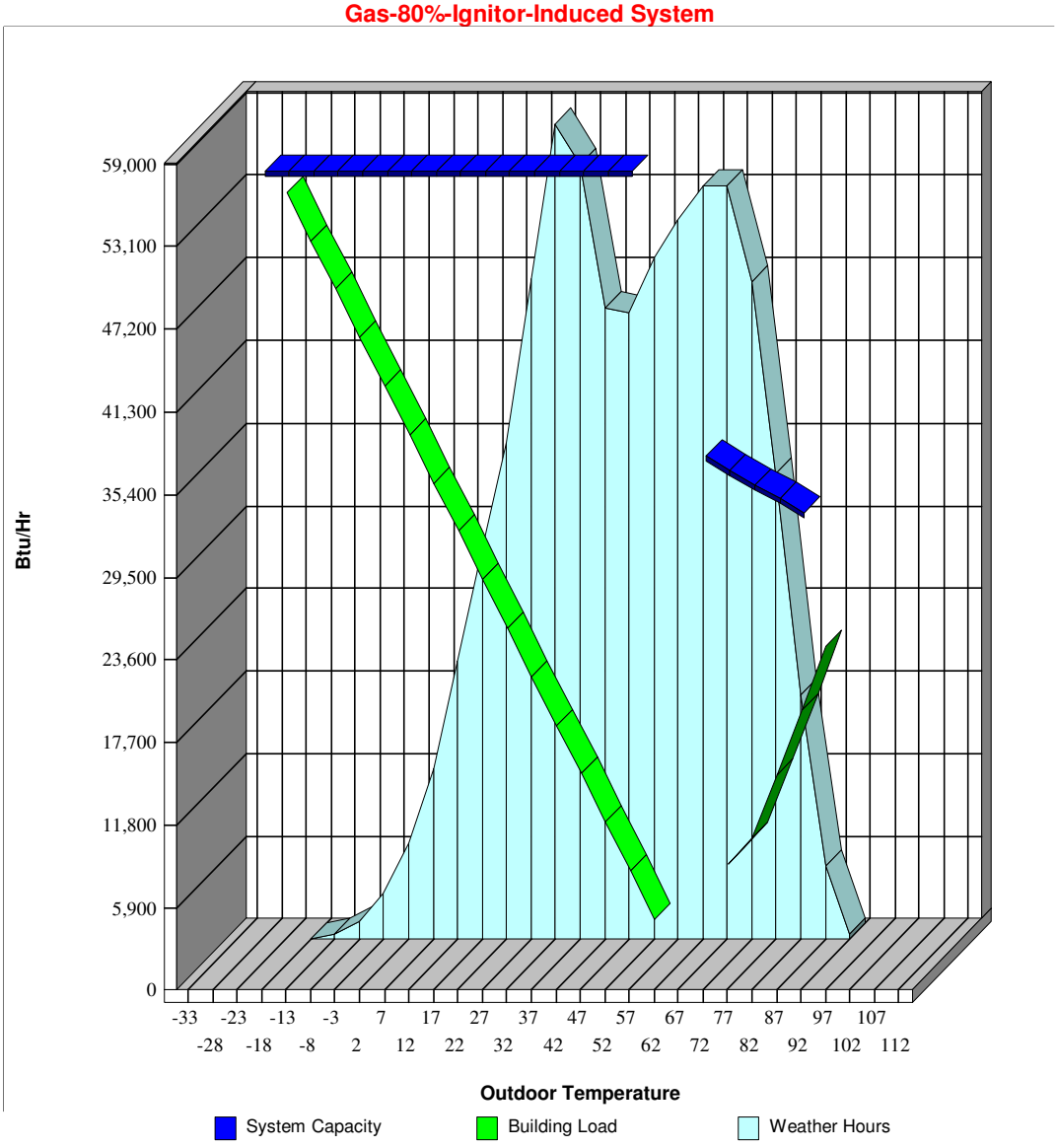

12/7/12

Appendix C

Thermistor Calibration

The Steinhart and Hart (1968) equation, Equation C.1, is the most commonly used empirical approximation formula for thermistors. This expression relates resistance of the thermistor to temperature.

$$\frac{1}{T} = A + B \ln R + C(\ln R)^3 \tag{C.1}$$

For higher accuracy or to accommodate a wider temperature range, a square term can be included to create Equation C.2, taken after Wood et al. (1978).

$$\frac{1}{T} = A + B \ln R + C(\ln R)^2 + D(\ln R)^3 \tag{C.2}$$

For this investigation the expected range of temperatures surrounding the geothermal loop was not expected to be significantly different than the control temperatures used to calibrate the sensors. To this end, Equation C.1 was calibrated to. With an equation of three variables, three equations are required to solve for them. The three reference temperatures were created using: an icebath ($\sim 0°C$), an environmental chamber ($\sim 18.2°C$), and a walk-in fridge ($\sim 5.2°C$). This produced a system of linear equations:

$$\begin{bmatrix} 1 & \ln R_1 & (\ln R_1)^3 \\ 1 & \ln R_2 & (\ln R_2)^3 \\ 1 & \ln R_3 & (\ln R_3)^3 \end{bmatrix} \begin{bmatrix} A \\ B \\ C \end{bmatrix} = \begin{bmatrix} \frac{1}{T_1} \\ \frac{1}{T_2} \\ \frac{1}{T_3} \end{bmatrix}$$

To check the precision of this calibration 3 sensors were examined at a fourth controlled temperature. Following the same system of equations, this produces a linear overdetermined system of 4 equations and 3 unknowns. The relative residual of these three sensor calibrations, as calculated by Equation C.3 were: 1.84E-04, 1.94E-04, and 1.97E-04. The three thermistors were all rated $30k\Omega$. This thermistor type comprised 59 out of 64 thermistors in the field.

$$R = \frac{||b - A \times A\backslash b||}{||A|| \times ||A\backslash b||} \tag{C.3}$$

All thermistors in the field were initially suspected to be calibrated acceptably using this method with the exception of one. The only $10k\Omega$ thermistor was recording resistances of over $1000k\Omega$ during the initial 36 hour test period. According to its calibration curve, this thermistor was recording temperatures of $-80°C$, which is unrealistic when contrasted with the coldest temperatures seen elsewhere on the system of $-2°C$. The "broken" thermistor was located on the farthest supply line off the manifold. It was recalibrated by assuming that the temperature differential on average between the two long trench systems was equivalent. This produced a system of 35 equations and 3 unknowns, which were used to recalibrate the sensor.

Appendix D

1-Dimensional Finite Difference Model Derivation

D.1 Energy Equation

Thermal energy in a fluid is defined as:

$$E = \rho c_p T \forall$$

where E is the total thermal energy in a volume of fluid in J; ρ is the density of the fluid in kg/m^3; T is the temperature of the fluid in $^\circ C$; and $\forall$ is the volume of the fluid in m^3. By

assuming, for the purposes of this thesis, that the heat exchange fluid is incompressible and changes in specific heat capacity and density of the fluid with temperature are negligible, the following can be written:

$$\frac{\partial c_p}{\partial t} = \frac{\partial \rho}{\partial t} = \frac{\partial \forall}{\partial t} = 0$$

and the change in thermal energy in a fluid can be written as:

$$\Delta E = \rho c_p \forall \Delta T \tag{D.1}$$

In order to develop an expression for the change in temperature in the heat exchange fluid, a thermal energy balance was applied to a cylindrical control volume representing a section of the GHX. Figure D.1 represents a finite section of the pipe showing energy entering and exiting the pipe through advection and dispersion, and entering the pipe as an energy flux from the surrounding environment.

Considering a pipe of total length L [m], the change in thermal energy in this control volume over time can be represented as:

$$\begin{aligned}
\frac{\Delta E}{\Delta t} &= \rho c_p A_p \left(-D\frac{\partial T}{\partial x} + vT\right)\Big|_{x=x_L} - \rho c_p A_p \left(-D\frac{\partial T}{\partial x} + vT\right)\Big|_{x=x_R} + Q_{source}\Delta x \\
&= \Delta x \frac{\partial}{\partial x}\left(\rho c_p A_p \left(D\frac{\partial T}{\partial x} - vT\right)\right) + Q_{source}\Delta x \\
\frac{\Delta E}{\Delta t} &= \Delta x \rho c_p A_p D\frac{\partial^2 T}{\partial x^2} - \Delta x \rho c_p A_p v\frac{\partial T}{\partial x} + Q_{source}\Delta x
\end{aligned}$$

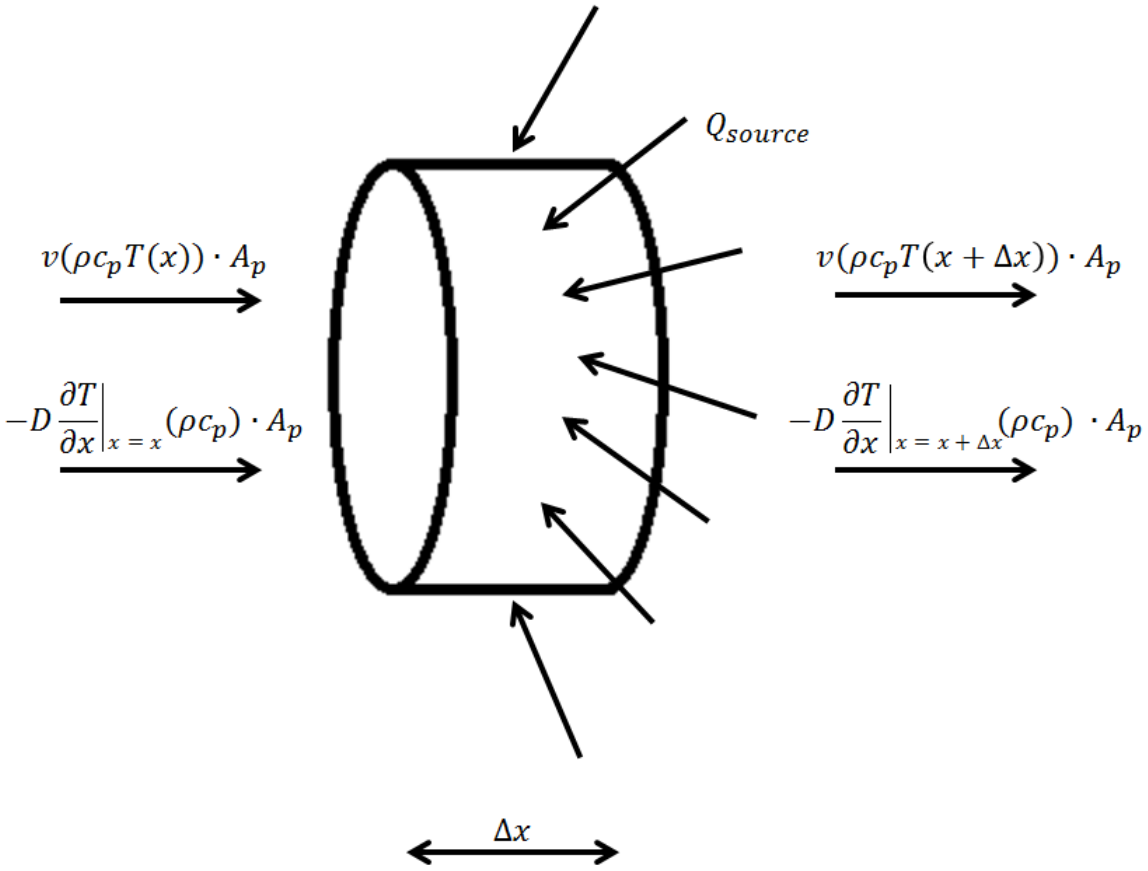

Figure D.1: Control volume used for energy balance

which, after substituting in Equation D.1, becomes:

$$\Delta x \rho c_p A_p \frac{\Delta T}{\Delta t} = \Delta x \rho c_p A_p D \frac{\partial^2 T}{\partial x^2} - \Delta x \rho c_p A_p v \frac{\partial T}{\partial x} + Q_{source} \Delta x$$

and reduces to:

$$\frac{\Delta T}{\Delta t} = D \frac{\partial^2 T}{\partial x^2} - v \frac{\partial T}{\partial x} + \frac{1}{\rho c_p A_p} Q_{source}$$

which, as the limit as $\Delta T \to 0$, is written as:

$$\frac{\partial T}{\partial t} = D \frac{\partial^2 T}{\partial x^2} - v \frac{\partial T}{\partial x} + \frac{1}{\rho c_p A_p} Q_{source} \tag{D.2}$$

Equation D.2 is the advection-dispersion equation for the temperature flux a fluid flowing through a pipe.

However, the thermal energy flux into the pipe is a combination of all energy sources and sinks surrounding the pipe, which in this case are the adjacent pipe and the surrounding subsurface:

$$Q_{source} = Q_{source}^{pipes} + Q_{source}^{soil}$$

where Q_{source}^{pipes} is the heat flux from the adjacent pipe per metre [J/sm] and Q_{source}^{soil} is the heat flux from the subsurface per meter [J/sm].

To represent the energy transfer into the pipe an expression for the total energy flux

per unit length of pipe was adapted after Yovanovich (1973) as:

$$Q_{source}^{pipes} = \frac{\Delta T}{R} = -\frac{T - T'}{R_p} \tag{D.3}$$

Similarly, to represent the energy transfer from the the surrounding soil at some distance into the fluid in the pipe, the total energy flux per unit length was adapted after Yovanovich (1973) as:

$$Q_{source}^{soil} = -\frac{T - T_s}{R_s} \tag{D.4}$$

Therefore, using Equations D.3 and D.4, Equation D.2 becomes:

$$\frac{\partial T}{\partial t} = D\frac{\partial^2 T}{\partial x^2} - v\frac{\partial T}{\partial x} - \frac{1}{\rho c_p A_p}\frac{T - T'}{R_p} - \frac{1}{\rho c_p A_p}\frac{T - T_s}{R_s} \tag{D.5}$$

and using the substitutions:

$$\beta_1 = \frac{1}{R_p \rho c_p A_p} \qquad \& \qquad \beta_2 = \frac{1}{R_s \rho c_p A_p}$$

Equation D.5 becomes:

$$\frac{\partial T}{\partial t} = D\frac{\partial^2 T}{\partial x^2} - v\frac{\partial T}{\partial x} - \beta_1 \left[T - T'\right] - \beta_2 \left[T - T_s\right] \tag{D.6}$$

D.2 Coupled Equations

Considering the temperature, T_s, at some intermediate point in the subsurface at a radial distance, r_s, between the pipe and the far field, Equation D.2 can be represented using two coupled equations:

$$\frac{\partial T}{\partial t} = D\frac{\partial^2 T}{\partial x^2} - v\frac{\partial T}{\partial x} - \beta_1[T - T'] - \beta_2[T - T_s] \tag{D.7}$$

$$\frac{\partial T_s}{\partial t} = -\beta_3[T_s - T] - \beta_3[T_s - T'] - \beta_4[T_s - T_\infty] \tag{D.8}$$

Where:

$$\begin{aligned}
\beta_1 &= \frac{1}{R_p \rho c_p A_p}; \\
\beta_2 &= \frac{1}{R_s \rho c_p A_p}; \\
\beta_3 &= \frac{1}{R_s \rho_{soil} c_{p_s} \forall_{inter}} = \frac{1}{R_s \rho_s c_{p_s} \pi (r_s^2 - r_o^2)}; \\
\beta_4 &= \frac{1}{R_\infty \rho_{soil} c_{p_s} \forall_\infty} = \frac{1}{R_\infty \rho_s c_{p_s} \pi (r_\infty^2 - r_s^2)};
\end{aligned}$$

and $\forall_s$ is the volume [m^3] of soil between the outer pipe radius, r_o, and the intermediate soil radius, r_s, and $\forall_\infty$ is the volume [m^3] of the hollow cylinder of soil created between the

intermediate soil radius, r_s, and the radius of influence, r_∞:

$$\forall_s = \pi(r_s^2 - r_o^2)\Delta x \qquad \& \qquad \forall_\infty = \pi(r_\infty^2 - r_s^2)\Delta x$$

Since the model represents a pipe of length L in a U-tube shape, the length of the soil domain is $L/2$. Therefore, the soil temperature, T_s, is equivalent at x and $L - x$.

D.3 Effective Thermal Resistance

Effective thermal resistances were divided into sections and combined in series:

$$\begin{aligned} R_p &= R_{soil}^{pipes} + 2R_{pipe} \\ R_s &= R_{inter} + R_{pipe} \end{aligned} \tag{D.9}$$

where expressions for R_{soil}^{pipes} and R_{inter} were estimated after Yovanovich (1973) in Chapter 4 as Equation D.10 and Equation D.11, respectively.

$$R_{soil}^{pipes} = \frac{1}{2\pi k_{soil}} \left[ln \left\{ \sqrt{\left(\frac{w}{r_{1_o}}\right)^2 - 1} + \left(\frac{w}{r_{1_o}}\right) \right\} - \left\{ \sqrt{\left(\frac{w}{r_{2_o}}\right)^2 - 1} + \left(\frac{w}{r_{2_o}}\right) \right\} \right] \tag{D.10}$$

$$R_{inter} = \frac{1}{2\pi k_{soil}} \left[ln \left\{ \sqrt{\left(\frac{w}{r_o}\right)^2 - 1} + \left(\frac{w}{r_o}\right) \right\} + \left\{ \sqrt{\left(\frac{w}{r_s}\right)^2 - 1} + \left(\frac{w}{r_s}\right) \right\} \right] \tag{D.11}$$

The effective thermal resistances R_{pipe} and R_{inter}, were derived from Fourier's Law:

$$q = -kA\frac{\partial T}{\partial \eta} \tag{D.12}$$

For heat flux through the wall of a hollow cylindrical control volume:

$$A = 2\pi r \Delta x \qquad \& \qquad \eta = r$$

where r is the radius of the control volume [m] and Δx is the length of the control volume [m]. Thus, Equation D.12 becomes:

$$q = -k2\pi r \Delta x \frac{\partial T}{\partial r}$$

Separating and integrating this equation from the inner radius, r_1, at T_1 to the outer radius, r_2, at T_2:

$$\int_{r_1}^{r_2} \frac{q}{r} \partial r = \int_{T_1}^{T_2} -2\pi k \Delta x \partial T$$

$$q \left[ln(r) \right]_{r_1}^{r_2} = -2\pi k \Delta x \left[T \right]_{T_1}^{T_2}$$

$$q[ln(r_2) - ln(r_2)] = -2\pi k\Delta x(T_2 - T_1) = 2\pi kLT(T_1 - T_2)$$

$$q = \frac{2\pi k\Delta x(T_1 - T_2)}{ln(\frac{r_2}{r_1})} \tag{D.13}$$

Equation D.13 defines the total heat flux across the wall of a hollow, cylindrical control volume. Defining the heat flux per unit length of pipe, Q, in J/sm as:

$$Q = \frac{q}{\Delta x} = \frac{2\pi k(T_2 - T_1)}{ln(\frac{r_2}{r_1})}$$

and using the definition for heat flux per unit length after Yovanovich (1973):

$$Q = \frac{(T_2 - T_1)}{R}$$

where R is effective thermal resistance of the cylindrical control volume in smK/J, this effective thermal resistance can be expressed as:

$$R = \frac{ln(\frac{r_2}{r_1})}{2\pi k} \tag{D.14}$$

Equation D.15 defines the effective thermal resistance across the wall of a hollow cylindrical control volume, which can be used to estimate the effective thermal resistances, R_{pipe} and R_{inter}. Substituting the appropriate parameters for the effective thermal resistance of

the pipe into Equation D.15, R_{pipe} is estimated as:

$$R_{pipe} = \frac{ln(\frac{r_o}{r_i})}{2\pi k_{pipe}} \tag{D.15}$$

where R_{pipe} is the effective thermal resistance across the pipe wall [smK/J]; r_o and r_i are the outer and inner radii of the pipe [m]; and k_{pipe} is the thermal conductivity of the pipe material [J/(smK)]. Substituting the appropriate parameters for the effective thermal resistance of the soil between the intermediate radius and the far field into Equation D.15, R_{inter} is estimated as:

$$R_{\infty} = \frac{ln(\frac{r_{\infty}}{r_s})}{2\pi k_{soil}} \tag{D.16}$$

Where R_{∞} is the effective thermal resistance of the annulus of soil between the intermediate radius and the far field [smK/J]; r_{∞} and r_s are the far field and intermediate soil radii [m]; and k_{soil} is the average thermal conductivity of the soil [J/(smK)]. Equation D.16 describes the effective thermal resistance, R_{∞} as used in Equation 4.5 to define β_4.

Substituting Equation D.10, Equation D.11, and Equation D.15 into Equation D.9 to complete the expressions describing the effective thermal resistances R_p and R_s as used in Equation 4.5 to define β_1, β_2, and β_3

D.4 Finite Difference Approximation

The finite difference approximation was employed to solve Equations D.7 and D.8 using a grid of 3×N discrete nodes to represent the physical system. The system is composed of a U-tube shaped pipe in a cylindrical soil domain. The fluid flowing away from the heat pump and the fluid returning to the heat are contained in identical, parallel lengths of pipe surrounded by a cylindrical subsurface. Therefore, using nodes to represent the system, nodes $1...N$ represent the fluid in the pipe flowing away from the heat pump, nodes $N+1...2N$ represent the fluid in the pipe returning to the heat pump, and nodes $2N+1...3N$ represent the soil at an intermediate radius from the centre of the two pipes. This node distribution is presented in Figure D.2, which represents N nodes in each of the supply pipe (black), the return pipe (black), and the soil (blue).

Using Crank-Nicholson weighted average in time, Equation D.7, for $1 \leq i \leq 2N$:

$$\begin{aligned}\frac{T_i^{n+1}-T_i^n}{\Delta t} &= \frac{1}{2}\Bigg[D\left(\frac{T_{i-1}^{n+1}-2T_i^{n+1}+T_{i+1}^{n+1}}{\Delta x^2}\right)-v\left(\frac{T_{i+1}^{n+1}-T_{i-1}^{n+1}}{2\Delta x}\right)\\ &\quad -\beta_1\left(T_i^{n+1}-T_{2N-i+1}^{n+1}\right)-\beta_2\left(T_i^{n+1}-T_{s_i}^{n+1}\right)\Bigg]\\ &\quad \frac{1}{2}\Bigg[D\left(\frac{T_{i-1}^{n}-2T_i^{n}+T_{i+1}^{n}}{\Delta x^2}\right)-v\left(\frac{T_{i+1}^{n}-T_{i-1}^{n}}{2\Delta x}\right)\\ &\quad -\beta_1\left(T_i^{n}-T_{2N-i+1}^{n}\right)-\beta_2\left(T_i^{n}-T_{s_i}^{n}\right)\Bigg]\end{aligned}$$

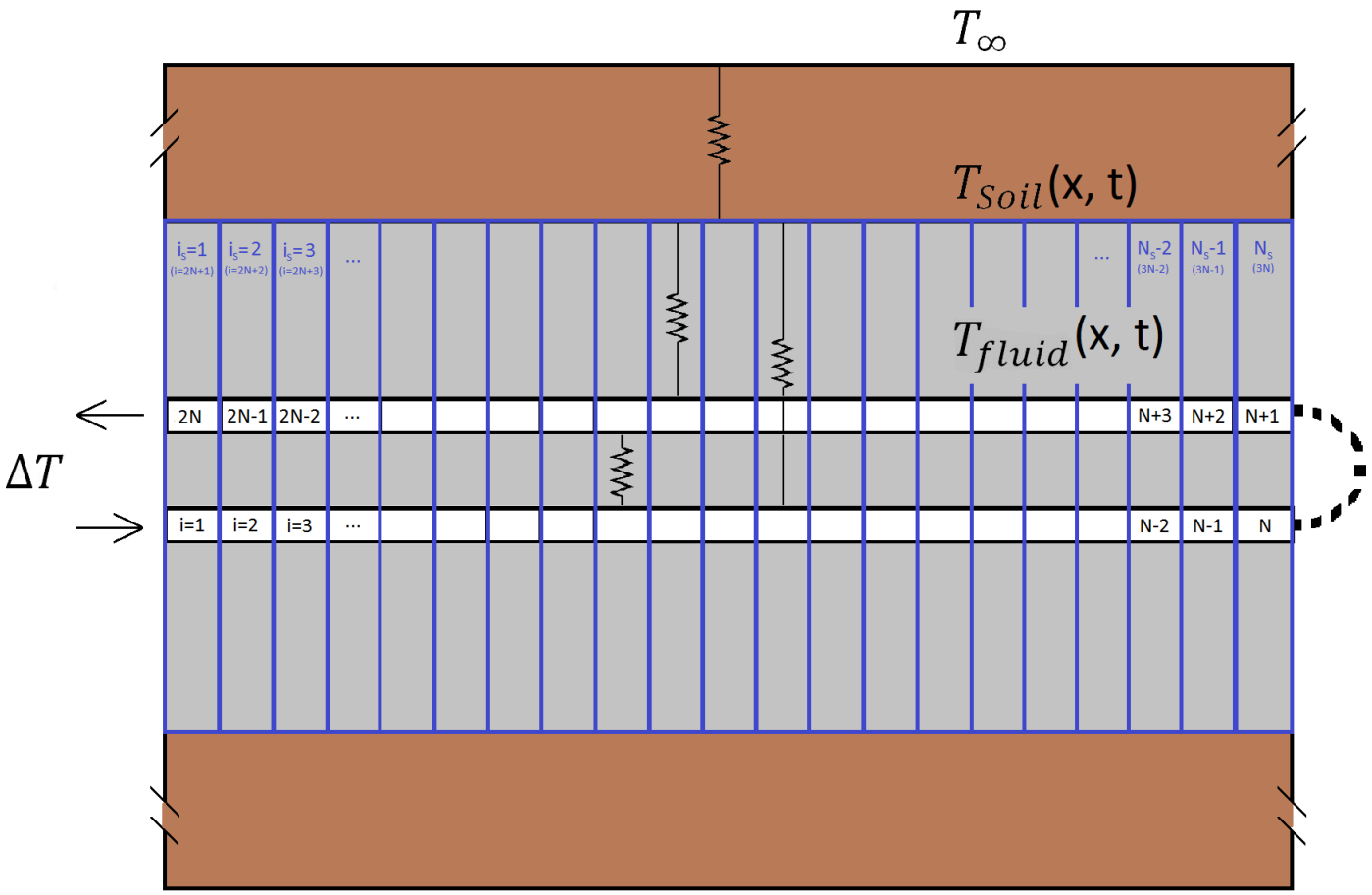

Figure D.2: Node distribution for the supply and return pipes and the soil - not to scale

which rearranges to:

$$T_{i-1}^{n+1}\left(-\frac{a}{2}\right)+T_{i}^{n+1}\left(\frac{1}{\Delta t}-\frac{b}{2}\right)+T_{i+1}^{n+1}\left(-\frac{c}{2}\right)+T_{2N-i+1}^{n+1}\left(-\frac{\beta_1}{2}\right)+T_{s_i}^{n+1}\left(-\frac{\beta_2}{2}\right)$$
$$=T_{i-1}^{n}\left(\frac{a}{2}\right)+T_{i}^{n}\left(\frac{1}{\Delta t}+\frac{b}{2}\right)+T_{i+1}^{n}\left(\frac{c}{2}\right)+T_{2N-i+1}^{n}\left(\frac{\beta_1}{2}\right)+T_{s_i}^{n}\left(\frac{\beta_2}{2}\right) \tag{D.17}$$

where:

$$a=\frac{D}{\Delta x^2}+\frac{v}{2\Delta x}$$
$$b=\frac{-2D}{\Delta x^2}-\beta_1-\beta_2$$
$$c=\frac{D}{\Delta x^2}-\frac{v}{2\Delta x}$$

With a finite difference approximation using Crank-Nicholson weighted average in time, Equation D.8 becomes, for $1 \leq i \leq N$:

$$\begin{aligned}\frac{T_{s_i}^{n+1}-T_{s_i}^{n}}{\Delta t} &= -\frac{\beta_3}{2}\left(T_{s_i}^{n+1}-T_i\right)-\frac{\beta_3}{2}\left(T_{s_i}^{n}-T_i\right)\\ &- \frac{\beta_3}{2}\left(T_{s_i}^{n+1}-T_{2N-i+1}^{n+1}\right)-\frac{\beta_3}{2}\left(T_{s_i}^{n}-T_{2N-i+1}\right)\\ &- \frac{\beta_4}{2}\left(T_{s_i}^{n+1}-T_\infty\right)-\frac{\beta_4}{2}\left(T_{s_i}^{n}-T_\infty\right)\end{aligned}$$

which rearranges to:

$$T_{s_i}^{n+1}\left(\frac{1}{\Delta t}+\frac{\beta_3}{2}+\frac{\beta_3}{2}+\frac{\beta_4}{2}\right)+T_i^{n+1}\left(\frac{-\beta_3}{2}\right)+T_{2N-i+1}^{n+1}\left(\frac{-\beta_3}{2}\right)$$
$$=T_{s_i}^{n}\left(\frac{1}{\Delta t}-\frac{\beta_3}{2}-\frac{\beta_3}{2}-\frac{\beta_4}{2}\right)+T_i^{n}\left(\frac{\beta_3}{2}\right)+T_{2N-i+1}^{n}\left(\frac{\beta_3}{2}\right)+T_\infty\left(\beta_4\right)$$

and, after the substitution $d=-\beta_3-\frac{\beta_4}{2}$, becomes:

$$T_{s_i}^{n+1}\left(\frac{1}{\Delta t}-\frac{d}{2}\right)+T_i^{n+1}\left(\frac{-\beta_3}{2}\right)+T_{2N-i+1}^{n+1}\left(\frac{-\beta_3}{2}\right)$$
$$=T_{s_i}^{n}\left(\frac{1}{\Delta t}+\frac{d}{2}\right)+T_i^{n}\left(\frac{\beta_3}{2}\right)+T_{2N-i+1}^{n}\left(\frac{\beta_3}{2}\right)+T_\infty\left(\beta_4\right)$$

D.5 Boundary Conditions

While the system is operating there is a fixed temperature delta boundary condition at $x=0$ representing the energy change in the fluid caused by the heat pump:

$$T\left(x=0,t\right)=T_{in}=T_{out}+\Delta T$$

where $T_{out}=T_{2N}$. So the boundary condition at $i=1$ can be defined using:

$$T_{i-1}=T_{in}=T_{out}+\Delta T=T_{2N}+\Delta T$$

It follows that the solution at $i = 1$ for the fixed temperature delta boundary condition at $x = 0$ becomes:

$$\begin{aligned} &T_i^{n+1}\left(\frac{1}{\Delta t}-\frac{b}{2}\right)+T_{i+1}^{n+1}\left(-\frac{c}{2}\right)+T_{2N-i+1}^{n+1}\left(-\frac{\beta_1}{2}\right)+T_{2N}^{n+1}\left(-\frac{a}{2}\right)+T_{s_i}^{n+1}\left(-\frac{\beta_2}{2}\right) \\ &=T_i^{n}\left(\frac{1}{\Delta t}+\frac{b}{2}\right)+T_{i+1}^{n}\left(\frac{c}{2}\right)+T_{2N-i+1}^{n}\left(\frac{\beta_1}{2}\right)+T_{2N}^{n}\left(\frac{a}{2}\right)+T_{s_i}^{n}\left(\frac{\beta_2}{2}\right)+\Delta T\,(a) \end{aligned} \tag{D.18}$$

When the system is not in operation the velocity and mechanical dispersion of the fluid in the pipe are zero. While the system is not operating a no thermal energy flux boundary condition is defined at $x = 0$:

$$\frac{\partial T}{\partial x}\Big|_{x=0} = 0$$

where $T(x = 0) = T_1$. So the boundary condition at $i = 1$ can be defined using:

$$\frac{\partial T}{\partial x}\Big|_{x=0} = \frac{T_{i-1} - T_i}{\Delta x} = 0 \quad \Rightarrow \quad T_i = T_{i-1}$$

It follows that when the system is not operating, using $v = D_L = 0$, the solution at $i = 1$

for the no thermal energy flux boundary condition at $x = 0$ becomes:

$$\begin{aligned} &T_i^{n+1}\left(-\frac{a}{2}+\frac{1}{\Delta t}-\frac{b}{2}\right)+T_{i+1}^{n+1}\left(\frac{-c}{2}\right)+T_{2N-i+1}^{n+1}\left(-\frac{\beta_1}{2}\right)+T_{s_i}^{n+1}\left(-\frac{\beta_2}{2}\right) \\ &=T_i^{n}\left(\frac{a}{2}+\frac{1}{\Delta t}+\frac{b}{2}\right)+T_{i+1}^{n}\left(\frac{c}{2}\right)+T_{2N-i+1}^{n}\left(\frac{\beta_1}{2}\right)+T_{s_i}^{n}\left(\frac{\beta_2}{2}\right) \end{aligned} \tag{D.19}$$

At all times an advective-only boundary condition is defined at $x = L$:

$$\frac{\partial T}{\partial x}\Big|_{x=L} = 0$$

where $T(x = L) = T_{2N}$. So the boundary condition at $i = 2N$ can be defined using:

$$\frac{\partial T}{\partial x}\Big|_{x=L} = \frac{T_{i+1} - T_i}{\Delta x} = 0 \quad \Rightarrow \quad T_{i+1} = T_i$$

It follows that the solution at $i = 2N$ for the no thermal flux boundary condition at $x = L$ becomes:

$$\begin{aligned} &T_{i-1}^{n+1}\left(-\frac{a}{2}\right)+T_i^{n+1}\left(\frac{1}{\Delta t}-\frac{b}{2}-\frac{c}{2}\right)+T_{2N-i+1}^{n+1}\left(-\frac{\beta_1}{2}\right)+T_{s_i}^{n+1}\left(-\frac{\beta_2}{2}\right) \\ &=T_{i-1}^{n}\left(\frac{a}{2}\right)+T_i^{n}\left(\frac{1}{\Delta t}+\frac{b}{2}+\frac{c}{2}\right)+T_{2N-i+1}^{n}\left(\frac{\beta_1}{2}\right)+T_{s_i}^{n}\left(-\frac{\beta_2}{2}\right) \end{aligned} \tag{D.20}$$

Appendix E

Base Case Calculations

E.1 In-Pipe Dispersion

Using the Elora Test Site as a basis for calculations, a base-case dispersion coefficient was calculated. The total volumetric flow rate through six identical pipes is 15 GPM, or 9.5×10^{-4} m^3/s. The pipe used for the GHX at Elora is 3/4" IPS SDR11, which has an average inner diameter of 0.827 inches, or 2.1×10^{-2} m (Cli, 2012).

The heat exchange fluid circulating through the GHX at the Elora Field Site is a mixture of water and 20% by volume propylene glycol. However, above 0°C the density of propylene glycol is taken to be 1000 kg/m^3 (Cli, 2012) and to simplify for the base-case,

the fluid properties were assumed to be that of water at 10°C. Water at 10° C has a density of 999.8 kg/m^3 and a dynamic viscosity of 1.31×10^{-3} Pa $\cdot$ s (Siegenthaler, 2004).

Based on these parameters, the base-case coefficient of longitudinal dispersion, D_L, of the fluid in the pipe was calculated using Equation 4.14 as 0.034 ft^2/s or 0.0032 m^2/s.

The thermal diffusivity, α, of the heat exchange fluid was defined as that of water of water at 10°C, 1.4x10$^{-7}m^2/s$ (Siegenthaler, 2004), which is negligible compared to the longitudinal dispersion coefficient. Therefore, the final dispersion coefficient was taken to be the longitudinal dispersion coefficient defined by Equation 4.14, 0.013 m^2/s.

E.2 Radius of Influence

Simms (2013) performed a study using a 3D finite element model describing a system representing the Elora Test Site. The study investigated the change in soil temperature with distance away from the ground loop for a range of heterogeneous soil thermal conductivities and the homogeneous case. Each simulation was a 400 day simulation utilizing the measured heating and cooling loads, surface temperatures, and fluid properties from the Elora Field Site. The bulk soil thermal properties from the Elora Field Site were used as a basis upon which a range of soil thermal properties were generated for these simulations. The results of this investigation are presented in Figure E.1 (Simms, 2013).

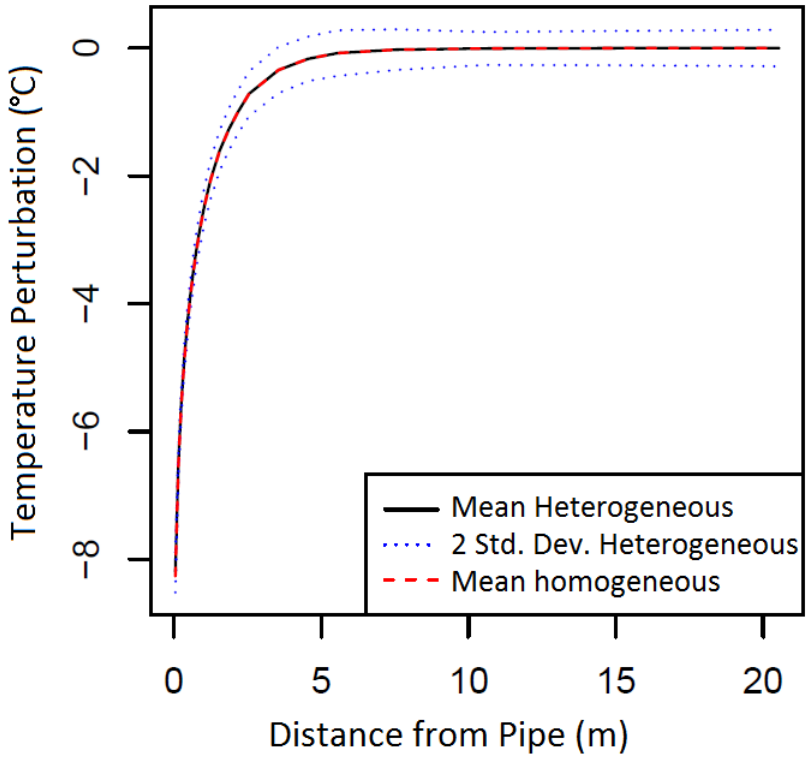

Figure E.1: Soil temperature perturbation caused by ground loop (Simms, 2013)

Figure E.1 illustrates that after the 400 day simulations there was negligible change in soil temperature at a radius of approximately 5 m from the ground loop for the mean heterogeneous and homogeneous cases. Therefore, the radius of influence, r_∞, was initially defined as 5 m in the developed finite difference model.

To investigate the sensitivity of the model to changes in the radius of influence, a range of simulations were conducted in which only this parameter was changed. All other

parameters were as defined in Section 5.1.1. Figure E.2 shows the results of this sensitivity analysis as it relates to the average coefficient of performance (COP) of the GSHP.

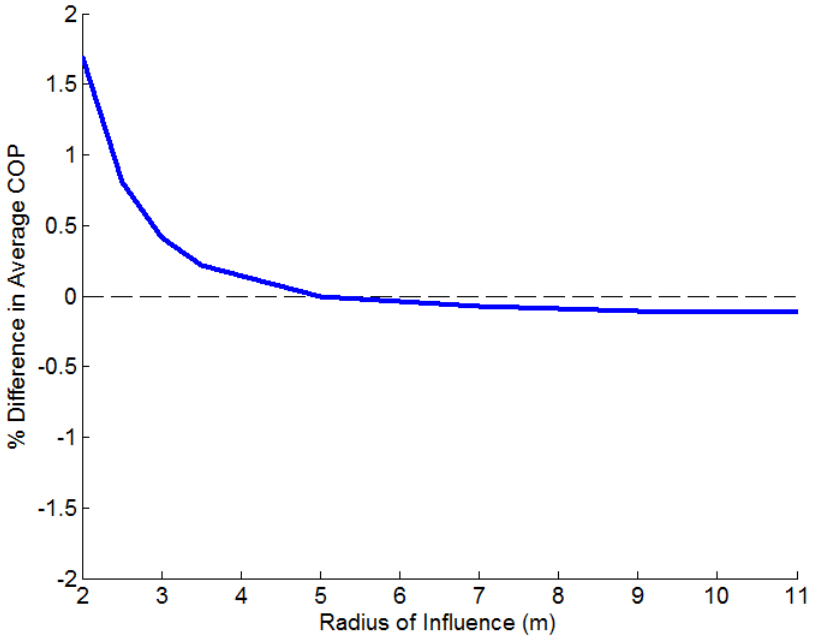

Figure E.2: Sensitivity of model COP to radius of influence, r_∞

Figure E.2 shows the effect of changing the radius of influence relative to the initial value of 5 m discussed above. The sensitivity to changes in this parameter are not significant ($<$0.2%) when r_∞ was increased above 5 m. However, the sensitivity to changes in the radius of influence became more significant ($\leq$2%) when r_∞ was reduced from 5 m to 2 m. Therefore, 5 m was used as the base value for the radius of influence.

E.3 Intermediate Soil Radius

This section summarizes the investigation into the sensitivity of the model to changes in the intermediate soil radius over a range of simulations. While all other parameters were representative of the Elora Field Site, only the intermediate soil radius, r_s, was altered. Figure E.3 shows the results of this sensitivity analysis as it relates to the average coefficient of performance (COP) of the GSHP.

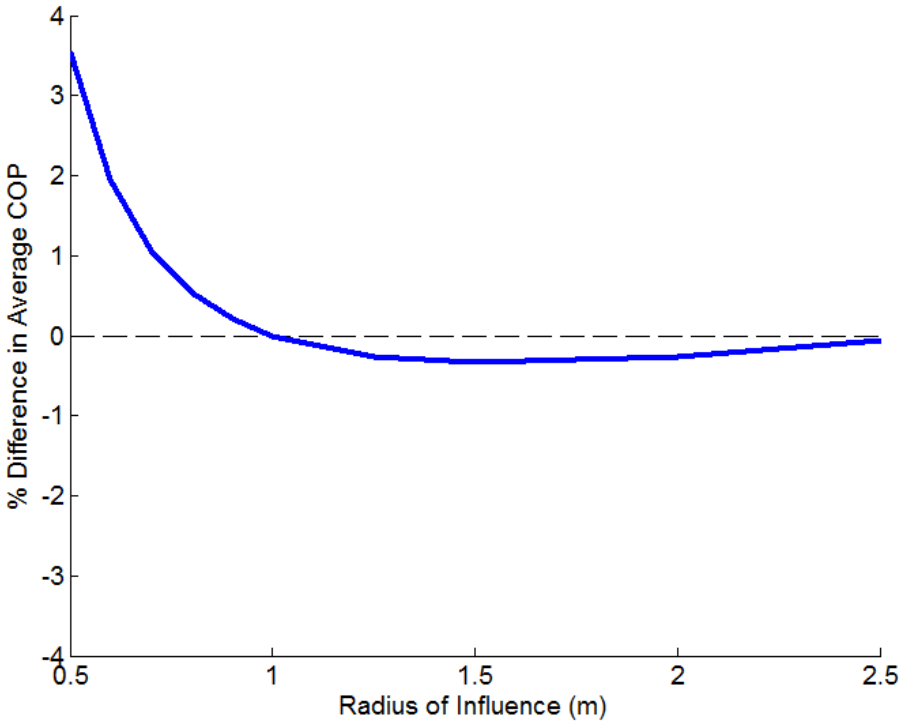

Figure E.3: Sensitivity of model COP to intermediate soil radius, r_s

Figure E.3 illustrates the effect of changing the intermediate soil radius relative to a base-case value of 1 m. The changes due to this parameter are slightly more significant than the radius of influence for the range considered. However, the variation in COP due to changes in the intermediate soil radius were only significant (>1%) below 1 m. Therefore, 1 m was used as the base value for the intermediate soil radius.

Appendix F

Constant Versus Pulsed Pumping Comparison Results

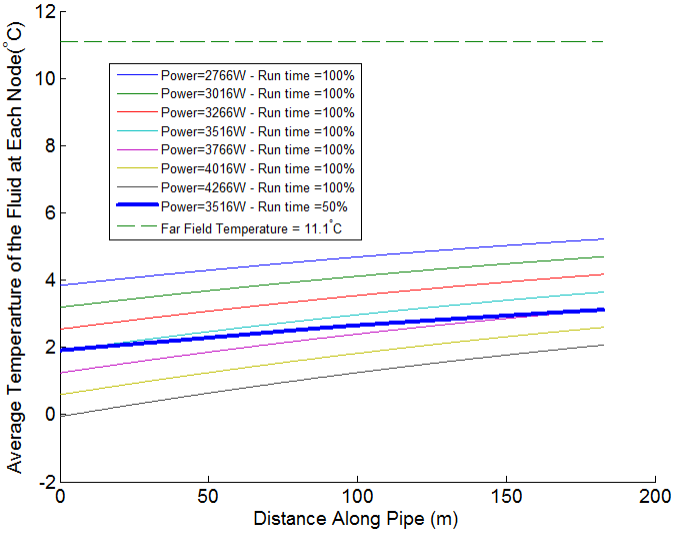

Figure F.1: Average temperature of the fluid in each element after 30 day simulation - comparison between pulsed and constant pumping cases

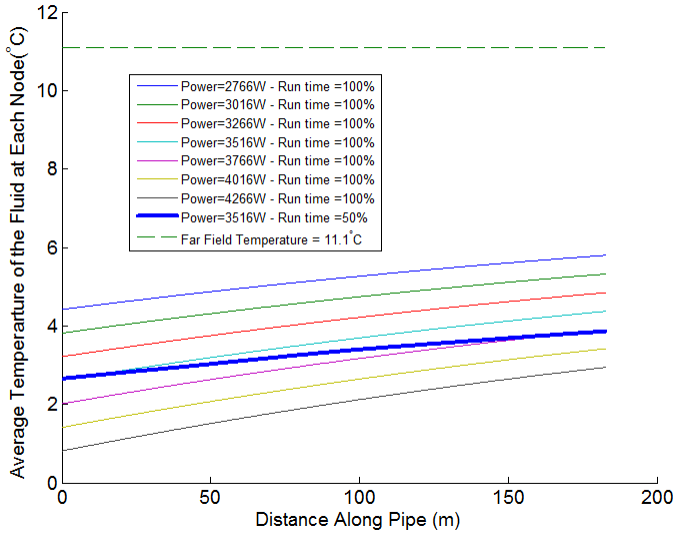

Figure F.2: Average temperature of the fluid in each element after 14 day simulation - comparison between pulsed and constant pumping cases

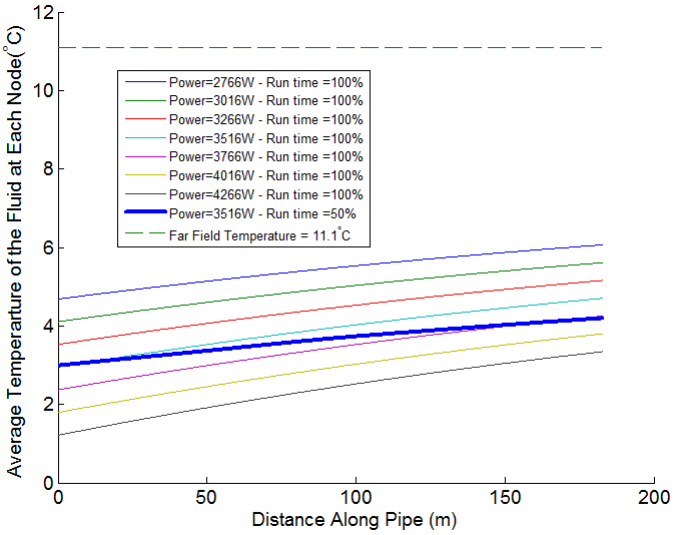

Figure F.3: Average temperature of the fluid in each element after 7 day simulation - comparison between pulsed and constant pumping cases

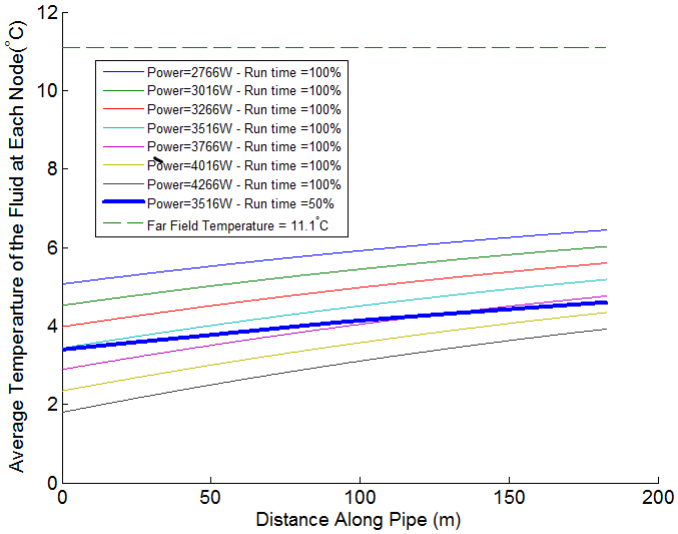

Figure F.4: Average temperature of the fluid in each element after 1 day simulation - comparison between pulsed and constant pumping cases

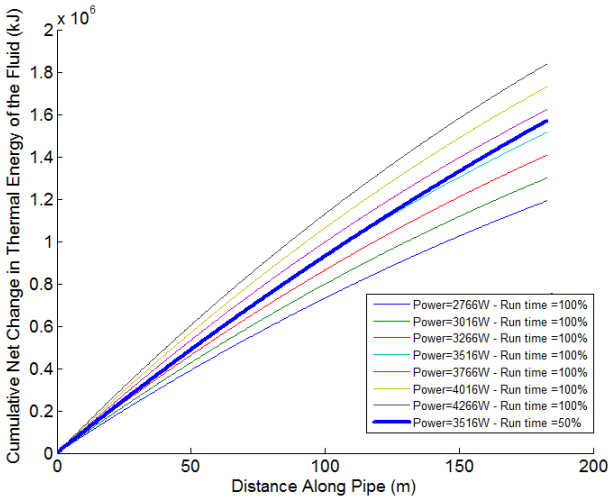

Figure F.5: Cumulative energy change of the fluid in each element after 30 day simulation - comparison between pulsed and constant pumping cases

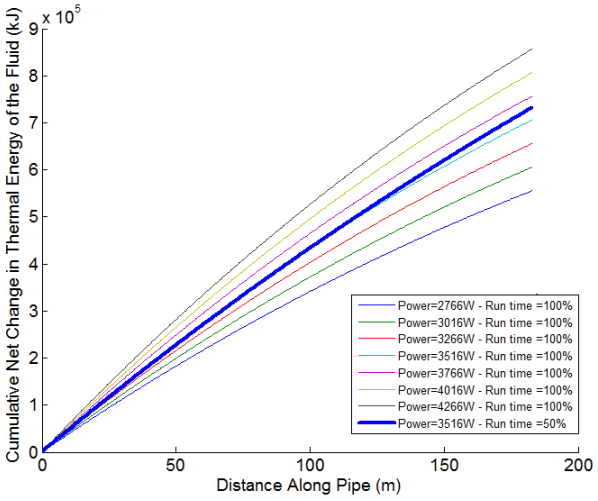

Figure F.6: Cumulative energy change of the fluid in each element after 14 day simulation - comparison between pulsed and constant pumping cases

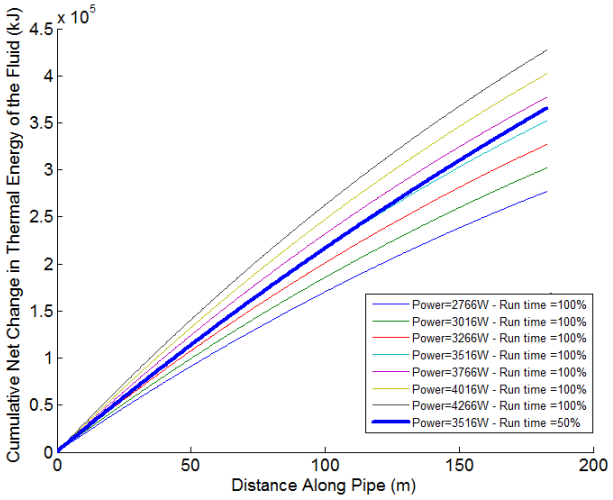

Figure F.7: Cumulative energy change of the fluid in each element after 7 day simulation - comparison between pulsed and constant pumping cases

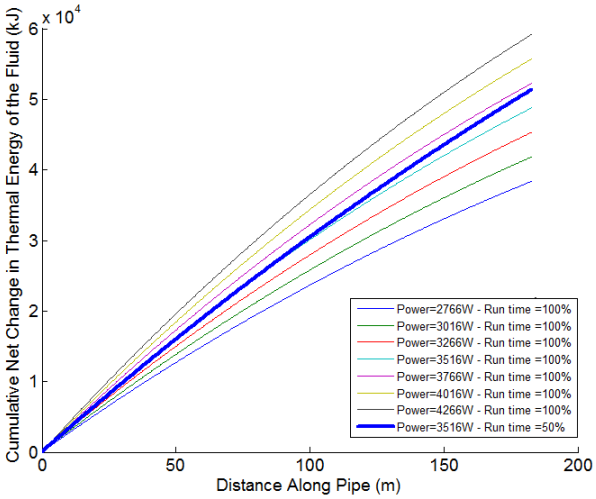

Figure F.8: Cumulative energy change of the fluid in each element after 1 day simulation - comparison between pulsed and constant pumping cases

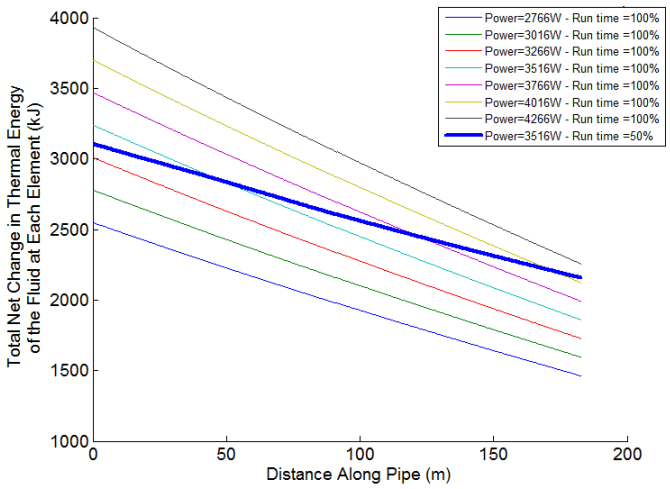

Figure F.9: Total energy change of the fluid in each element after 30 day simulation - comparison between pulsed and constant pumping cases

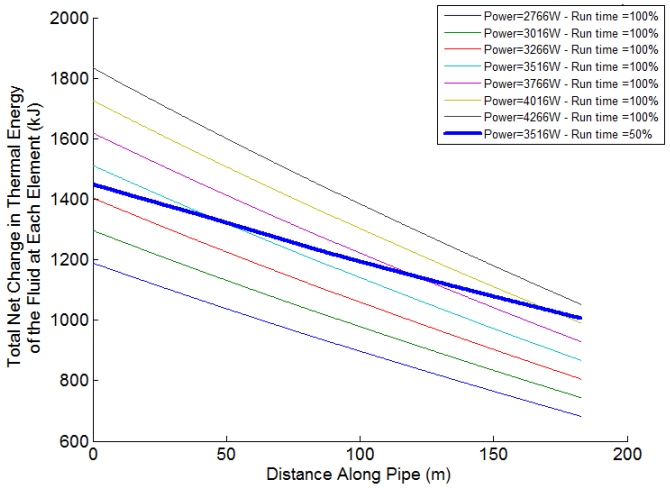

Figure F.10: Total energy change of the fluid in each element after 14 day simulation - comparison between pulsed and constant pumping cases

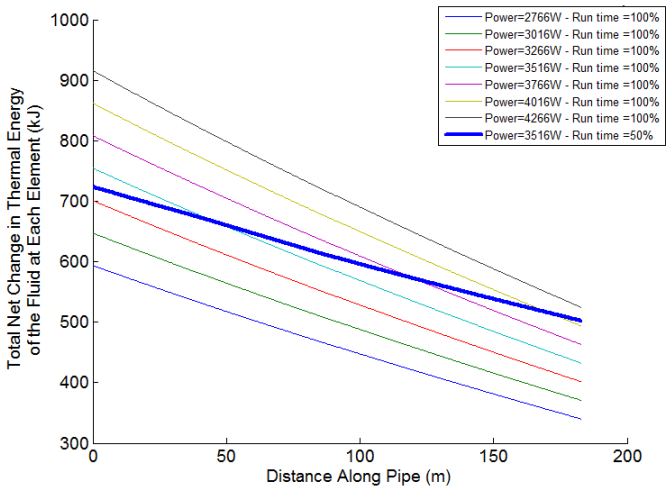

Figure F.11: Total energy change of the fluid in each element after 7 day simulation - comparison between pulsed and constant pumping cases

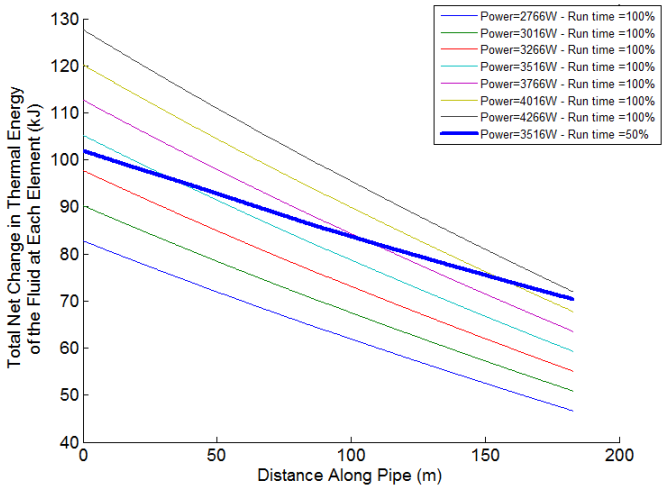

Figure F.12: Total energy change of the fluid in each element after 1 day simulation - comparison between pulsed and constant pumping cases